NTNU

NORWEGIAN UNIVERSITY OF SCIENCE AND TECHNOLOGY

Kavli Institute For Systems Neuroscience And Centre For Neural Computation

Analysis Of Contralateral-Projecting Cells In Medial Entorhinal Cortex Layer II/III Using Electrophysiological Recordings Combined With Optogenetics Application

Nader Marzban

Master thesis Supervised by

Sheng-Jia Zhang

Jing Ye

Faculty of Medicine, Department of Neuroscience

Trondheim, Norway

May 2015

ABSTRACT

Recent studies have revealed that all functional cell types in superficial layers of medial entorhinal cortex have projections to the hippocampus. Furthermore, hippocampal functions in connection with neural circuits in medial entorhinal cortex offer a good systems approach to understanding the basic functions of episodic memory formation. Then, we draw our attentions to the connections complexity between both medial entorhinal cortex (MEC) hemispheres to investigate the pattern of connectivity of MEC-MEC functional cell type neurons, furthermore, providing further data associated with spatial memory formation for future research. There are several functional spatial cell types in superficial layer 2 of MEC that code various spatially information in navigational system. These cells including; grid cells, head-direction cells, border cells, conjunctive grid x head-direction cells, conjunctive border x head-direction cells, unknown principal cells and interneurons. By injecting retrogradely transportable recombinant adeno-associated virus carrying channelrhodopsin-2 transgene in the left MEC of two rats and also right MEC of three rats, optogenetic control over entorhinal neurons with direct projections to the contralateral MEC has been presented. Optogenetics application together with electrophysiological recordings *in vivo*, enabled us to determine functionally specialized spatial cell types in MEC projecting to the contralateral MEC, as these cells contained minimal response latencies to laser stimulations in MEC. We here show that, unknown principal cells and interneurons, among all functional cell types presented in MEC, had a strong projection from left MEC to the contralateral right MEC and vise versa. Grid cells that are recently found to have a massive projections to the hippocampus, here in our study, only a small number, showed responses to light that might suggest the probability of their contralateral MEC connections. However, these responses were too much weak to convince us that these cells had projections to contralateral MEC. No more data were discovered to support projections of other detected spatial cell types to the contralateral MEC at this study.

PREFACE AND ACKNOWLEDGMENTS

This work was part of the Master of Science in Neuroscience at the Norwegian University of Science and Technology (NTNU), and it was carried out at the Kavli Institute for Systems Neuroscience and Centre for Neural Computation, Faculty of Medicine, NTNU, in Trondheim, Norway.

This master thesis, along with most of my education, has been driven forward with the encouragement, support and assistance of many advisors, colleagues, and friends. Actually, I am indebted to them all, but can only thank few of them here:

I would like to thank my principal supervisor Sheng-Jia Zhang, who took a great leap of faith in taking an overly eager and slightly odd foreigner student into his lab and trusting me to be part of his group working on his interesting project. I am extremely thankful and indebted to Jing Ye for sharing expertise, and sincere and valuable guidance and encouragement extended to me. She gave me more than could be expected. I thank Jean Wu due to help me at this project through histochemistry part. I wish to express my sincere thanks to Anne Bjerkhagen, the Executive officer of the neuroscience department and June Larsen senior Executive officer of Faculty of medicine, for their kindly supports and assistance over those hard period time passed over me. I am also so grateful to Ignas Cerniauskas and Rine Sørlie Wågan as my lab mates for their help and supports. I take this opportunity to express gratitude to all my family members, in special my parents as they deserve a mention, because without their supports all happened would not be happened. I would like to nominate some of friends who made my student life as it should be: Axel, Javier, Sacha, Fahad as my dear flat mates, and my close friends: Reza, Saman, Sarry, Nuttawut, Vincent, Yassine, Behzad ,Jasem Estakhr. These friends are amazing and will be always kept in my heart and mind forever.

I also place on record, my sense of gratitude to one and all, who directly or indirectly, have lent their hand in this venture.

TABLE OF CONTENTS

List of figures

List of Tables

ABBREVIATIONS

AAV	Adeno-associated virus
AMPA	α-amino-3-hydroxy-5-methyl-4-isoxazole-propionic acid
BR	Bacteriorhodopsin
BSA	Bovine serum albumin
CA	*Cornu ammonis*
ChR	Channelrhodopsin
DIO	Doublefloxed inverted
ER	Endoplasmic reticulum
GFAP	Glial fibrillary acidic protein
HD	Head direction
HF	Hippocampal formation
HR	Halorhodopsin
HSV	Herpes-simplex virus
ISIH	Interspike interval histogram
ITR	Inverted terminal repeat
LEC	Lateral entorhinal cortex
LED	Light emitting diode
MEC	Medial entorhinal cortex
NGS	Natural goat serum
NMDA	*N*-methyl-D-aspartate
ORF	Open reading frame
PaS	Parasubiculum
PBS	Phosphate buffered saline solution
PHR	Parahippocampal region
PrS	Presubuculum
rAAV	Recombinant adeno-associated virus
SDC	Sodium dodecylcholate
SFO	Step function opsin

1. INTRODUCTION

Navigational system relies on information about changes in position and direction of animal in the environmental space (1). In fact, a network in the brain regions collectively represent animal location in local environment, but the underlying nature of this 'cognitive map' has not been fully understood yet. In recent years, evidence has increased supporting the notion that both hippocampus and entorhinal cortex containing neuronal information that allows the animal to navigate in the environment (2,3,4,5). The history of the last 40 years of research in navigation and path integration aimed at characterizing Hippocampal neuronal activity in freely behaving rats has been rich and has been achieved by the discovery that when animal had located itself in a local environment (by using environmental stimuli) the hippocampus could calculate subsequent locations in that space, on the basis of how far and in what direction the animal navigated in the environment (6). The persistence of hippocampal place cells in the dark phase have encouraged the inclusion of a neuronal path integrator. Place cells are those classes of cells in hippocampal region whose activities are tuned to rat's position and orientation in a specific field of environment (7). After almost more than three decades of spatially selective hippocampal place cells, and this proposal that hippocampus is the only basis of cognitive map, an interesting study turned the point of neuroscientists' views on entorhinal cortex area. By disruption of all intrahippocampal signals, place cells were still active in firing action potential suggesting there is another inputs origin further than intrahippocampal inputs and then studies shifted to the adjacent parahippocampal areas specially medial entorhinal region (8). A number of distinctive cells types discovered in medial entorhinal cortex which play an significant role together with hippocampal place cells to constitute a neuronal cognitive map in representing spatial movement of the brain in mammals to enable them to locate themselves and navigate to a goal. Four of these cells types and their anatomical locations are further illustrated in following. These cells are aforementioned hippocampal place cells which code for a unique location in space; head direction (HD) cells, which code a direction of animal's head and fire whenever the animal is facing a particular direction in space irrespective of where the animal is in the environment (7,9), grid cells which fire in regularly repeating positions, may be responsible for a distance metric (7), forming a specific triangular firing pattern (10) by having multiple periodic firing fields, arranged for each cell in a hexagonal pattern that run a metric that place cells don't have this ability on their own (11) and boundary vector /border cells which fire in response to barriers to movement. Whereas, hippocampal place cells were initially believed to have general navigational functions, it became

clearer that sensory information about space is distinguished by hippocampus into a mass of context- specific representations, which can be retrieved independently from degraded original inputs (10). This diversification of information is related to a principal role for hippocampus in event specific memory, and increases the probability that context-independent position information is computed upstream of the hippocampus area (10). Recent works has shown that location is represented accurately before the hippocampus in the superficial layers of the medial entorhinal cortex (MEC) (10). So we recorded neuronal firing activity in medial entorhinal cortex area while rats ran in an enclosure that was large enough (1 m × 1 m × 0.5 m) to get possible regularities in the spatial organization of neuronal activity.

1.1 Representations of the Hippocampal Formation and the Parahippocampal Regions

Hippocampal formation (HF) and Parahippocampal area of the rat is distinguished by general differences like the number of cortical layers and the pattern of connectivity (12,13). Situated in the caudal part of the brain, there is a C-shaped structure that is called hippocampal formation (HF) (Fig. 1). Three distinct subregions can be differentiated to the dentate gyrus (DG), the hippocampus (CA1, CA2 and CA3) and the subiculum. HF cortex has a three-layered appearance. The first layer of HF is a deep layer, consisting of a combination of afferent and efferent fibers and interneurons. This layer in DG is called the hilus, whereas in the CA areas it is referred to stratum oriens. A layer with mixture of principal cells and interneurons is superficial to this layer. This layer is referred to as the granule layer in the DG, whereas in the CA areas and the subiculum it is called the pyramidal cell layer (stratum pyramidale). Molecular layer (the stratum moleculare) is the most superficial layer of DG and subiculum. In the CA area the molecular layer is further divided into several sublayers. Three sublayers are detected in CA3: the stratum lucidum, which receives projections from the DG, the stratum radiatum, and most superficially, the stratum lacunosum-moleculare, comprising the apical tufts of the apical dendrites. The parahippocampus (PHR) area is next to the HF, bordering the subiculum and comprised of five subregions: the presubiculum (prS), the parasubiculum (paS), the entorhinal cortex (EC), the perirhinal cortex (PER), including the Brodmann areas 35 and 36 and the postrhinal cortex (POR). The entorhinal

cortex (EC) is further divided into medial entorhinal cortex (MEC) and lateral entorhinal (LEC) cortex. In general, the PHR contains six layers (13).

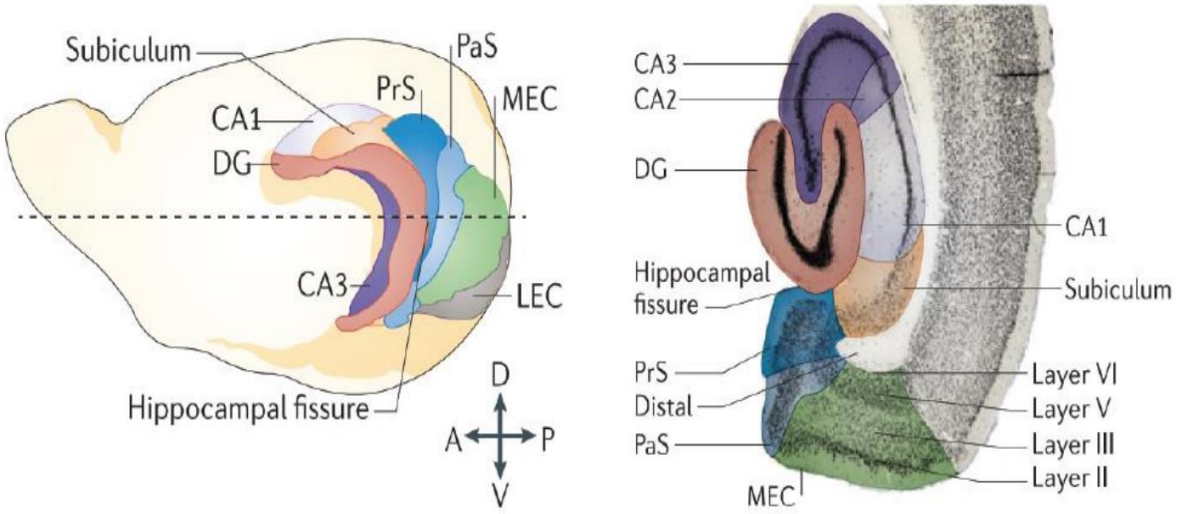

Fig. 1. Representations of the Hippocampal Formation and the Parahippocampal regions in the rat brain. Left: a mid-sagittal view. Note that the dorsoventral position of the section is shown by dashed lines through the hemisphere. Right: A Nissl-stained horizontal cross section. Various subregions in hippocampal formation and parahippocampah region are indicated by different colors. Abbreviations: A, anterior; D, dorsal; P, posterior; V, ventral; CA, cornu ammonis; DG, dentate gyrus; LEC, lateral enthorhinal cortex; MEC, medial enthorhinal cortex; PaS, parasubiculum; Prs, presubiculum. Adapted from (27).

1.1.2 Circuits Within Hippocampal Formation

Hippocampal formation (HF) consisting of three subregions called the dentate gyrus, the hippocampus proper (CA1, CA2, CA3), and the subiculum (Sub) differentiated with different layers. The connectivity in HF is formed by a unidirectional pathway from the DG to CA3 with mossy fibers and then from CA3, schaffer collaterals, project information to CA1. Interestingly, the distal part of CA3 region conveys information to proximal CA1 and on the other hand the proximal part of CA3 sends signals to distal CA1. Then information from CA1 goes to the subiculum. Distal part of subiculum receives projections from pyramidal cell layer of proximal CA1, whereas proximal part of subiculum receive signal from distal CA1. In contrast to this

projection model, there are a number of backprojections in the HF. CA3, conversely, sends projections to the hilus and molecular layer of the DG and also CA1 projects back to the same layers in CA3. Another backprojection is also occurs between subiculum and CA1 that is stratum pyramidal cells of subiculum projects back to all layers of CA1 (13).

1.1.3 Circuits Within Parahippocampal Region

A set of intra-PHR circuit is the connections between the EC, the presubiculum and the parasubiculum. The parahippocampus (PHR) area consists of five subregions including: the presubiculum (prS), the parasubiculum (paS), the entorhinal cortex (EC), the perirhinal cortex (PER), including the Brodmann areas 35 and 36 and the postrhinal cortex (POR). The entorhinal cortex (EC) is further divided into medial entorhinal cortex (MEC) and lateral entorhinal (LEC) cortex. In general, the PHR contains six layers. There is a projection pathway of PER-to-LEC and POR-to-MEC in parahippocampal area. In addition to MEC, POR also projects to LEC, however lesser information than PER. Per also sends signals to the MEC. In layers II, III, V and VI of A35 area and in A36 of the PER, neurons project to layers II and III of LEA whereas the PER output to the MEA arises largely from A36. The inputs from POR to the LEA arises mainly from layers II, III, V and VI and ends in layers II and III. The POR signals to the MEA initiates from the similar layers and terminates differently in the superficial layers, while some fibers are reported in the deep layers of the MEA. Information then from layers III and V of the LEC goes to all layers of A35 and A36 and from the MEC goes to all layers of A35. MEC and LEC both, through a reciprocal pathway, also send projections to presubiculum and the parasubiculum. There are several other connections have not been described here (13).

1.1.4 Parahippocampal- Hippocampal Circuits

Based on various circuitry models, neocortical projections are marked at the parahippocampal region (PHR), which in turn delivers the large source of input to the hippocampal formation (HF). In the PHR, two parallel projection pathways are found, the perirhinal cortex (PER) delivers signals to the lateral entorhinal cortex (LEA), and the postrhinal cortex (POR) sends input to the medial entorhinal cortex (MEA). As mentioned above, the entorhinal cortex (EC) has a reciprocal pathway with PER and the POR. Moreover, the EC receives excitatory signals from the presubiculum (PrS). The EC-to-HF connections are known as perforant pathway and EC is believed to be the source of the performant pathway, which send excitatory signals to all subregions of the hippocampal formation. Pyramidal-like cells in layer II of entorhinal cortex

projects to the dentate gyrus (DG), CA2 and CA3, whereas principal cells in layer III projects to CA1 and the subiculum (Sub) through angular boundle (13,14,15). The polysynaptic pathway, an extended version of the traditional trisynaptic pathway, describes a unidirectional pathway that links all subregions of the HF serially. In summary, the DG granule cells leads to the mossy fiber pathway, which projects to CA3 and then the CA3 Schaffer collaterals terminate to CA1 and, finally, CA1 sends signals from CA3 to the Subiculum. Then, Output from the HF ascends from CA1 and Subiculum and is directed to the PHR, in particular to the deep layers of the EC (13). (Fig. 2).

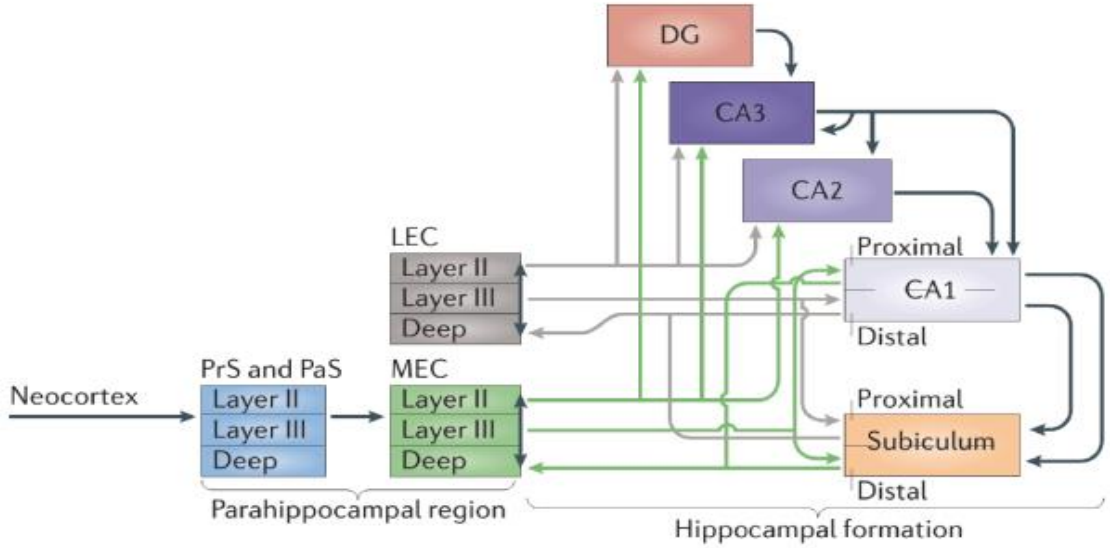

Fig. 2. The current model of the parahippocampal-hippocampal circuitry. According to this standard connectivity model, parahippocampal region (PHR) is targeted from neuocortical excitatory projections, which in turn provides the primary source of input to the hippocampal formation (HF). All enthorhinal layers are reciprocally connected. Medial enthorhinal cortex (MEC) selectively receives information from the presubiculum (PrS) and the parasubiculum (PaS). Lateral enthorhinal cortex (LEC) together with the medial enthorhinal cortex (MEC) send information to the HF, with layer II projecting to the DG, CA3 and CA2. And layer III projecting to CA1 and the subiculum. CA1 and the subiculum send projections to layer V of the enthorhinal cortex (EC). Projections from and to the MEC connect to the proximal CA1 and the distal subiculum, however pattern is opposite for projections from and to the LEC. Adapted from (27).

1.1.5 Entorhinal Cortex Anatomy

The entorhinal cortex (Brodman area 28) derives its name because it is partially enclosed by rhinal (olfactory) sulcus. The EC is superficial to the amygdala, and hereby forming the anterior part of

the parahippocampal gyrus and has two –way monosynaptic and polysynaptic signals with the amygdala, the hippocampus and the medial septum, Indeed, EC is the primary gateway by which hippocampal formation (HF) is interconnected with other areas in the brain (16,17). The entorhinal cortex is part of parahippocampal region and is further divided to the medial entorhinal cortex (MEC) and lateral entorhinal cortex (LEC) based on connectivity pattern and cytoarchitecture. As shown in Fig. 3, six layers typically observed in these two distinct areas of the entorhinal cortex which has lots of similarities in between (14,15). In general, the lamination of the EC is referred to the prototype of the transition between the three-layered allocortex and the six-layered neocortex.

The superficial layer called molecular layer (layer I), in general, consists of a dense band of transversely oriented fibers (14). The cell layer II varies considerably in appearance, but mainly contains so-called "stellate" in MEC and "Fan cells" in LEC. Fan cells are similar to stellate cell morphologically but different in electrophysiological characteristics (14,15). In overall, layer II cells are fairly large in entorhinal cortex. Another cell type found in deeper in layer II are "modified pyramidal cells" that are triangular soma shaped. Principal neurons in layer II sends excitatory signals to the angular bundle and join the main pathway of EC-to-HF by sending signals to the dentate gyrus and CA3. This pathway, as mentioned before, is called preforant pathway (14,17). Layer III is a wide layer and mostly contains large-to-medium sized pyramidal cells. A cell-sparse fiber layer called the lamina dissecans (sometimes as layer IV) is located in the deep border of layer III and is better developed in the MEC than LEC. Layers II and III also contain different interneurons, and mostly make local inhibition (17). The next cell layer (layer V) is noticeably stratified and sometimes subdivided into a superficial layer of large to medium-sized pyramidal cells, large pyramidal cells located just below the lamina dissecans. These large pyramidal cells continue their apical dendrites to the superficial layers and from there receiving inputs from presubiculum (18). On the other hand, they reach the deep layers with their basal dendrites and receiving signals from CA1 and the subiculum (14). The basal dendrites of MEC

layer V pyramidal cells also might get some inputs from retrosplenial cortex and medial prefrontal cortex (19). Principal cells in either MEC or LEC in layer V are quite similar in morphology and electrophysiological characteristics. All principal cells in layer V transfer a main axon into the white matter (20). Multiple layers can be distinguished in the deepest cell layer VI, which is delineated by the white matter. However, since the appearance of layer VI is very changing at different lateromedial and rostrocaudal levels, then no more differentiation between sublayers is

made. These multipolar cells sometimes reach angular bundle and layer v (14) and then their axons lastly project to the thalamic midline nuclei through underlying white matter (21).

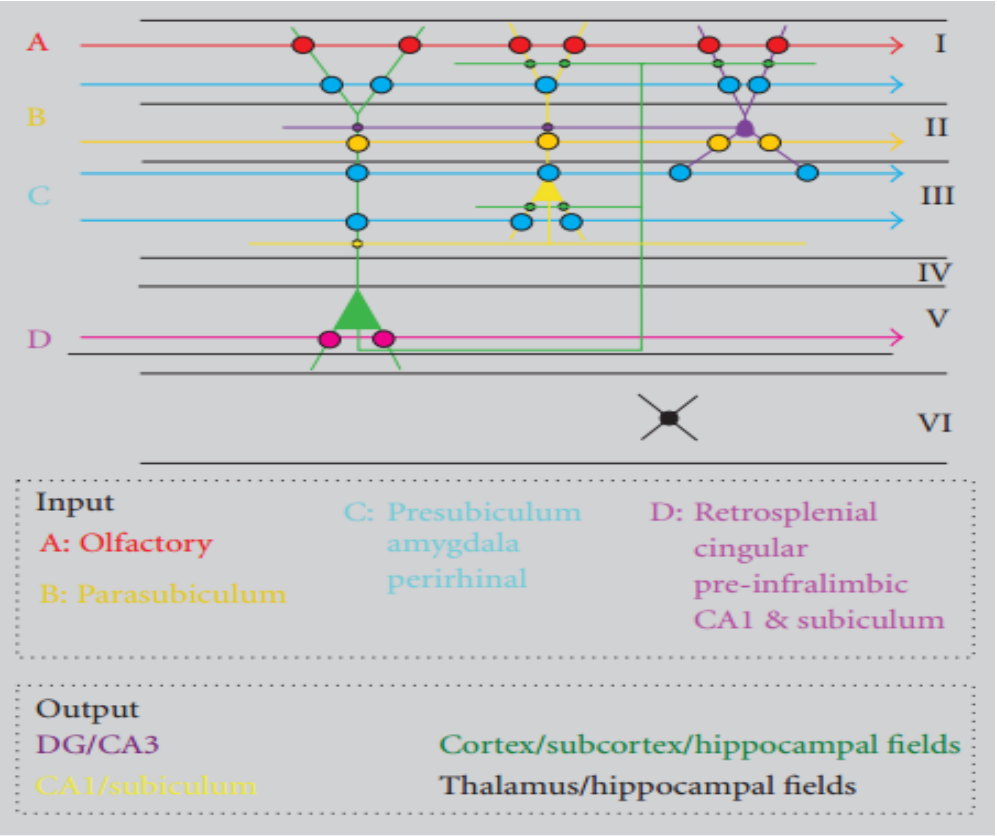

Fig. 3. Schematic representation of laminar distribution and synaptic interactions in entorhinal cortex. Color-coded arrows representing different inputs; position of the arrows specifies the main laminar distribution. Circles are synaptic contacts. Main output connectivity of principle cells is indicated as well. Adapted from (14).

1.2 Spatial Cell Types

1.2.1 Place Cells

John O'keefe and John Dostrovsky discovered many cells in the dorsal hippocampus of freely-awake moving rats that were intensely active only when the animal's head is in a particular part of its environment and, based on this, these such units called 'place cells' (22, 23). Different place cells are reported to have different firing positions, or place field. Although, the size of firing fields is larger in ventral hippocampus than dorsal part, location of animal in the environment is mapped nontopographically in the way that place fields of neighboring cells are no more similar than those

cells that are far apart (23).The combination of cells that are active in a special point of environment is unique suggesting there is a spatial map of the environment forming by these ensemble of cells in the hippocampus. Interestingly, place cells represent not only the current position of the animal but also the earlier locations that animal has faced before that shows the role of place cell in declarative memory(23,24). Edward Tolman several earlier decades proposed that behavior is guided by map-like representations in an internal cognitive phenomenon way (25). When the rat faces a new environment, new subsets of neurons are recruited in the hippocampus that shows that multiple representations in consistent with particular places are represented in the hippocampus (25). This fact that hippocampal place cells express previous experiences brings up this question whether place cells are formed by experiences or if an underlying component is at behind in the circuit. The firing pattern of place cells changes under the minor alternations of the same experimental environment like change in color or shape of environment while they are not dependent on visual cues since they thoroughly fire even during dark phase of environment (26) These findings suggest that hippocampal place cells representations are not involved in location computational metrics.so computation of metrics of spatial map remained a challenge for several decades after the discovery of place cells. So the adjacent area, entorhinal cortex, was a proper candidate for neuroscientists to look for more details in spatial map.

1.2.2 Grid Cells

Grid cells are one synapse upstream of place cells located in medial entorhinal cortex. These cells are place-selective cells that are active at multiple discrete and regularly spaced locations in the environment (27) In fact, when the animal is navigating through an environment, the grid cells show various firing pattern in response to different locations.(27,28). These firing locations provide a hexagonal pattern that covers the entire environment that is available for the animal (27). Whereas in distinct places, ensembles of place cells change unpredictably, the positional relationship between grid cells is kept, suggesting the structure of space independently of the contextual details of each single place. The rigid construction of the grid map, along with its spatial periodicity, introduces the grid cells as a part of the brain's metric for local space (27). The most obvious properties of grid cells are their hexagonal pattern of activity (Fig. 4).

However there are more properties of grid cells that distinguishes these cells than other cells. Grid cells varies in grid spacing meaning that the distances between grid fields are different. From dorsal entorhinal cortex to the ventral part there is almost a linear increase in distances between grid fields ranging from one field recurrence per 30cm to several meters (28,29). The rotation of grid axes (grid orientation) and the x–y locations of their firing vertices (grid phase) are also different (27). Grid cells show multiple degrees of asymmetry and generally the variety of grid cells defines a map of the rat's position in space. Since grid cells vary in spacing, then each point in the local environment is associated with a particular combination of active cells, enabling grid cells to get access in combined activity to read out the animal's location (27). The maps of grid cells are dynamic and get changed based on the animal movements in environment. In order to update grid activity based on ongoing movements, they get sensory inputs. These sensory inputs come from proprioceptive and kinaesthetic feedback as well as vestibular information and also optic signals. Independently of landmark identities, gird cells tend to keep their hexagonal firing pattern across environments unlike the place cells, however their phase and orientation is variable over different environment (27, 30).

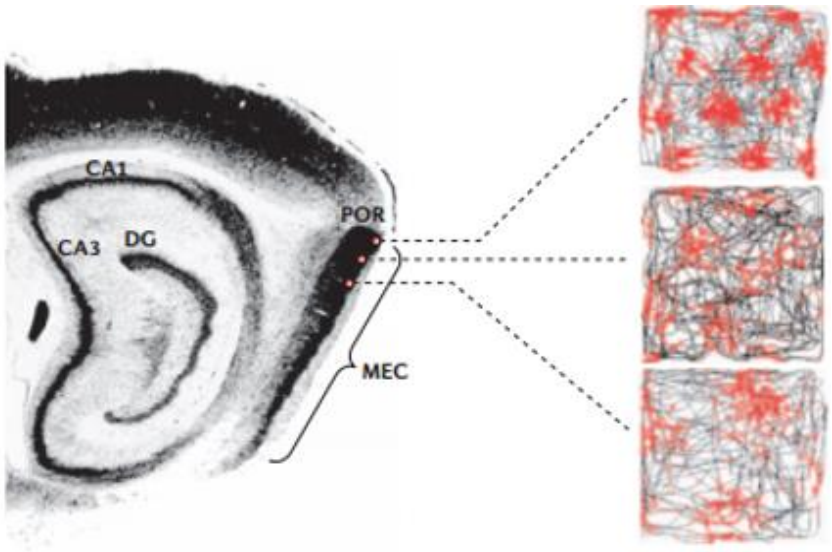

Fig. 4. Grid cells in the medial entorhinal cortex. Left; Medial enthorhinal area is shown on a sagittal section of brain. Right; squares representing the recorded grid field of one MEC neuron in layer II during

10 min running session. The spike locations are illustrated with red dots; the trajectory paths of the rat as grey lines. Note that the grid scale rises with distance from the border of the MEC with the postrhinal cortex (POR). Adapted from (6).

1.2.3 Border Cells

Less than 10% of the local cell population of those distinct cell types in parahippocampal-hippocampal network found in the Medial entorhinal cortex and the adjacent parasubiculum is called border cells (30). These cells fire when the animal is moving close to borders of the proximal environment. Irrespective of their length and connections with other borders, border cells contain firing fields that continue firing beside selected geometric borders of the proximal environment (30,31). Border cells are scattered widely in the circuit, information about obstacles and borders should be open to the majority of the entorhinal grid cells and external target areas involved in path planning (30,32). Although, the population of border cells is spars (less than 10%), their role can be still significant in spatial representations due to presence in all layers of MEC and they might play an important role in planning trajectories and anchoring grid fields and place fields to geometric reference frame (24,30).

1.2.4 Head Direction Cells

Head direction (HD) cell were found in layers III, V and VI of the MEC and consisting 26% of the cells of the entorhinal cortex (9,33). Each HD cell fires action potential maximally when the animal's head is in the preferred direction, independent of the animal's behavior, position, or trunk circumstance, in the horizontal plane. Their peak firing range varies from 5 to 115 spikes per second. Similar to grid cells, based on self-motion and sensory inputs, notably from the vestibular system, they update directional heading from moment to moment in a way called angular path integration (34). The preferred direction of HD cell's firing is continuous for about 15 minute and this is showing that the HD cells are able to keep a directional reference memory over at least this period (7).

1.2.5 Conjunctive Cells

Head-direction cells usually encounter together with grid cells. Below layer II of the MEC, grid cells sometimes co-localize with head-direction cells, that is, grid cells and head-direction cells form overlapping populations, and then following that receiving some general properties similar

to those of head-direction cells (35). The 2D distribution of gridness and directional tuning is continuous, such that some grid cells are directionally tuned and some HD cells contain grid correlates The population of grid cells with conjunctive properties differs in different layers. The largest proportion is in layers III and V, where 66% and 90% of the grid cells response to preferred direction respectively. The proportion in VI is 28% and no conjunctive cells are found in layer II yet (35). Those conjunctive cells with different gridness and directionality always react as a coherent ensemble during environmental manipulations such as the rotation of a polarizing cue card in experimental training box.

Conjunctive grid x head-directional cells may update the representation of spatial map by integrating position and direction sensory inputs when the animal navigates in the environment. They are found to be connected to place cells in the hippocampus supplying information for path integration (40).

Furthermore, there are cells found in superficial layers of MEC that in addition to a high firing rate along the borders, showed preferred directionality. These cells representing information about boundaries and head directionality while navigation in environment, These cells are called conjunctive border x head-direction cells.

1.3 The Brain Spatial Map

So far, two neural systems are identified to encode self-location in the brain: Place cells in the hippocampus that respond to particular locations in particular environments, whereas grid cells, border cells and head-direction (HD) cells, all located in MEC, in the parahippocampal area that give the animal a universal metric for mapping locations and directions in all its environments. These systems have been studied in very simple environments (24). However, natural environments are sorted, nested and quite variable in time. Recent studies show that hippocampal and entorhinal spatial maps reflect this complexity (19,24,29,35).

1.3.1 Entorhino–Hippocampal Connectivity

Sensory inputs that first process in several distinct pathways throughout a number of cortical areas, are further sent from associated areas to the entorhinal cortex, and finally entorhinal subdivisions project these information to the hippocampus (36).These inputs have been a matter of debate among scientists for years that which cell types send these inputs from entorhinal area to

hippocampal place cells forming a special map. Recent studies showed that the pathway through the medial entorhinal cortex (MEC) apparently is special for computing and sending spatial information to the hippocampus while the pathway through the lateral entorhinal cortex (LEC) is for transferring object and object/ place-related information (36). MEC layer III contains principal cells that are mostly grid cells project to CA1 and subiculum while layer II has two distinct principal cell group called calbindin-positive pyramidal cells that project sparsely to hippocampal subregions and do not project to the dentate gurus and reelin-positive stellate cells that targeting the dentate gyrus and CA3 by performant pathway (36,37,38,39). This suggests that that only reelin positive cells project via the perforant path to the hippocampus and calbindin neurons project extra-hippocampally (39). In addition to grid cells, other cell types have also prominent projections to the hippocampus such as boundary/border cells, HD cells any many other cells (around 50%) known as non-spatial cells. These projections of entorhinal cell types to the hippocampus indicate that these cell types play important role in maintaining hippocampal firing pattern (36). These findings came up by a study for identifying the cell types projecting to hippocampus based on optogenetics combined with electrophysiological recording method (39).This study confirmed that a large number of cells projecting to hippocampus were grid cells, but also border cells and HD cells and cells with irregular firing pattern (nonspatial) showed some connections indicating that place fields in the hippocampus may be generated by convergence of signals from a broad spectrum of entorhinal functional cell types (39).

1.3.2 Path Integration

Path integration is a navigational process by which processing inertial cues, proprioceptive feedback and stored motor signals, received during locomotion, allow the animal to update its position in association with its point of departure (40). This system allows the animal to find the location of the goal, for example its home, even when external cues are absent in the enclosure. However, without the use of external cues, the path integration system gives the subject an ability to reach a specific position by rapid accumulation of errors involving both the direction and distance of the goal and integrating angular and linear motion according to the contextual cues (40,41). A neurobiological study have consistently shown that a central structure for path integration whose place cells are selectively active in specific locations in space (42). These place cells, as a group, encode a representation of location in space (25) which could be used for navigational system. A long-standing question concerns how hippocampal place cells decide where to fire. Basically, place fields are landmark dependent meaning they are only associated to

one particular location in space and hereby do not provide any universal code for representation of metric in environment (43,44). Recent findings in entorhinal cortex (29,40) shed light on this issue. Lesions in MEC leads the rat to not be able to indicate the location only based on idiothetic cues. Grid cells, head-direction cells, boundary/border cells and conjunctive grid-head directional cells located in MEC can play an important role in path integration by supplying information to place cell. For instance, boundaries supply place cells with a linear distance metric, telling the place cells, in effect, how far the rat is from (some of) them (43) and the head direction cells convey directional orientation inputs and providing a sense of directionality to the path integration as well as showing the same directional tuning in different environments (9,45). A characteristics of grid cells that distinguishes grid cells from place cells is that in various environments, the distances between grid fields does not change and is stable. Furthermore, in a new environment, grid fields quickly get active and showing a hexagonal firing pattern even without any external landmark. In fact, this regular firing pattern of MEC grid cells, the independency of their spatial relationship from external influences and also their co-localization with conjunctive cells and sensitivity of all these cells to motion is sufficient for path integration (6,24,25).

In addition to all abovementioned cells activities in MEC, conjunctive grid-head directional cells put all the required information for the path integration in the local circuit by co-localization of grid and head direction cells. These conjunctive cells, with different gridness and directionality, always react as a coherent ensemble during environmental changes such as the rotation of a polarizing cue card in experimental training box. Intriguingly, hippocampal inactivation gives rise to grid field destabilization in medial entorhinal cortex (Note that hippocampal formation is connected to entorhinal cortex through by backprojections from hippocampus mainly to deep layers of MEC) (46). All in all, it seems that entorhinal cortex, in particular medial entorhinal cortex, paly an essential role in cooperation with hippocampal place cells to implement path integration.

1.4 Grid Maps Models

The initial insights into some general principles that might underlie grid network development came from a theoretical proposal by Alan Turing (47). The discovery of grid cells in MEC and indicating their unique properties at neural processing where firing properties are shaped not by

sensory signals but rather by internal self-organizing principles opened a new insight towards these unique MEC cell type. Some models have been published to explain the formation of grid organization in MEC cells. Almost in all models, Periodic firing positions are found by path integration of velocity-modulated input signals, with other sensory information give rise to only setting the early phase and orientation of the grid (49,50). However, this does not rule out this likelihood that grid network could be formed only from spatial inputs.

1.4.1 Oscillatory Interference Model

Early studies of grid cells suggested that the grid pattern is as a result of each single neuron activity (51). In this model, the firing activity of a grid cell occurs within the neuron as an interference pattern between a constant theta oscillation and other internal or external velocity-controlled theta oscillators (51,52). The frequency of these oscillators is modulated by the sudden running speed of the animal at its preferred direction. The interference of each such oscillator with the reference membrane oscillation give rises to the formation of bands of activity with similar orientation as the preferred orientation of the associated velocity-modulated oscillator (51). Then, by separation of orientations of the velocity-controlled oscillators at 60 degree, a hexagonal periodic spatial pattern can be observed (51). However this model is simple and successfully explains some of the firing properties of grid cells, the models are facing serious challenges. A major problem is that the 60 degree separation has to manually be added into the model. In addition, when it comes to test this model in experimental testing of whether the component of the model exist, studies have failed (53).

1.4.2 Attractor Network Models

A neuronal network with a self-stabilizing activity state is defined as an attractor network. In fact the models show that grid firing activities are formed in local circuits with attractor properties. Based on this type of models, hexagonally pattern of activity of grid cells occurs as a consequence of connections between recurrently connected neurons, and this neural activity moves across the connection matrix according to the animal's motions through the space (54). A significant feature of these models is that the hexagonal pattern emerges within network by itself. Early attractor models for grid cells were based on Mexican-hat connectivity. Mexican-hat connectivity is a strong excitatory interactions between cells with the same grid phases and gradually weaker interactions between cells with increasingly different phases (55,56). At this model inhibition surrounds the local excitation to prevent it from spreading. However, these models are valid when entorhinal network actually has the recurrent connectivity needed for spontaneous formation of hexagonally patterned firing fields. The main problem with the attractor network models is that

static noise in the recurrent connectivity leading to unwanted drift in the recurrent connectivity and such drift destroys the grid hexagonal pattern (54).

1.5 Optogenetics

1.5.1 Definition of Optogenetic

Optogenetics is a newly-introduced technology in the life sciences and, as the term has come to be commonly used, talks about the mixture of optical technologies and genetic methods to control, in precise, the activity of specific cell type in living tissue by manipulation of these cells (57,58). This recently developed technology has evolved so rapid and provided considerable interest in neuroscience research field. This method allows neurons to express light-sensitive genes that enable the identification, dissection, and manipulation of specific cell types and their interactions in the tissues and organs of the animal.

1.5.2 Early Efforts Toward Optical Control

A major challenge facing neuroscience is lack of a chance to precisely control a single cell type while the other cells are kept unaltered (Francis Crick 1979) (57). Later on, he suggested that light might be a relevant control tool but at that time he had no concept about how light could alter the activity of a single cell without manipulation of other cells. In earlier years, bacteriorhodopsin as a microbial single-component light-activated ion pump was found. This bright breakthrough led further studies in more understanding of bacteriorhodopsin and then led researchers to discover many more new members of this microbial opsin family such as halorhodopsins (58) and channelrhodopsins (59) that transport ions across the membrane in response to light photons (57).

Decades later, these two separate concepts came together by neuroscientists. Although microbial opsin genes were thoroughly known as a single-component light-activated regulators Of transmembrane ion conductance, there were several assumptions indicating that opsin protein is not a proper choice for activation of single cells by light. First, the presumption was that photocurrents would be highly weak and slow to control neurons efficiently. The second presumption was that microbial membrane proteins in fragile mammalian neurons would be poorly expressed or toxic, and the last most importantly presumption was that additional cofactors, such as all-*trans* retinal, would need to be added to any intact-tissue experimental system (57).

These preconceptions were all reasonable enough in arrear several more years for optogenetics advent.

1.5.3 An Optimal Optogenetic Design

An optimal optogenetic design consists of several steps (58). First, suitable optogenetic tools (opsin proteins) are required to alter neuronal activities. These opsin proteins that are light-activated, allow various interventions in neuronal activities for specific purposes. Examples of these proteins are the original microbial opsins, ChRs, that are applied for neuronal excitation and called excitatory optogenetic tools, while halorhodopsins (NpHR) and bacteriorhodopsin (BR) are inhibitory optogenetic tools. As mentioned above, these proteins are not efficient to activate a single neuron by light. So, In order to optimize these optogenetic tools, Researchers, in recent years, combined the light-activated opsins and G protein-coupled receptors with engineering approaches and found that this is efficient enough to control neuronal activity. Second, optogenetic tools (opsin proteins) can be delivered to targeted neuronal system by definite vectors. Viral delivering is the most widely used method which is fast targeting and constant load. Amongst studied viruses, adeno-associated virus (AAV) and lentivirus are the most widely used viruses for delivering optogenetic tools to neuronal cells (58). Third, light acts as the operator of neuronal activity. Since different opsin proteins are activated in different light specific wavelengths, the delivery of light determines either the excitation or inhibition of neurons. For example, halorhodopsin (HR) absorption maximum is at ~580 nm, while channelrhodopsin-2 (Chr2) is not responsive at that wavelength. Finally, a readout system with high resolution is fundamentally essential to study and analyzing the collected data.

1.5.4 Opsin Proteins

Rhodopsin, the visual pigment in retinal photoreceptor cells, contains a seven transmembrane alpha helix protein part called opsin that does not absorb light by itself. The light-absorbing component, retinal, that is a vitamin A derivative, is a small molecule whose 11-cis isomer is bound to a lysine residue of opsin (Fig. 5).

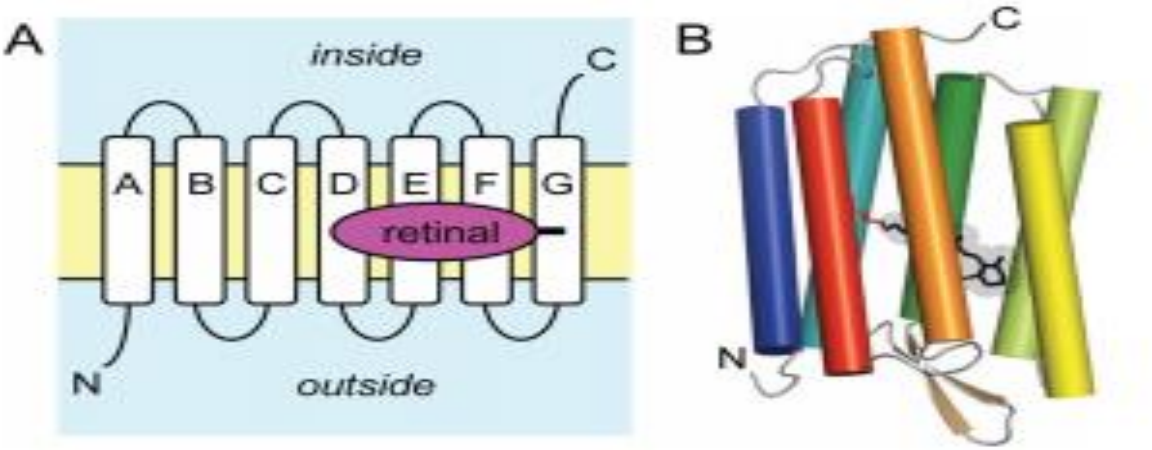

Fig. 5. Schematic form of the retinal proteins. (A) These membrane proteins consist of seven α-helices (helix A to G in microbial opsins and TM1 to 7 in the animal opsins) with a leg on each side of the lipid bilayer. The N-terminus faces the outside of the cell and the C terminus the inside. Retinal in microbial opsins and animal opsins is covalently attached to a lysine side chain on helix G or TM7, respectively. (B) Schematic representation of the helical arrangement of a microbial rhodopsin with attached all-transretinal. Adapted (27).

A photon absorption causes retinal to flip from the 11-cis to all-trans configuration. When retinal isomerizes, this contributes to a configuration in rhodopsin leading the ion channels open and the activity of the single neuron either increases (depolarization) or decreases (hyperpolarization) based on the type of transferred ionic current. Opsin genes contain two distinct superfamilies. The first one is called microbial opsins (type I) present in prokaryotes, algae, and fungi that is involved in phototaxis, retinal synthesis and energy storage and the second one is animal opsins (type II) that are found in higher eukaryotes and are mainly involved in vision (61). Based on some differences between these two types of opsins (61), only microbial opsins (type I) are used in optogenetic purposes and animal opsins type II) are applied in biochemical modulations in cells (61). Initially, all approaches to achieve optical control by microbial opsin genes, had serious limitations in meeting this goal due to inadequate control capability, toxicity and challenges about light delivery (57). The key properties of microbial optogenetic tools is routed in the ecology of their original host organisms which response to the environment by seven-transmembrane proteins of opsin (type I) gene (57). Microbial opsin (type I) further discussed in following based on their original host organism. The first type I protein is haloarchaeal proton pump bacteriorhodopsin (BR) that expresses in low-oxygen conditions and is involved in energy-production system. These light-gated proton pumps have also been indicated in marine proteobacteria to do similar photocycles (62,63).A second type of microbial opsin genes is involved in halorhodopsins (HR). Halorhodopsin is a light-activated chloride pump found in archaebacteria (64) transporting

chloride ions from extracellular to the intracellular space of the cell. Then in optogenetics, these pumps can be used for inhibiting neurons by further chloride influx inside the neuron and followed by hyperpolarization of the cell (65). Another type of the single-component microbial transmembrane ion conductance protein is channelrhodopsins (ChR). These proetins discovered in the green algae *Chlamydomonas reinhardtii* and containing light-activation ion-flux properties that conduct H+, Na+, K+ ions down to their electrochemical gradient and are using for exciting neuronal activity by illumination in optogenetic applications (66). These all single-component optogenetic tools are now available to neuroscientists to apply fast excitation, fast inhibition, bistable modulation and control of intracellular biochemical signaling in neurons and other cell types. In the following part, chanelrhodopsin (ChR) as a main optogenetic tool for excitation of single neurons involved in my project has been further discussed.

1.5.5 Channelrhodopsins as Light-Gated Cation Channels

As mentioned before, Chanelrhodopsins are single-component microbial with 7-transmembrane proteins conducting cation flow across the membrane of neuron as a result of illumination. Ionic conduction by ChRs can be fast, repetitively, reproducibly, and non-invasively (67) (Fig. 5). ChRs have a similar homology to bacteriorhodopsin (BR) in residues associated with their retinal-binding pocket and proton-conducting system. ChRs is highly homologous to BR in structure of retinal-binding pocket, containing an effective water-filled cation channel pore that makes their proton conductance activity to be independent of retinal isomerization which implies that ion flux depends on the kinetics of channel closure (57,68). Over last years, up to thirteen ChR sequences have been found in other green algae that are distinct from each other based on their cation selectivity, kinetics, light wavelength sensitivity, and light intensity sensitivity (67). The first detected chanelrhodopsins (ChRs), named chanelrhodopsin 1 (ChR1) (68) and chanelrhodopsin 2 (ChR2) (69). These both channels naturally were identified in unicellular algaes called *Chlamydomonas reinhardtii.* IN case of ionic conduction, *ChRs* both transport cations including Na^+, K^+, and also Ca^{2+} ions. However, ChR2 conducts Na+ and K+ ions two times more than other protons, (70) and both exhibiting fast *On* and *Off* kinetics (71). Upon illumination in optogenetic, ChRs rapidly increase their cations conductance, and give rise to a depolarization of the cell membrane in milliseconds. Such a property has made ChRs a proper candidate for optogenetic to change the membrane potential of the targeted neuron. Optogenetic activation precisely has focused on the opsin-expressing neurons in particular chanelrhodopsin properties (60).

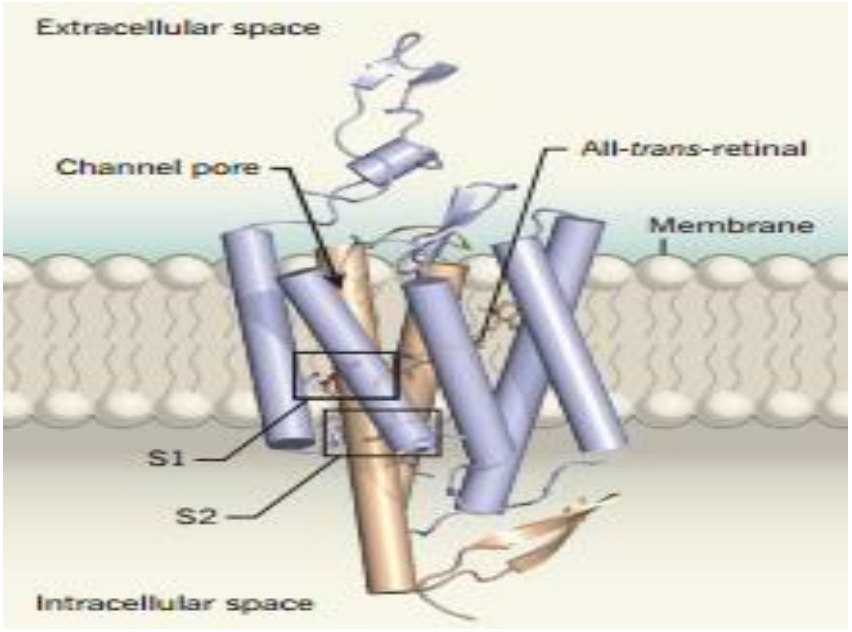

Fig. 6. Structure of a closed light-gated cation channel. Channelrhodopsins (ChRs) are proteins structures present in microbial cell membranes including seven transmembrane helices (shown as cylinders) and open in response to light, allowing cations influx through the cellular membrane. The light sensitivity of these channels is due to a molecule, all-trans-retinal, that is covalently attached to the protein. The X-ray crystal structure of a chimaeric ChR constructed from two other ChRs, ChR1 and ChR2; the purple cylinders of the protein are from ChR1 and the brown parts are from ChR2. A negatively charged pore places between helices 1, 2, 3 and 7 and is interrupted by two trios of amino acids, which form gates S1 and S2. light-induced isomerization of the retinal give rises to opening gates, and, in turn, extending the pore to the cytoplasm. Adapted from (60).

1.5.6 Delivering Optogenetic Tools into Neuronal System

Optogenetics essentially relies on light-delivery technology, In vitro, experiment optogenetic tools are usually stimulated with filtered light from mercury arc lamps (72,73,74), lasers (75,76,77), light-emitting diodes (LEDs) (78,79), or LED arrays for multiple sites stimulation (80). However, In vivo, stimulation of freely moving animals has been convoyed with laser light to the transduced tissue by optical fibers that is inserted through implanted cannulas (81,82, 83) or with fiber-coupled high-power LEDs (84).To achieve these goals in vivo, various strategies is needed including: viral promotor targeting, transgenic animal targeting, projection targeting.

1.5.7 Viral Gene Delivery

Opsin genes can be transfected to targeted neuronal cells by specific vectors. The most widely used vectors are viruses due to their fast targeting and constant long-term expression and high infectivity. Among the different viral vector systems developed so far, adeno-associated virus

(AAV) and lentivirus are the most used viruses for delivering optogenetic tools to neuronal cells (58). Thanks to the fact that AAV vectors do not integrate into the genome of the targeted neuron, whereas lentivirus vector does, AAV vectors are more common used vectors to delivery opsin gens in order to avoiding the host genome disruptions (85). Although, these two methods are the most common used ways to deliver opsin genes into the targeted neuronal cells, only short promoter fragments can be transfected and this is because of AAV and lentiviruses limited genomic packaging capacity of ~5 kb and ~8 kb, respectively (86,87). A larger carrying capacity including adenoviral or herpes simplex-based (HSV) vectors are other optional viral systems, however, HSV is of some shortcomings including higher toxicity as well as inconsistency between experiments (*88*). Therefore, an increasing interest in AAV vectors, in comparison with other viral vector systems such as the retrolentiviral and adenoviral vectors, can be justified by their unique features. Up to now, 11 AAV serotypes with different intrinsic properties have been identified (89). There is a high sequence homology among these diverse serotypes, however, the greatest difference lies in their capsid proteins (90,91,92) that making them different in both tropism and serological neutralization (93). Due to a tremendous amount of study on understanding the biology of AAV2, therefore, it has been the most widely used serotype and among all naturally discovered serotypes it is the best characterized one. In case of opsin delivery, the most common used AAV serotype is recombinant adeno-associated virus (AAV) type 2 (rAAV) vectors. These vectors have been recently demonstrated to have a great utility in gene transduction both in vitro and in vivo (88). There are several diverse serotypes of AAV2 that is pseudotyped with viral capsids from serotypes 1, 2, and 5 (rAAV2/1, rAAV2/2, and rAAV2/5, respectively). Indeed, the extent of viral spread in CNS differentiates these all serotypes from one another (94). For instance, when these serotypes are injected into a rat hippocampus region, rAAV2/1 and rAAV2/5 diffuse more deeply and targeting CA1-CA3 areas, however, rAAV2/2 and lentivirus are more restricted in dentate gyrus and subfields of CA1 region respectively (*94*). Then these various serotypes seem to only expand targeting strategies.

1.5.8 Cell Type Specific Expression of Opsins

Opsins can be selectively presented into specific neurons based on their molecular signature, projection pattern, anatomical organization, and functional activity (95). Then, Various cell types can be targeted to express opsins by using their genomic promoters. To limit the expression of opsins to specific neuronal population, it can be relied on promoter sequences, which are often huge and owing to limited packaging capacity of viruses, only a short fraction of these promoters can be transferred by viral system (96). However, depending on the genomic structure, some

promoters are small enough to be packed into viral vectors so that specific cell types can be used to target across animal models. Those cell types with too-large promoters can be targeted by using transgenic technologies that are limited to mice and rats (95). Thus, transgenic animal, employing the entire promoter sequence elements, can achieve high specificity.

1.5.9 Transgenic Approaches

By transgenic animals, neuroscientists are now able to access and manipulate many cell types in mammalian brain in order to study synaptic and circuitry connectivity function, and dysfunction. In comparison with mice, rats are a superior model for behavioral studies involving training paradigms for goal-directed tasks (97). Thus, it is expected that efforts directed at developing transgenic rat lines with expression of engineered opsins will significantly simplify advances in behavioral neuroscience and then represent a welcome addition to viral gene delivery methods for achieving functional opsin expression in rats. The first transgenic animal line was transgenic mice expressing ChR2 under Thy-1 promoter and the first ChR2 transgenic rat lines were also developed by using the Thy1.2 plasmid (97, 98). Expression of ChR2 was discovered in neocortical layer 5 projection neurons and some subcortical structures (98). For promoters that are larger than packaging maximum of viral vectors, transgenic animal lines can be a great strategy to express optogenetic constructs in a cell-type-specific approach. Transgenic constructs can be presented into transgenic animal either through bacterial artificial chromosomes or using recombinant cell-type-specific promoters (95).

A major challenge with producing transgenic animals expressing microbial opsins is an inability of some cell-type-specific promoters in driving strong expression of the downstream gene. Due to this fact that many of the opsins possess low conductance or pumping powers (88), high expression rates of opsin are needed to achieve a consistent neural activation or silencing. To amplify the expression rate of opsin, AAV vectors that carry double-floxed inverse open reading frame (DIO) of microbial opsin genes (DIO AAV vectors), can be conveyed to the transgenic animals brain expressing Cre recombinase under the control of cell-type-specific promoters. Cre recombinase will identify the double-floxed opsin construct and facilitate transgene expression after recombination (99,100). Here the DIO AAV system enables the interested gene to be expressed using ubiquitous promoters, while deriving cell-type specificity from Cre recombinase expression.

A wider group of available cell type specificities can be obtained because here promoter size is not limited by the genetic capacity of virus. Thus, Virus load itself is constructed by doublefloxed inverted ORF (DIO) strategy where opsin gene is sited in inverted orientation and flanked on both

sides by two Cre recombinase sequences. When such virus enters a cell expressing Cre recombinase, ORF is inverted and in turn expression of opsin gene begins. The accessibility of abundant Cre transgenic animal lines from these groups as Allen Brain Institute for Brain Science, Jackson Laboratory, Gene Expression Nervous System Atlas (GENSAT), offers a convenient solution for targeting a wide range of cell types in the brain.

As a result, Compared with viral delivery, one disadvantage with this strategy is the amount of time needed to generate and breed transgenic animal lines. Besides, due to the untargeted nature of the transgene insertion, each transgenic animal line must be carefully characterized to prevent the animal from an undesirable gene interruption.

1.5.10 Light Illumination and Electrophysiology Recordings

The advent of fine electrode recordings in 1940s, shifted our focus to the study of the neuronal activities and in turn allowed neural recordings to be analyzed at the level of neuronal assembly, as well as the single-neuron level (101). Over time, this method has given rise to the development of a variety of electrode arrays and electronic devices for these purposes. Nowadays, chronically implanted electrode arrays are used because they allow stable recordings of single neuron of interest and/or field potentials from up to hundreds of electrodes over long time period 'Microdrive recording technology' and 'Versadrives' devices are both designed for tetrode recordings from either single neuron or neural network activity. Indeed, the use of these recording techniques coupled to multiple tetrodes allow investigators to obtain neural signals and electrical activity of single neurons recorded intracellularly in small mammalians brain for up to two months after implantation (102). The application of tetrodes, at these electrophysiological recordings, has some major benefits for unit identification purposes and allows the high accuracy acquisition and discrimination of multiple single-units (103). Tetrodes allow signals from putative individual neurons to be triangulated between a number of recording points for improved unit discrimination.

The microdrive device contains 4 tetrodes and each individual tetrode has 4 insulated electrodes twisted together in which each wire has a diameter of 12.5 μm (102,104) (Fig. 7). This system runs eight recording channels, but the design can be modified to provide additional channels (105).

Microdrive and headstage recording system utilizes printed circuit boards and light, flexible cables to enable the animal free movement for behavioral testing. There are several advantages in using this recording system including: reduced weight and size of assembly that is approximately 1.5-

2.0 g and also simplified microdrive that is a set screw pushing a piston-like holder that protects the top of the cannulae covering electrodes. Each full rotation of the screw pushes down the electrodes by 0.2 mm (200 µm). The screw turner slots also allow quarter-turns to be made quite easily, which result in 0.05 mm (50 µm) electrode movement (106). Moreover, recordings from several brain regions at various depths can be simultaneously possible because every tetrode can be positioned independently. Last but not least, use of small guide tubes (0.3 mm) in microdrive device reducing the possibility of tissue damage and the smaller recording probes (0.01–0.02 mm) record smaller cells and lower amplitude signals (107).

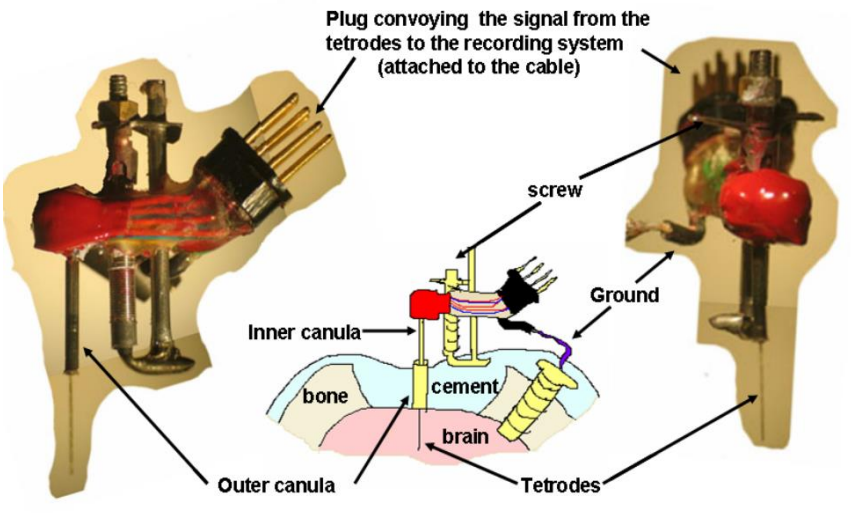

Fig. 7. The structure of a Microdrive device. The tetrodes are slid into an inner cannula of a microdrive. One tetrode consists of 4 insulated electrodes twisted together and each microdrive contains 4 tetrodes.

Another electrophysiological device that are versatile and new designs used in neuronal recording for small animals are Versadrive technology (Fig. 8). These devices are aimed for tetrode recordings from either an individual brain structure or from two or more structures that are in one line extending from the skull surface into the depth of the brain. However, there are more complex models of versadrive in which tetrodes are arranged in a way to target brain structures whose locations are not co-linear. Different numbers of tetrodes are available for this design. For instance, there are versadrives with 4 or 8 tetrodes that are moveable independent of one another. At this model, each drive contains a shuttle, a guide tube, 2 drive pins, a drive screw and a tetrode and as mentioned above each drive is independently moveable. One complete turn of this screw pushes the movable drives down by 0.25 mm (250 µm) by consideration of the maximum practical

travel of the moveable drives from initial to bottom-most location that is 4.0 mm (4000 µm).In general, versadrives weigh approximately 3.2 g and can easily be carried by small animals (104).

Fig. 8. An example of a VersaDrive 8 Optical with and without the optical cable. 8 tetrodes including 32 wires go down to the brain areas from the external place located down the drive.

At the end, although, by these tetrode devices, long-term multichannel single-unit recordings in several cortical and subcortical regions have been greatly achieved in various animal species such as birds, rats, and primates, long-lasting electrode implantation in even more brain areas while recording from larger mass of neurons is an aim that could be attained in the near future (108).

2. MATERIALS AND METHODS

Note:

The virus preparation procedure such as AAV plasmid construction, surgery, serotyping and virus transfection was all performed by Sheng-Jia Zhang. The process of histology was mostly performed by Jing ye and Juan Wu and perfusion procedure was performed by the help of Ignas Cerniauskas.

2.1 Animals

At this experiment, recordings of neuronal activities in medial entorhinal cortex was conducted on 5 male Long-Evans rats (Approximately 2-3 months old, 350-550 g at surgery time). Each rat was housed in a transparent plexiglass cages (45 × 30 × 35 cm) in a vivarium which had a controlled temperature and humidity. The animal living room was approximately 10 m far from the recording room. Prior to any experimental process, the rats were allowed to familiarize to their housing, which comprised of single-unit (one-rat) cages kept in a temperature-controlled laminar airflow unit. Rats were handled for at least five days prior to experimental training to allow for familiarization with the experimenter. In between recordings, rats were kept in their housing in living room and maintained in a reverse 12:12 light-dark cycle. Recordings were carried out between the hours of 09:00 and 19:00, in the dark phase. All the rats were kept at 85-90% free-feeding body weight but water was available ad libitum. The animals were food deprived almost 18-24 h before training or recording session. All experiments were conducted in accordance with Norwegian Animal Welfare Act and the European Convention for animals' protections used for experimental and other scientific purposes. Forsøksdyrutvalget regulations. (**http://www.mattilsynet.no/fdu/**).

2.2 Surgical procedure

Before tetrode implantation, for anaesthesia, isoflurane (Abbot Laboratories, UK) via a gas anaesthesia system (Medical Supply Services, UK) with an average flow rate of 1.0 ± 0.2 liter per minute was used. Isoflurane was persistently administered throughout the process. For the surgical procedure, rats were located in a stereotaxic tool (Kopf Instruments, US). rAAV2/1 (1.0×10^{12} viral genomic particles/ml) was injected in the left MEC with the injection volumes of

0.5-1 µl for three rats with indication numbers of 19081-19082 and 19083. The same viral vector was injected into the right MEC of two rats (rats number 18851 and 18916) with the same volumes of 0.5-1 µl. Then for electrode implantation the skull was exposed and a small burr-hole was drilled over the anticipated site (ideally for medial entorhinal area: 0.1-0.5 mm in front of the transverse sinus, 4.5-4.7 mm lateral to the midline, 1.6-1.8 mm below dura, and oriented at an 8-20 degree angle in the anterior direction in the sagittal plane). The electrodes were implanted in both right (rats numbers 19081-19082-1903) and left hemisphere (rats number 18581 and 18916). Five bone-screws were made around the exposed skull to stabilize the microdrive on the animal's head, with one screw acting as a ground tetrode bundle containing four tetrodes cut flat at the same level. Optical fiber tip was placed 500 µm above the tetrode tips in MEC; what is more, 26G cannula was implanted adjacent to the optrode in MEC for drug infusion. The tetrodes were made of 17 µm polyimide- coated platinum-iridium (9:1) wire with platinum-plated electrode tips.

2.3 Electrodes and Electrophysiological Devices

Electrodes used for recording neuronal signals included either 8 tetrode bundles (32 channel versadrive) or 4 tetrode bundles (16 channel Microdrive) consisting of 4 entwined platinum-iridium wires (90% platinum, 10% iridium; HM-L insulated, 25 µm bare wire diameter, California Fine Wire Ltd., USA). Each tetrode bundle was cut at the same level to make all wires to have similar length. Tetrode wires in turn were mounted onto small drivable microdrive (Axona Ltd., UK) and versadrive (Axona Ltd., UK) in preparation for implantation.

At the end, microdrives and versadrives was put in place over the intended implantation location, and the electrodes were carefully lowered to the required depth into the previously made hole. We used microdrives device for three rats with indication numbers of 18916-19081-19082 and Versadrive device was used for two rats with indication numbers of 18581 and 19083.

2.4 Training session

For both recovery and getting adapted to the new environment after the surgical procedure, the rats had a rest of approximately 10 to 14 days before training began. Then each animal was trained to run in a 1 x 1 x 0.5 m square box two times per day. The training box was electrically grounded to avoid signal noise and containing black walls and black floor with a surrounding

curtain to make it dark during recording. To polarizing the box, a white cue card (21 x 30 cm) was on one of the box's walls. During 10 minutes training, animals were motivated to run and cover the whole square enclosure by throwing in crumbs of crushed chocolate cereal towards random locations within the area in almost each 20 seconds, and the rats were able to freely move around to obtain the crushed chocolates. This encourages the animals to remain in continuous locomotion and sufficiently sample the entire square enclosure and then, following by, getting the best possible running coverage of the enclosure. This process of training was kept for about 10 days until the running coverage was acceptable. The floor mat was washed by water in between successive sessions. Before and between the recording sessions, the animal rested on a towel in the flower pot on the pedestal located nearby the recording enclosure.

2.5 Experimental Recordings Session

During this experiment, two types of data collecting sessions was carried out : a 2 minutes session, on a towel in an almost large flower pot on a pedestal, or 10-15 min running session in the aforementioned square-black box. while moving freely in the pot, the rat was connected to the recording system ("dacqUSB Recording System"; Axona, UK) via the attached head stage amplifier on animal's head. In fact, the cables connecting to the animals head were weight-counterbalanced allowing easily animal's movement either in the pot or inside the box. The tetrodes were lowered in 50 μm steps (never more than 100 μm per day) until single cells could be extracted from recording sessions. When the experimental procedures showed no recognizable changes in the firing pattern of the cells, then it was the time to lowering in the tetrodes further 50 μm in the same way until the new cells got discovered from recordings of the animal's neuronal activities while navigation in the environment. Then, recorded signals were amplified between 8,000x and 20,000x and filtered between 380 Hz and 6 kHz to allow for single-unit detection. For separation of signals from noises, only signals that exceeded a pre-defined user threshold (at least three times the noise level) were recorded by the system. To provide a baseline for noise 10 level, each channel was referenced to another channel whose background noise was similar and contained no neuronal activity.

2.6 Analysis Software , Spike Sorting , Cell Classification

Recorded neuronal activities was then transferred to a graphical cluster-cutting software TINT® (Tetrode Interface (Tint), Axona, UK). Clustering was carried out manually in two-dimensional projections of the multidimensional parameter space including waveform amplitude and waveform energies, using autocorrelations functions as additional tools to separate waveforms were separated and evaluated by using specific spike characteristics for instance amplitude, duration, maximum and minimum spike voltage, the time of occurrence of maximum and minimum spike voltages, and the voltage at a specific time point. By using cluster-cutting software, spike sorting was carried out based on abovementioned characteristics. This program yields scatterplots by pairwise evaluations of the 4 electrodes of a single tetrode. The clustering of the scatterplots was done by hand drawn polygons using two of the parameters the software suggests: peak-through amplitude and voltage at time t.

To ensure that recorded cells were not included in more than one data set, then cells were compared with successive sessions in next day. However, if two cells with same clusters in one tetrode contained indistinguishable firing fields on two successive recording session, we only chose one of them (the cells that contained better coverage and better signal-to-noise ratio) for further analysis.

Please note that in order to get rate maps the rat's location was tracked by an overhead video camera which recorded the position of two head stage LEDs (approximately 5 cm separated from each other).

2.7 Criteria for Data Inclusion

A cell to be included in the data analysis, needed to have either more than 50 spikes during the 10 minute training session recording period or having low or an absence of firing activity before the 2ms (refractory period) of the -10/10ms autocorrelogram. Some neurons were discarded based upon these criteria that suggested that the signal was noise instead of being a cellular unit. These criteria contained a waveform that showed oscillations at its tail and very few total correlations in the -10/10 autocorrelogram.

2.8 Laser Stimulation Sessions

When animal was moving freely on the towel in flower pot, laser stimulation procedure was carried out in order to identify ChR2 expressing cells. In order to couple laser setup to the optical cannula on the animal's head, an optical fiber was used to arrange for light delivery while the rat was moving around on the towel in the flower pot. For the 2 minute stimulation at with frequency of 1 Hz, Laser light of 473 nm (473 nm Blue DPSS laser (T3); Shanghai Laser & Optics Century, P. R. China) was used. The light pulses were 3.5ms long lasting with power of light delivering, at the tip of fiber, at around 20mW. If any cell were detected in the recorded data during 2 min training in the pot, both right and left MEC neurons would receive a 2 min laser stimulation before the rat was decoupled from the laser setup and put into the square box to run for 10 min to provide data to identify different spatial cell types. If in any case, a responsive cell was detected, some laser tests were performed. First a normal session of 2 min 1Hz with laser power of 25mW, then sessions contain a laser power of 5mW, 10mW, 15mW and 20mW all for 2 min with a pulse frequency of 1 Hz. After all, a 2 min session of 5 Hz and then a 20Hz stimulation session lasting for 30 seconds with the light pulses of every 5 seconds was done.

2.9 Perfusion Procedure

After hundreds μm of further lowering the tetrode in and finding no more new neuronal signals, the experimental protocol was stopped meaning experimental recordings were done. Food limitation regime for the animals was also stopped and food was presented ad libitum. Tetrodes position remained at the same place till the perfusion was done. To obtain the proper amount of pentobarbital, animals' weight was measured before perfusion work. Then the rat was placed in a transparent gas chamber (16 cm x 20 cm x 20 cm) with a paper towel with a few drops of 100% isoflurane at the bottom of the anaesthegia transparent gas chamber. This procedure drove the animal unconscious after few minutes and then an overdose of 100 mg/ml pentobarbital solution (3ml for a 600g rat) was injected intraperitoneally in the abdominal area with a 25G needle (Sterican®; Braun Melsungen, Germany). A toe pinch reflexes test was done to check if the animal is truly unconscious. If no signs of senses were detected during pinch reflexes test, the animal was set on the perfusion bath while its limbs are taped preventing possible movements of animal during surgery. To access the animal's heart, its chest area got opened and a 21G needle with running 0.9% saline solution was injected into the left ventricle of heart while still beating. The heart was still beating at the time, and to lead the blood out of the

body, in special the brain, and obtain the animal's brain free of blood, a small cut was made in the right atrium of the heart. The saline solution was running for about 15-20 min until the whole blood was washed out, and then the saline was replaced with formaldehyde 4 % solution (pH 7.4) for about 10-15 min. Formaldehyde makes the brain tissue to be fixed. After another 15-20 min the rat's head cut off and soaked in a glass of 4% formaldehyde solution for about 1 hour. At last the tetrodes all were turned all the way back up and the brain tissue was carefully removed from the caudal part of the skull by removing the skull bones. The removed brain tissue was kept in a glass of 4 % formaldehyde solution for few days to be prepared for histology and immunohistochemistry session analysis.

2.10 Immunohistochemistry

Before transferring the brain tissue to the slicing part, the brain tissue , which was already washed out by saline were stored in the formaldehyde 4% glass in the refrigerator for about 2-4 days. The brain tissues were fixed onto the microtome holder by mounting medium (Neg -50; Richard-Allan Scientific, USA) and enclosed by pulverised dry ice (101 Cold Spray; Taerosol, Finland). They were kept for 20-30 min at temperature of -21°C and then cut (Microm HM505E; Midwest Lab Equipment, USA) in 30 μm sections in the sagittal plane. During slicing, 6-well plate of sections containing 1 × PBS solution were collected and every seventh section was laid on "gelatin" glass slides (Polysine™; Gerhard Menzel, Germany) (1% gelatin was added to each glass slide manually). Sections on glass slides collected for Nissl (Cresyl violet) staining part. Sections were put in dH2O for 2 minute and then dehydrated by rinsing (10 times dipping up and down) in ethanol respectively with different concentrations of 70%, 80%, 90% and at last 3 times in 100% ethanol. After the putting the brain slices in a container of xylene 100% for 2 minute, they were put in rehydration stage. In rehydration part they soaked three times in athanol 100%, and following by athanol with concentrations of 90 %, 80%, and 70% one time per each respectively. Then they spent 5 minute in a fixing solution (70% ethanol, 0,,005% acetic acid). Sliced tissues were bathed in water and then stained in Cresyl violet solution (0.001% Cresyl violet in dH_2O) on the shaker for 5 minute. At this stage, there might be additional color which would be washed away by water and dipping tissues in the fixing solution. Another dehydration stage mentioned above was carried out (70%, 80%, 90%, 3 × 100% ethanol) and tissues soaked for at least 10 min in xylene once again. By MIRAX MIDI software (Carl Zeiss, Germany), Scanning and measurements were followed. 6-well plate sections were used for immunostaining part. At the first, tissues experienced 3 times 1% Triton X-100 solution

(in 1 × PBS) for 10 min to be washed. When the washing section was truly done, sections were kept in blocking buffer (0.1% Triton X-100, 1% BSA, 5% NGS in 1 × PBS) on a shaker at 4°C during night. 2µl rabbit polyclonal FLAG (1mg/ml), as the primary antibody, was added to 2 ml dilution buffer (0.1 Triton X-100, 1% BSA, 1% NGS in 1 x PBS). Reactions of the antibodies with 2 ml dilution buffer (1mg/ml) and 10 µl mouse monoclonal NeuN antibody (1mg/ml) were carried out and then the FLAG antibody was used to recognize the position of neurons expressing ChR2, whereas NeuN, as a background stain, reacts with most neuronal cell types. Reactions continued for approximately between 2 to 3 days on the shaker at 4°C. When the reactions were done, sections were washed twice for 15 min each and twice for 30 min each in PBST (0.1% Tween-20 in 1 × PBS). The secondary antibodies also reacted with 2 ml dilution buffer and 4 µl goat anti-rabbit antibody with Cy3 cyanine dye and 4 µl goat anti-mouse antibody with Alexa Fluor® 488 dye. Cy3 dye is of an emission maximum light at 570 nm showing red color in staining sections and its antibody binds to rabbit polyclonal FLAG primary antibody. Alexa Fluor® 488 dye is of an emission maximum light at 519 nm and shows a green color to staining sections and its antibody binds to NeuN antibody. Secondary antibodies reactions were executed on a shaker at room temperature of about 24 °C for approximately 2 h. After washing the tissues again with PBST (2 x 15 min, 2 x 30 min), they were fixed on a glass slides covered by gelatin and letting them to be dried during night. Then tissues stored for 5 min in 0.002 mg/ml Hoechst stain at about 24 °C (room temperature), and then washed 2 × 30 s in 1 × PBS and then kept for 1 min in dH_2O. The Purpose of using Hoechst was only to getdigital pictures with higher qualities.

3. RESULTS

'' it is not the finding that make science, science, it is the method, as stodgy and grumpy as it may seem, that is far more important than the findings of science. '' – Carl Sagan

To isolate, characterize as well as analysis of the cells that recorded during experiments period, much of the work, skills, and time was required for extracellular, single-unit recordings in vivo. To ensure that the research is precise, based on a set of experiment-specific criteria, the experimenter must be able to sufficiently, discriminate, classify, and evaluate recorded data. Based on this, the following sections show analysis of specific cell types in medial enthorhinal cortex area (MEC) further in depth. Each case demonstrates analysis of sample cells including grid cells, head direction cells, border cells, conjunctive grid-head direction cells, conjunctive border-head direction cells, unknown principal cells and interneurons.

3.1 Electrophysiological Recordings *in Vivo*

Recorded data from tetrode-optical fiber implanted in MEC of 5 male Long Evans rats transferred to the cluster cutting software TINT (Axona) for electrophysiological recordings of nuronal activities in MEC. The reason by using tetrodes instead of single electrodes (stereotrode) is that tetrodes enable to access isolated action potential of a single neurons from the surrounding action potentials in a neuronal essambly. The amplitude of the received signal is plotted against one another in each channel and a neuronal's signal can be isolated based upon distinct clusters formed by a consistent differential of the waveform's amplitude. This amplitude of the recorded neuronal signal and followed by discrete waveform results from a functional distance between the single neuron and the implanted electrode. Then, by electrode-pair scatterplots generated by the software, these recorded action potentials plotted in two dimensions in each channel due to their distance to two discrete electrodes that represent 6 distinct plots for different electrode pairs in the tetrode. Clustering of single units carried out manually by hand drawn polygons and two factors were chosen as parameters including: peak-to-trough amplitude and amplitude at user-defined time (Fig. 9).

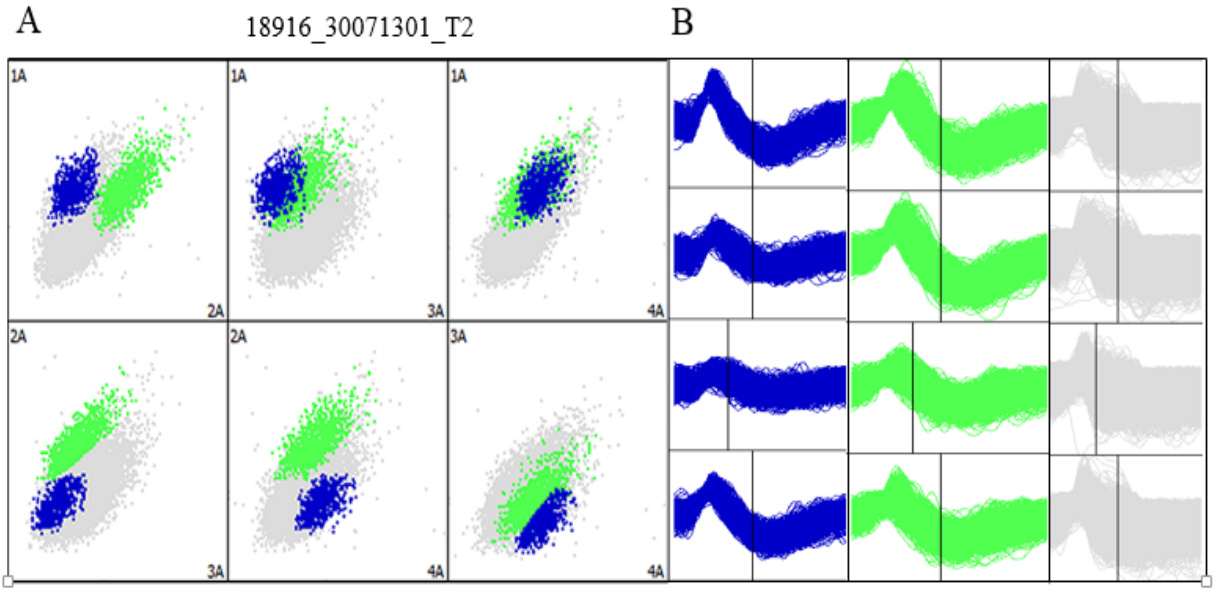

Fig. 9. Unit isolation using cluster-cutting software TINT Axona. **(A)** Electrode-pair scatterplots by 10 min recording of neuronal signals in MEC. The number shown above the scatterplots 18916_30071301_t2 is a representative of the recording session where 18916 stands for the rat number, 30071301 – date 30.07.13 and 01 means the first recording session, T2 shows the second tetrode. Each individual grey dot in scatterplot is representative of one recorded spike plotted in accordance to its distance to 4 electrodes of the tetrode (1A–4A). Each box shows the recorded action potential by a single electrode. Two representative units (blue and green) shown in two distinct clusters identified manually by hand drawn polygons. **(B)** shows the waveforms of neuronal spikes that are represented by two clusters with distinct colors (blue and green) in (A). The column with gray waveforms represents the mean waveform taken from all the waveforms in the left columns. If two neuronal spikes are mainly similar or if there is noise that has a similar waveform like the cell signal, signals can be further isolated from either other signals or noises by comparing amplitude to voltage at a user-specific time point.

Sensitivity of the recording system (dacqUSB Recording System";Axona, UK) to the low frequency enables to detect instantaneously electrical activities generated by several cells in neuronal ensembles in MEC. These neurons are isolated from each other and noises by different amplitudes shown in distinct signal waveforms. As shown in Fig. 9, the cut window displays the different action potentials either as waveforms in columns B on the right or as gray dots in a two-dimensional section of multi-dimensional space in column A on the left. Each single dot is derived by plotting the peak-though amplitude on one electrode-pair scatterplots. Although, there are a wide range of neuronal activities in a single surrounding place, tetrodes detect

simultaneously action potentials of multiple neurons and it is possible to isolate all single units based on parameters mentioned above.

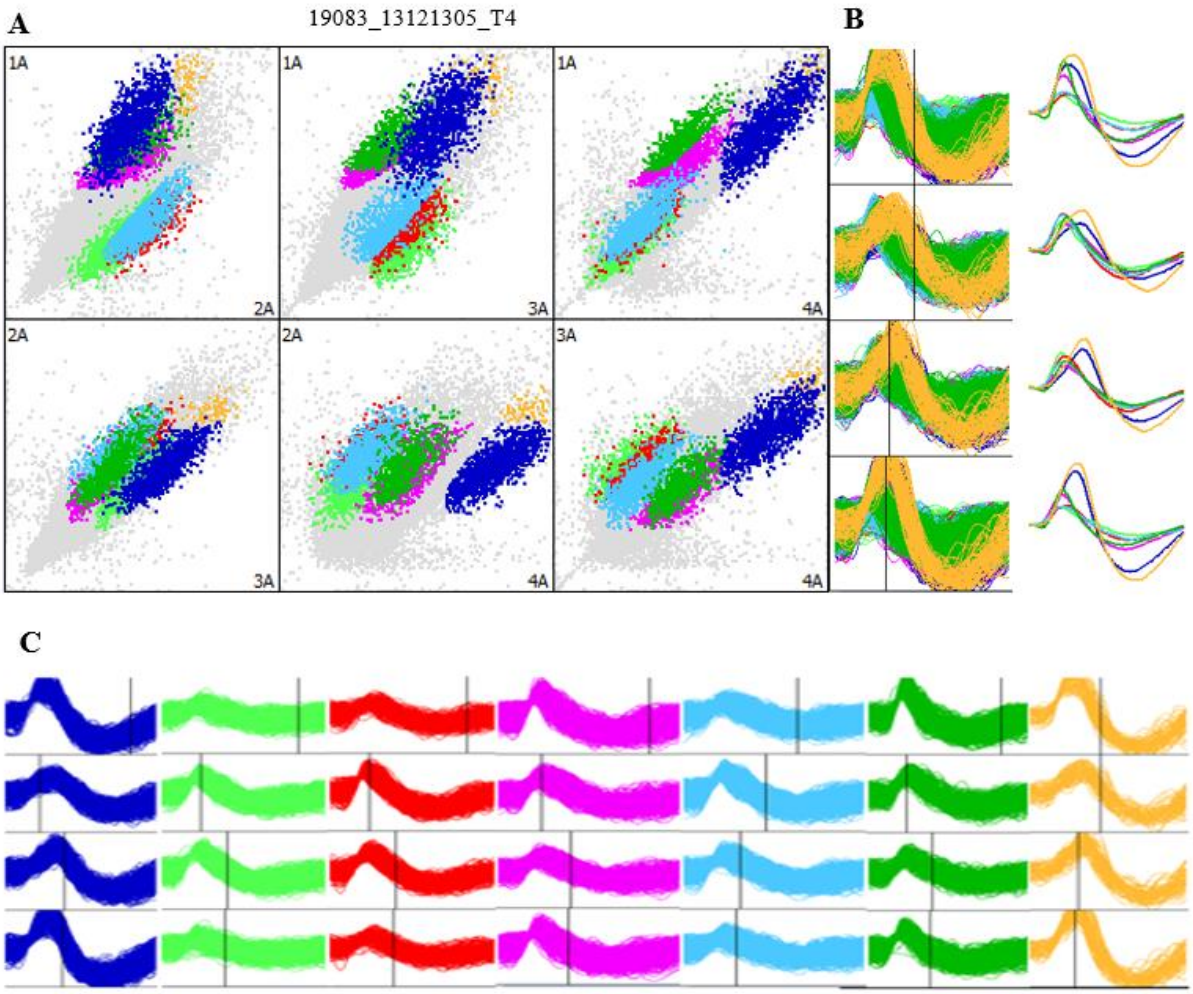

Fig. 10. Numerous detected action potentials generated by multiple neurons with a close amplitude in MEC for 10 min recording session. **(A)** shows the scatterplot representing neuronal activities in MEC plotted by the amplitudes of all recorded signals across four electrodes of a single tetrode. Seven various cells with different amplitudes are shown in different colors. On the right columns **(B)**, a comparison of the various amplitudes of the cells are shown. As can be seen, although, some cells (blue and orange) looks to be the same cells (look at **(C)** waveforms) with the first look in cluster cutting, by a comparison of waveforms, it gets more clear that there is differential cells with various amplitudes than a single cell.

The tetrodes were lowered in 50 μm steps (never more than 100 μm per day) until single cells could be observed from recording sessions. Then the rats were put into a $1m^2$ square box to run freely around for 10-15 min and neuronal signal activity was recorded in both left MEC (for two rats with numbers; 18581-18916) and right MEC (for three rats with numbers; 19081

19082-19083). When the experimental procedures showed no recognizable changes in the pattern of the neuronal firing, then tetrodes were further 50 μm lowered in. later on, in order to classify functional identity of MEC recorded neurons, the information recorded such as action potentials, positional data and preferred directional heading of the animal were all used. In total there were 124 cells recorded in MEC. After the experimental recordings was completed (almost 2 months), rats were perfused transcardially and their sagittal brain sections evaluated by Nissel staining method to see the location of tetrodes in MEC. The following figure of Nissl stained sagittal brain sections confirmed the presence of tetrodes in superficial layers of MEC (Fig. 11). However, the tetrodes for rat number 18916 seems to be initially sticked at superficial layers of MEC.

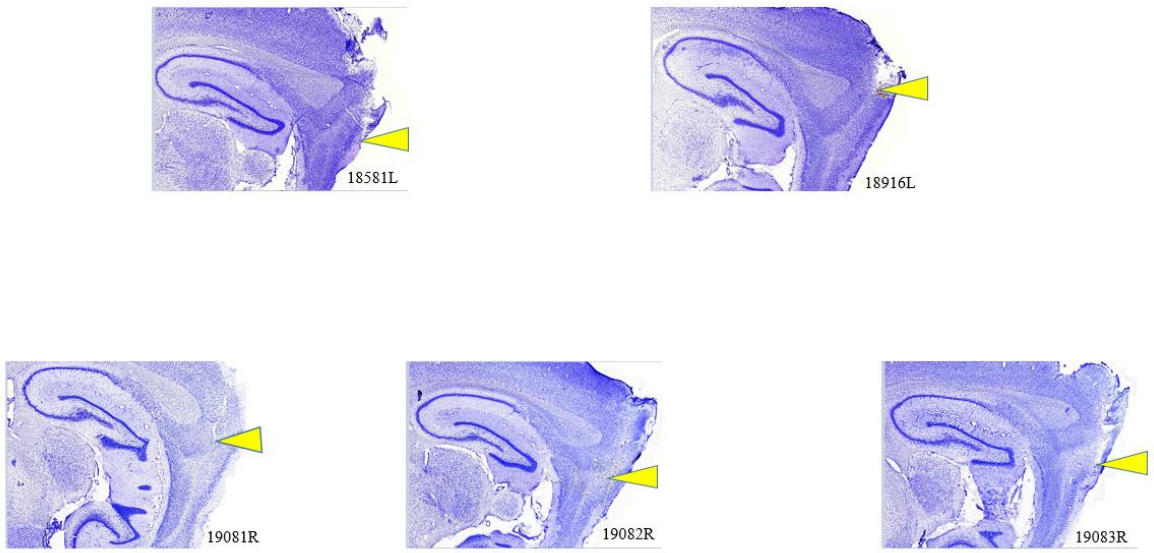

Fig. 11. Nissl-stained sagittal brain sections. Nissl-stained sagittal brain sections were studied to identify the trace of tetrodes. Yellow arrowhead represents the deepest recording position of tetrodes. The numbers indicate the numbers of the rats where ‘’R’’ refers to right brain hemisphere and L refers to left brain hemisphere.

3.2 Identification of Functional MEC Neurons

When a neuron detcted in superficial layers of MEC area, it is the time to see the type of the cell by using a combination of criteria suggesting that the signal is from grid cells, head-direction cells, border cells , conjunctive cells, unknown principal cells or interneurons. These criteria includes waveforms exhibiting oscillations of the signal, -10/10 ms autocorrelogram to indicate if the cell

isullated from noises and -1000/1000 ms interspike interval histogram (ISIH), path map, color-coded rate map, autocorrelogram, head directional polar map and firing rate of recorded cell.

Autocorrelograms show the firing pattern of the neurons by plotting spike correlation over specific intervals of time. All of the cells included in this study showed no firing pattern within the refractory period of the cell, that is, the first 2ms of the autocorrelogram, unless the correlation could be defined as noise signals. The interspike interval histogram (ISIH) indicates theta rhythmicity of the neuron in its firing pattern. Rhythmically firing neurons would have reveal picks, whose number depends on the type of rhythm, in an extensive interval autocorrelograms. In 1000 ms interval, delta rhythms, gamma rhythms and the most famous neuronal theta rhythms would have 1-4, 30-70 and 6-12 picks respectively. The color-coded rate map shows the pattern of firing distribution and path map represents the trajectory of the rat with spike locations. A polar plot shows the firing rate of the cell as a function of head direction and amount of time that the rat faced one specific direction. A cell was classified as grid cell if it showed a clear triangular firing pattern in the rate map with no head direction specificity in polar plot. Those cells that showed a clear firing field along the wall of the box as well as the inserted wall during wall session recording with no head direction specificity defined as border cells. Cells categorized as head-direction cells when polar firing rate map had a firing rate as a function of the rat's head direction with peak rate indicated towards a clear preferred direction with no pattern of grid cells and border cells activity. Conjunctive grid x head direction cells defined as those cells showing both grid structure and head direction modulation. Conjunctive cells with the properties of border cells and head direction cells classified in conjunctive border x head direction cells group and those cells that did not satisfy any of the criteria for aforementioned cells categorized in either unknown cells or interneuron groups. To distinguish these two cell types, interneurons have narrower waveform with higher frequency in their firing pattern than unknown principal cells.

Of the total number of 124 discovered cells in MEC, 25 grid cells, 16 head direction cells, 9 border cells, 10 conjunctive grid x head direction cells, 7 conjunctive border x head direction cells, 23 interneuron cells and 34 unknown principal cells identified. The table 1. Shows the number of cells and types of the cells detected at this study.

Table 1. Total cell types detected in MEC of rats.

ANIMAL	GRID CELLS	HD CELLS	BORDER CELLS	CONJUCTIVE GRID-HD CELLS	CONJUCTIVE BORDER-HD CELLS	UNKNOWN PRINCIPAL CELLS	INTERNEURONS	TOTAL
18581	8	5	3	3	2	10	6	**37**
18916	0	1	2	0	0	0	8	**11**
19081	5	4	2	0	1	6	2	**20**
19082	4	3	2	3	2	6	2	**22**
19083	8	3	0	4	2	12	5	**34**
TOTAL	**25**	**16**	**9**	**10**	**7**	**34**	**23**	**124**

3.2.1 Grid Cells

Gird cells contained the second most detected spatial cells in this experiment (25 grid cells out of total 124 discovered cells that is ~10 % (Table 1). These cells showed multiple triangular firing pattern with various sizes of their firing fields in their rate maps (Fig. 11. A, B section II). Two of grid examples are shown in Fig. 12.

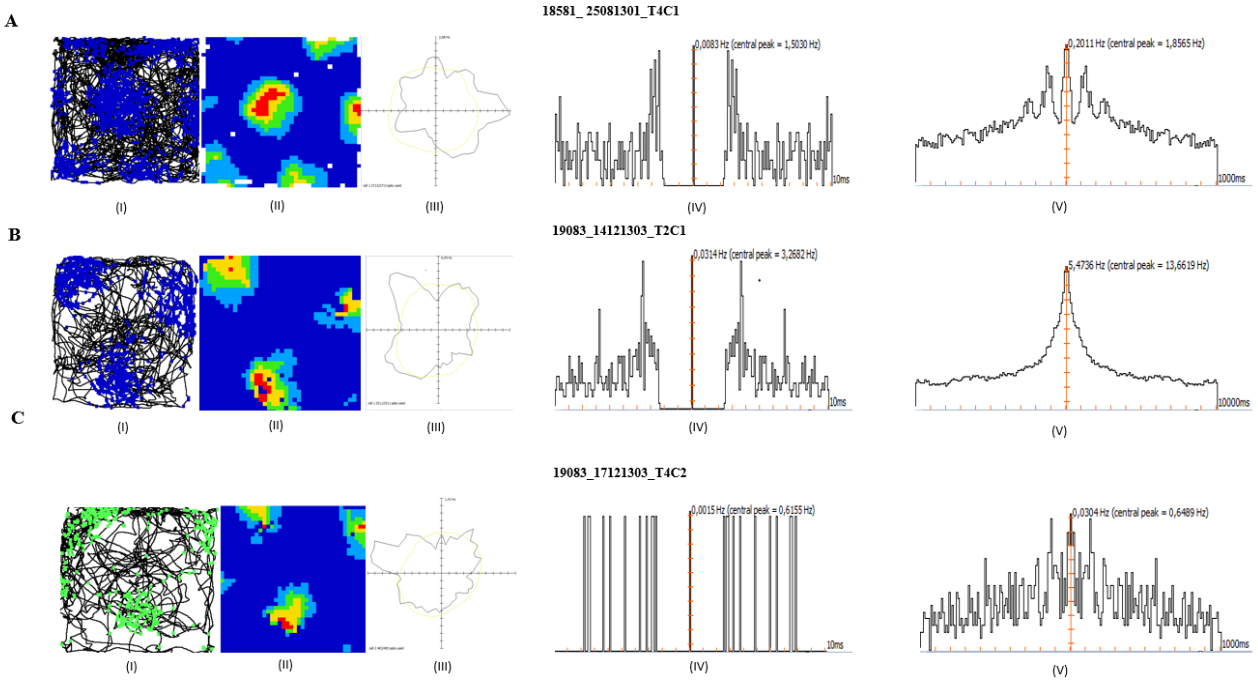

Fig. 12. Grid cells recorded in MEC of rats over 10 min running in a 1 x 1 x 0.5 m square box. Three grid cells are represented at this figure by **A**, **B** and **C**. From left to right: spike locations **(I)** (blue for **A** and **B**

and green dots for **C**) superimposed on the trajectory of the animal (black lines) showing a grid pattern of firing activity during 10 min recording period**.** Different colors (blue and green) here in spike locations map representing different cells recorded while neural clustering process by Tint program software. Color-coded rate maps **(II)** representing the distribution of firing pattern with maximum rate of firing representing by red and absence of action potentials by dark blue color. Polar maps **(III)** showing neural firing rate as a function of rat's head direction and. as seen, there is no preferred head directionality in their neuronal firing patterns of activity and if so, the cells would categorize as conjunctive cells. The autocorrelogram of firing pattern from intervals of -10/10 ms **(IV)** and -1000/1000 ms **(V)** indicate the correlation of firing frequency and showing how well a neuronal signal correlates with itself. In **A**, **B** and **C**, the accurate isolation of extracellular neuronal spikes was confirmed by the absence of firing within the first 2 ms of the -10/10 ms autocorrelogram **(IV).** The -1000/1000 ms autocorrelogram **(V)** in cell **A** shows a high correlation at the first few milliseconds with two distinct peaks, however the correlations decline over time. A lack of distinct peaks in ISIH of cell **B** and **C** indicates that there is no rhythmicity in the firing pattern of these cells. A consistent burst firing is seen in all cells with a correlation peak at around 3 ms that identifies these cells as burst cell. The letter '' C '' in the Sessions number, identified on the top, stands for a unit number.

3.2.2 Head –Direction Cells

Head direction cells contain an amazing ability to consolidate the external sensory and internal vestibular and proprioceptive inputs to encode for directional heading purposes. 16 cells identified as head direction cells. All of the recorded head direction cells showed a clear head directionally pattern in their polar plots. Among recorded cells, some cells were tuned sharply to a specific point of direction in environment (fig. 13,A), while others had a wider tuning specificity in their preferred directions (Fig. 13, B and C).

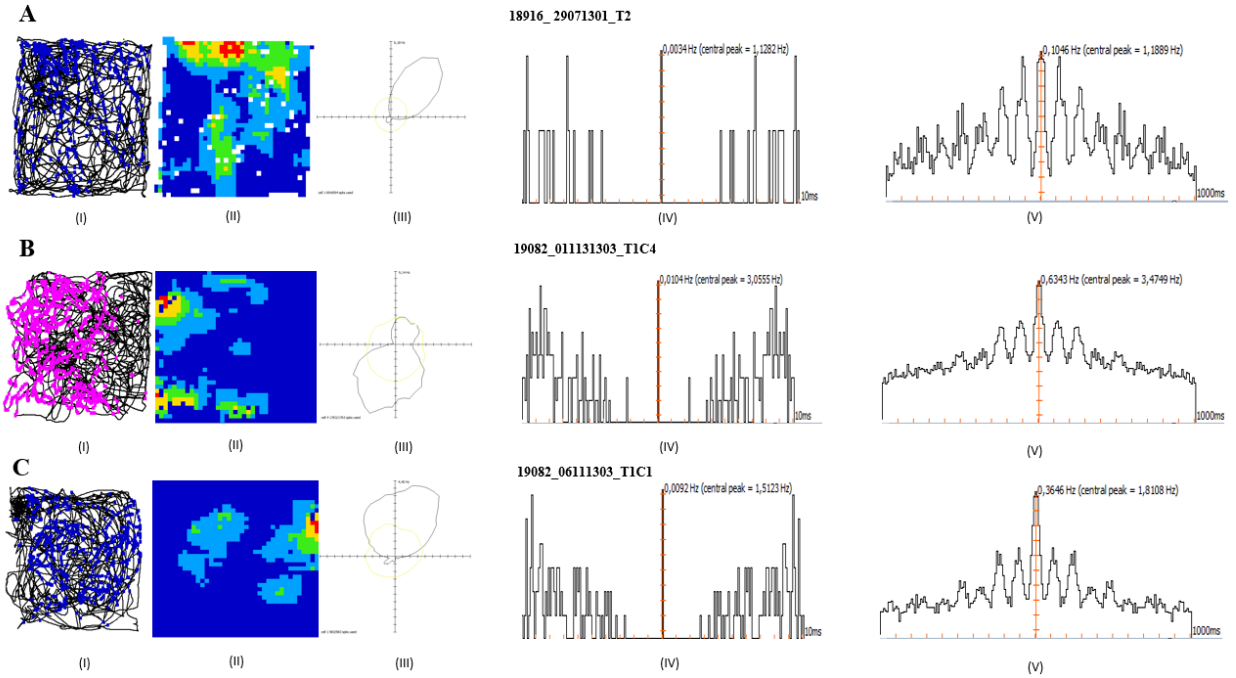

Fig. 13. Head-directional cells recorded in MEC of rats over 10 min running in a 1 x 1 x 0.5 m square box. Three head direction cells are represented by **A**, **B** and **C.** From left to right: spike locations (blue and pink dots) superimposed on the trajectory of the animal (black lines) showing the pattern of firing activity during 10 min recording period **(I).** Note that different colors, showing spike locations, in trajectory-with-spike-locations map is referring to different cells; blue dots, here, indicating the unit ‘’number 1‘‘ and pink refers to ‘’unit number 4’’. Color-coded rate maps **(II)** representing the distribution of firing pattern with maximum rate of firing representing by red and absence of action potentials by dark blue color. Polar maps **(III)** showing firing rate as a function of rat’s head direction with peak rate indicated towards northeast, southwest and north directions for **A**, **B** and **C** respectively. Note that, there is no evidence of either border selectivity pattern of firing or triangular firing pattern specialized for border and grid cells respectively in all presented rate maps **(II).** As clearly shown in B **(III),** there is a tuning head directionality from right part of the enclosure towards the left side differentiating the trajectory of animal into two separated parts (pink dots versus the black lines). The accurate isolation of extracellular neuronal spikes was confirmed in all cells (**A**, **B** and **C**) by the absence of firing within the first 2 ms of the -10/10 ms autocorrelogram **(IV).** The -1000/1000 ms autocorrelograms **(V)** show a high correlation with distinct peaks supporting a characteristic of theta firing cells with a sinusoidal decaying oscillations of 5,7 and 8 peaks in cell **B**, **A** and **C** respectively (from 0-1000 ms). The number of 5 , 7 and 8 correlation peaks found on both halves of -1000/1000 ms autocorrelogram is a strong evidence that suggest these cells are firing at theta frequency (6-12 Hz).

3.2.3 Border Cells

In all four rats, MEC contained a small but distinct population of border cells. Such cells identified by showing a high firing rate field along either one of the walls of the box (Fig. 14, C) as well as showing the same pattern of activity along the inserted wall into the enclosure. (Fig. 14, A and B). 9 out of 124 detected MEC cells (~7 %) passed the classification criterion. Although more cells found with characteristic of border cells (firing along the walls of enclosure), due to showing a preferred head directionality in their polar plot, another classification considered for these cells as conjunctive border x head direction cells.

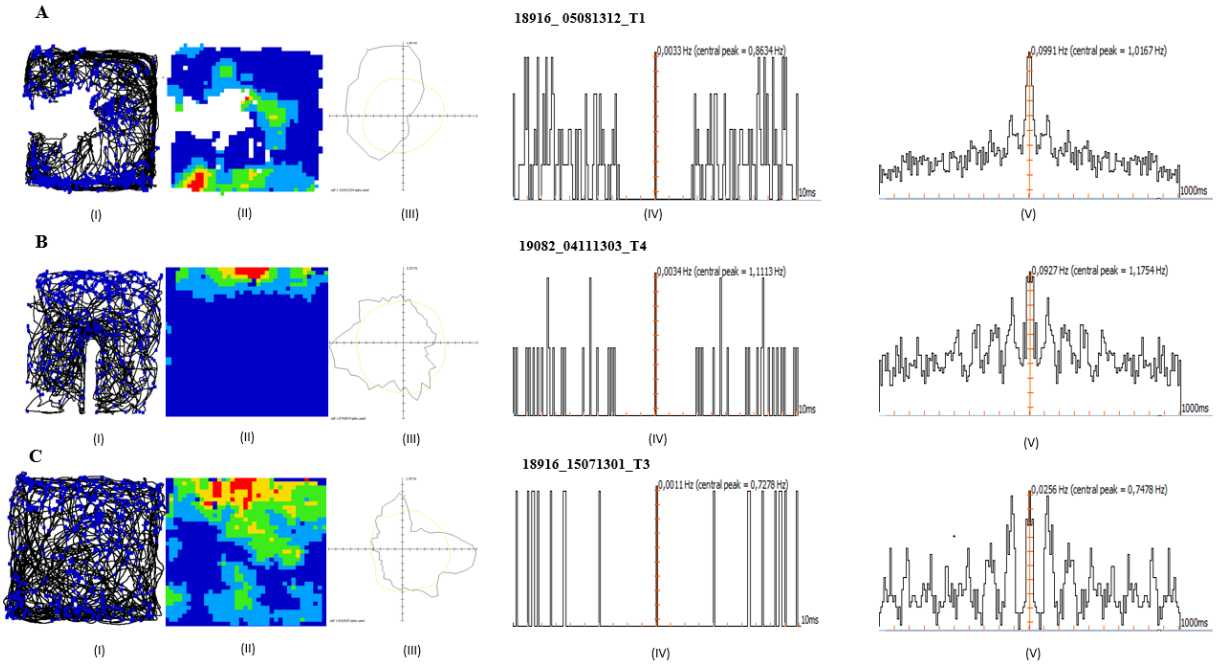

Fig. 14. Border cells in the MEC of rats over 10 min running in a 1 x 1 x 0.5 m square box. **A**, **B** and **C,** from left to right: spike locations (blue dots) superimposed on the trajectory of the animal (black lines) showing a high number of spike along the walls of the box during 10 min recording period **(I).** Color-coded rate maps **(II)** representing the distribution of firing pattern with maximum rate of firing representing by red and absence of action potentials by dark blue color. Polar maps **(III)** showing firing rate as a function of rat's head direction. As seen in polar plots **(III),** there is no direction selectivity while navigation in enclosure resulting that these cells are not conjunctive cells. The isolation of extracellular neuronal spikes was confirmed in all shown cells by the refractory time of 2 ms of the -10/10 ms autocorrelogram **(IV)**. The -1000/1000 ms autocorrelograms **(V)** show a high correlation with distinct peaks supporting a characteristic of theta firing cells (6-12 Hz) (**A**,**B**,**C**).

3.2.4 Conjunctive Grid x Head Direction Cells

To define a cell as a conjunctive grid-head direction cell, the cell should show a preferred direction selectivity in polar plot in addition to a triangular pattern of firing in rate maps. 10 out of 124 cells (~ 8%) passed this criterion and categorized as conjunctive grid x head direction cells. These cells show both grid structure and head direction modulation.

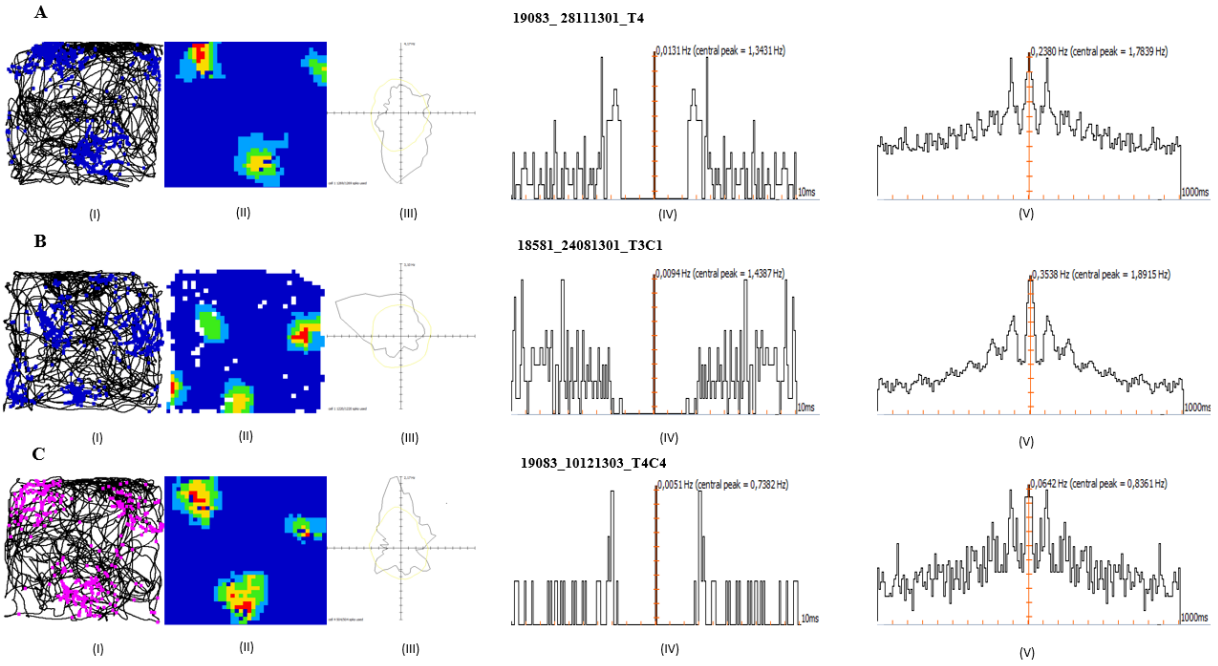

Fig. 15. Conjunctive grid x head direction cells in MEC of rats over 10 min running in a 1 x 1 x 0.5 m square box. **A**, **B**, and **C**, from left to right: spike locations (blue and pink dots) superimposed on the trajectory of the animal (black lines) showing a grid pattern of firing activity during 10 min recording period **(I).** Note that different colors, showing spike locations, in trajectory-with-spike-locations map is referring to different cells: blue dots, here, indicating the unit ‘’number 1‘‘ and pink refers to ‘’unit number 4’’ recorded in TINT program software. Color-coded rate maps **(II)** representing the distribution of firing pattern with maximum rate of firing representing by red and absence of action potentials by dark blue color. Polar maps **(III)** showing firing rates as a function of rat’s head direction with peak rate indicated towards the south, northwest and north directions for cells **A**, **B** and **C** respectively . Maximum firing rates indicated for all three rate maps showing a triangular pattern of activity as well as maximum occupancy in specific directions in polar plots are indicators of conjunctive grid x head direction structure of these cells. No firing activity over refractory period (0-2 ms) showing an accurate isolating extracellular neuronal spikes in -10/10 ms autocorrelograms **(IV)** of all three cells (**A**,**B**,**C**). The -1000/1000 ms autocorrelograms **(V)** show a high correlation with distinct peaks in **B** supporting a characteristic of theta firing cells (6-12 Hz). However, **A** and **C** show no rhythmicity pattern of firing.

3.2.5 Conjunctive Border x Head Direction Cells

We concluded that of 124 MEC cells 7 cells satisfied the criteria for both border and head direction cells. These cells in addition to a high firing rate field along either one of the walls of the box or the same pattern of activity along the inserted wall into the enclosure, showed a clear preferred direction in polar firing rate map (Fig. 16, **A** and **B**, section III).

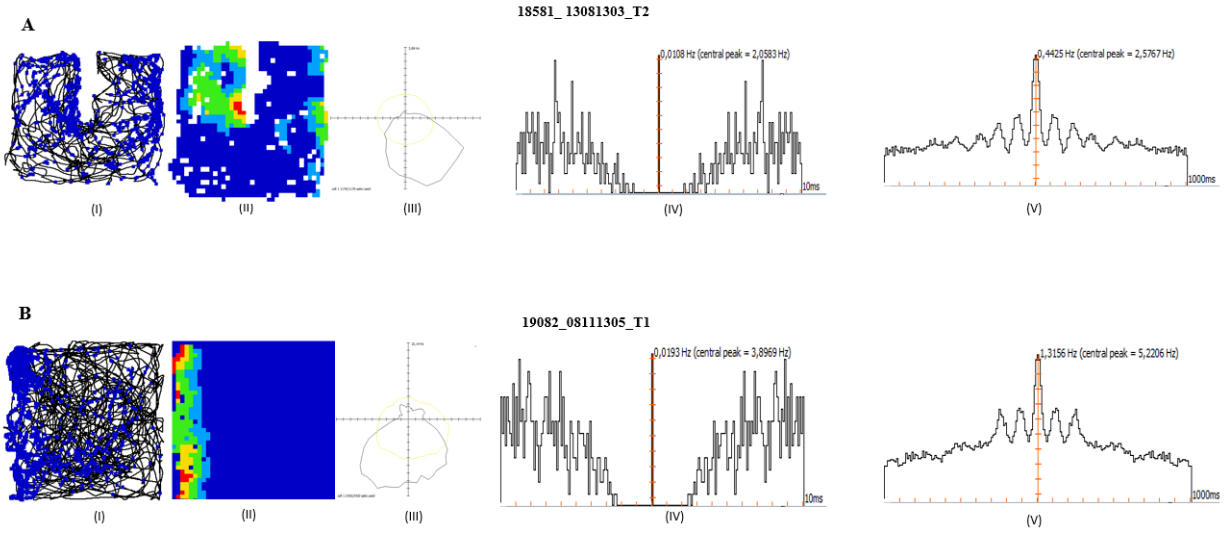

Fig. 16. Conjunctive border x head direction cells in MEC of rats over 10 min running in a 1 x 1 x 0.5 m square box. **A**, **B** and **C,** from left to right: spike locations (blue dots) superimposed on the trajectory of the animal (black lines) showing pattern of firing activity along the left wall of the box **(B, I)** and also along the left side of the inserted wall (**A**, **I**) during 10 min recording period. Color-coded rate maps **(II)** representing the distribution of firing pattern with maximum rate of firing representing by red and absence of action potentials by dark blue color. Polar maps **(III)** showing firing rate as a function of rat's head direction with peak rate indicated to the south direction. The isolation of extracellular neuronal spikes was confirmed by the refractory time of 2 ms of the -10/10 ms autocorrelogram **(IV).** However, a small correlation right before 2ms to compare with other correlations in the -10/10 ms autocorrelograms for Cell A **(A, IV)** suggests that a small amount of noise was isolated with this signal. The -1000/1000 ms autocorrelograms **(V)** show a correlation with distinct peaks supporting a characteristic of theta firing cells (6-12 Hz).

3.2.6 Unknown Principal Cells

The principal cells that did not support the criteria for grid cells, head direction cells, border cells, conjunctive grid x head direction cells and conjunctive border x head direction cells were classified as unknown principal cells. We concluded that of 124 detected MEC cells 34 cells (~28 %) were unknown principal cells that is the most cell type recorded in MEC at this study (Fig. 17).

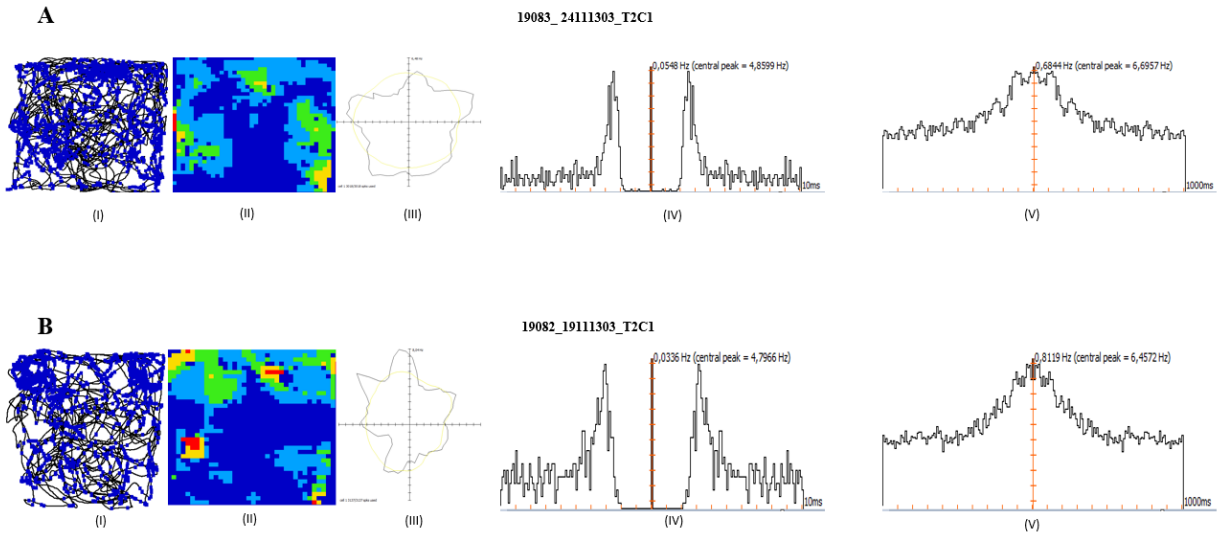

Fig. 17. Unknown principal cells in MEC of rats over 10 min running in a 1 x 1 x 0.5 m square box. **A** and **B**, from left to right: spike locations (blue dots) superimposed on the trajectory of the animal (black lines) showing uncertain pattern of firing activity during 10 min recording period **(I).** Color-coded rate maps **(II)** representing the distribution of firing pattern with maximum rate of firing representing by red and absence of action potentials by dark blue color. Polar maps **(III)** showing firing rate as a function of rat's head direction supporting no head directionality for both cells **A** and **B**. The silent activity over the refractory period (0-2 ms) in the -10/10 ms autocorrelograms of both cells **A** and **B (IV),** indicating how well the extracellular neuronal action potentials are isolated from surrounding neuronal spikes. No rhythmicity in the firing pattern of these cells is observed by lack of distinct peaks in -1000/1000 ms autocorrelograms **(V).**

3.2.7 Interneurons

Three criteria were required that the recorded cell would be counted as an interneuron: i. no clear directional or spatial modulation; ii. high firing rate ; iii. short and narrower waveform (peak- to-trough width (*109*). 23 cells recorded in the MEC supported these criteria and were categorized as intern0eurons (Fig. 18).

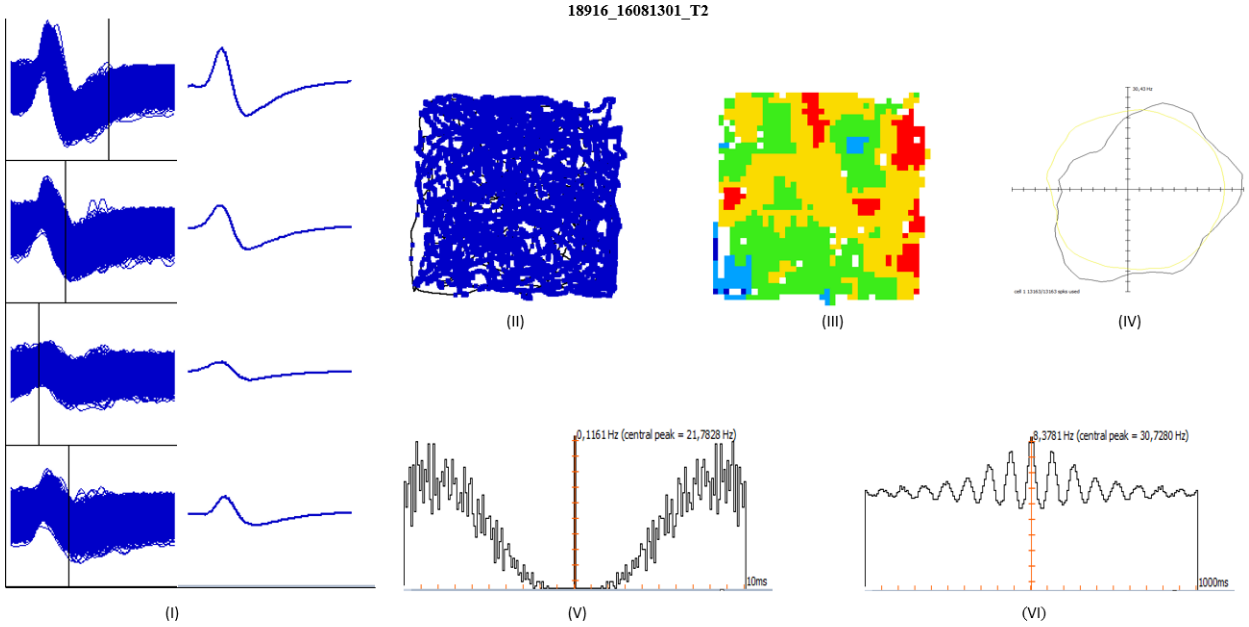

Fig. 18. Interneurons in MEC of rats over 10 min running in a 1 x 1 x 0.5 m square box. Action potentials are seen to be as short and narrow waveforms **(I).** spike locations superimposed on trajectory of the animal (black lines) showing tremendous firing activity of interneuron all over the enlcosure area during 10 min recording period **(II).** Color-coded rate maps **(III)** representing the distribution of firing pattern with maximum rate of firing representing by red and. Polar maps **(IV)** showing firing rates as a function of rat's head direction supporting no head directionality. The isolation of extracellular neuronal spikes was confirmed by the refractory time of 2 ms of the -10/10 ms autocorrelogram **(V).** The The -1000/1000 ms autocorrelograms **(VI)** show a high correlation with distinct peaks supporting a characteristic of theta firing cells (6-12 hz).

3.3 Retrograde Transduction of Entorhino-Entorhinal Projection Neurons

By applying a retrograde gene delivery strategy, we could target projection neurons in contralateral MEC. When a virus carrying immunohistochemical tag is being injected into a certain region of the brain, it gives an opportunity to track transduction of neurons either in injection area or other areas that contains neurons which retrogradely project to the injecting area. Due to this fact that a small fraction of entorhino-entorhinal fibers can only be discharged from a single electrode, by using a widely diffusible vector carrying a light-responsive transgene, we were able to tag larger proportion of incoming axons from left MEC to the contralateral right MEC and vise versa. We used adeno-assiciated virus (AAV) as vectors due to their properties of low toxicity and long-term gene expression. AAV2 serotype pseudotyped with AVV1 capsid proteins (AVV2/1) was selected to target transgenes to axon terminals of both left and right MEC. rAAV2/1 was packed with pAAV-ChR2-FLAG plasmid; ChR2 was used for optogenetic control. Note that FLAG is a non-fluorescent tag. In immunohistochemical staining, FLAG tag is bound by a primary antibody and then, in turn, bound by a secondary antibody conjugated with Cy3 fluorescent dye using to detect transduced neurons. The construct consists of potassium channel Kir2.1 derived 20 amino acid trafficking signal DYKDHDGDYKDHDIDYKDDDDK and ER export motif FCYNENEV for improved plasma membrane localization. Moreover, vector construction contained WPRE and BGH polyadenylation signal for higher transgene transcription and expression. When the optrode was implanted in left MEC (for rats number; 18581 and 18916) and right MEC (for rats number; 19081-19082 and 19083), rAAV2/1-ChR2-FLAG was injected into the contralateral sides of MEC. After experimental recordings, the rats were transcardially perfused. For further studies, by using immunostaining, transgene expression levels were evaluated on sagittal brain sections. By Immunofluorescent images, ChR2-FLAG expression was detected nearby the injection sites in both left and right entorhinal cortex as well as superficial layers of contralateral sides if injection regions in MEC (Fig.19). As the expression of ChR2-FLAG is detectable in the superficial layers of both left and right hemispheres of MEC, these results prove that the virus was retrogradely transduced from left MEC to right MEC and vise versa.

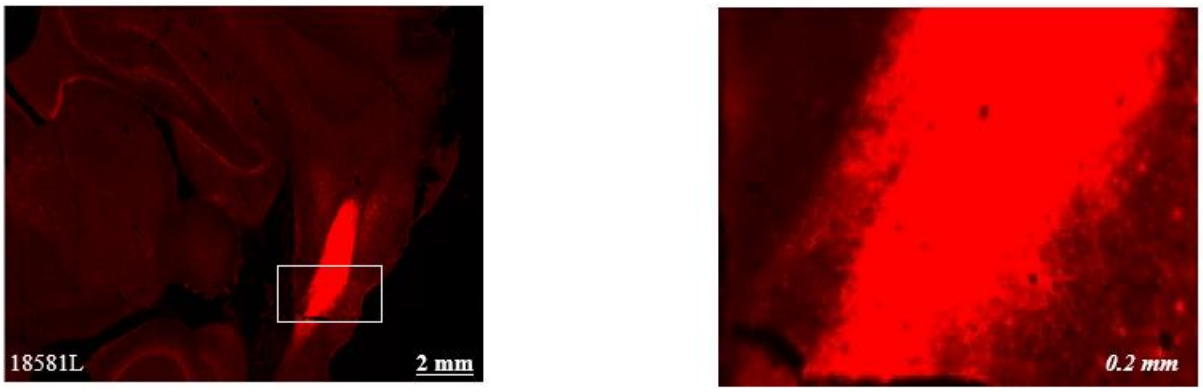

Fig. 19. The immunofluorescent images of rats' sagittal brain sections. ChR2-FLAG expressing MEC areas are indicated by the bright red fluorescence. In the immunohistochemical staining section, FLAG tag is bound by the primary FLAG antibody, which in turn is bound by the secondary antibody conjugated with Cy3 fluorescent dye. From left to right, the increasing magnification with the scale indicated on the bottom row, being 2 mm and 0.2 mm, respectively (the right image shows framed area in the left image magnified). The number indicates the rat number and '' L'' refers to the left hemisphere.

Thus, the retrograde gene delivery strategy can be used to tag medial entorhinal neurons projecting to contralateral neurons in MEC and hopefully gain optogenetic control over them. Furthermore, immunofluorescent images of 2 rats is shown in the following figure, (Fig. 20), representing the channelrhodopsin-2 expression in the right MEC as injected area and retrogradely ChR-2 expressed in left MEC. However, the other three immunofluorescent images in figure 21 showing the expression of ChR-2 in the left hemisphere of MEC as injected area and retrograde expression of ChR-2 in the right MEC of two other rats.

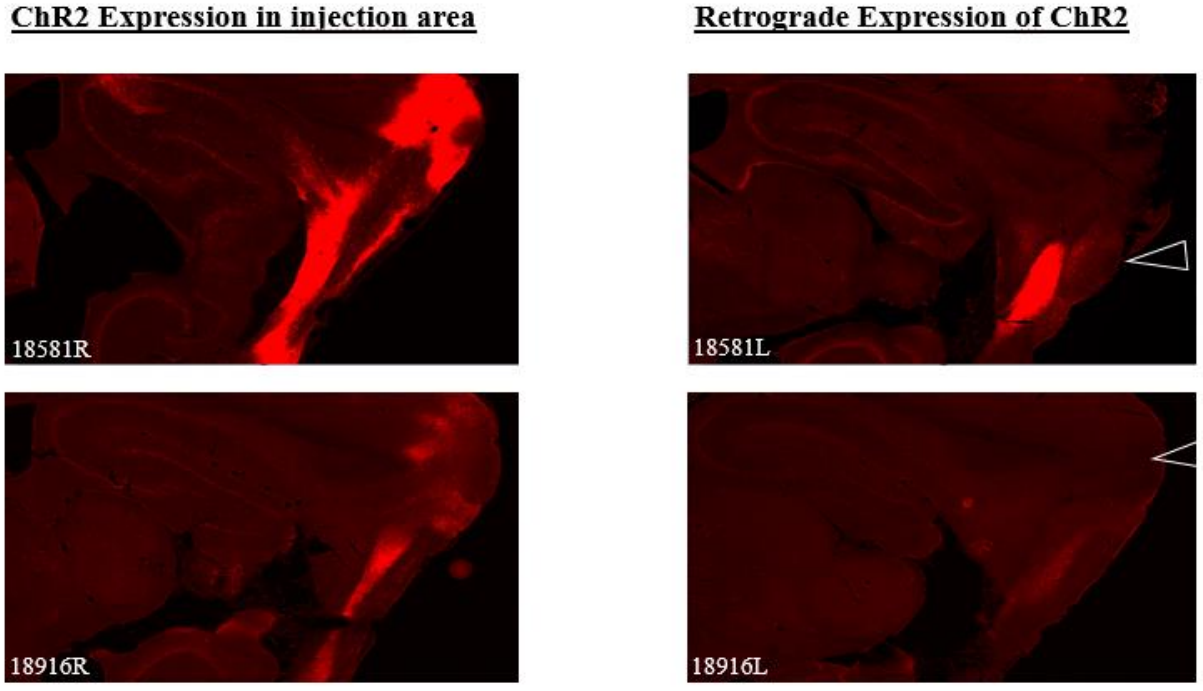

Fig. 20. Immofluorescent images indicating retrogradely ChR2-FlAG expression in the left MEC when the vectors injected in the right MEC. Immunofluorescent images of sagital brain section representing ChR2- FLAG expression in MEC. Bright red fluorescence (emission maximum at 570 nm), present the areas which express ChR2-FLAG (white rectangles as part of the expression area). The left images show expression of ChR2-Flag in right hemisphere where the viral vector was injected for two rats (with numbers: 18581 and 18916). Right images are sections of the left hemispheres Showing the ChR2-FLAG expression retrogradely transported from the injection site in the right hemisphere. The white arrow show where the recording tetrodes were located at its deepest position. R stands for Right hemisphere and L stands for Left hemisphere.

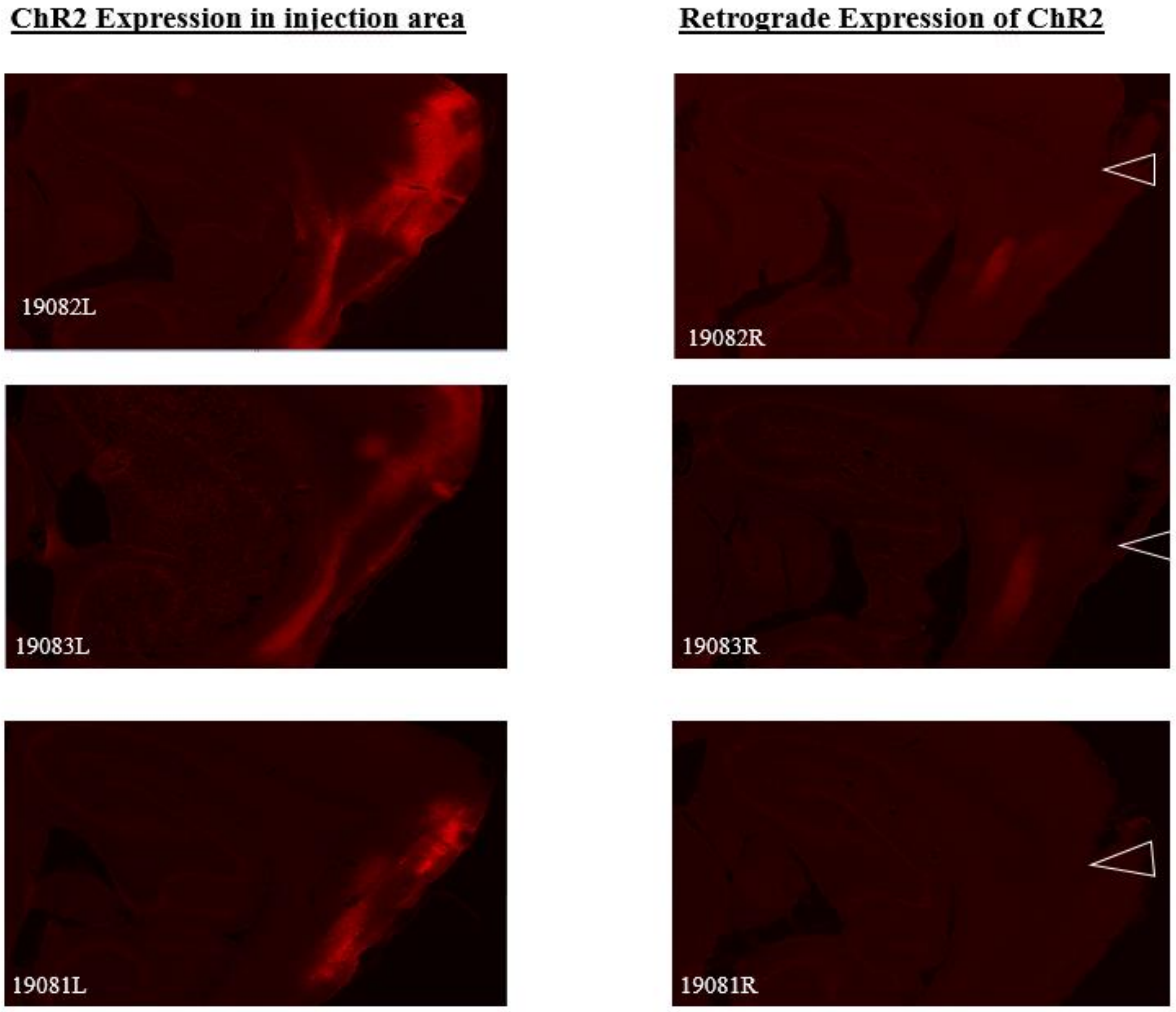

Fig. 21. Immofluorescent images indicating retrogradely ChR2-FlAG expression in the right MEC when the vectors injected in the left MEC. Immofluorescent images of sagital brain section representing ChR2-FLAG expression in MEC. Bright red fluorescence (emission maximum at 570 nm), showing the areas which express ChR2-FLAG (white rectangles as part of expression area). The left images show expression

of ChR2-Flag in left hemisphere where the viral vector was injected for three rats (with numbers: 19081-19082-19083). Right images are sections of the right hemispheres where the ChR2-FLAG are expressed retrogradely from transported vectors that injected in the left hemisphere. The white arrow show where the recording tetrodes were located at its deepest position. R stands for Right hemisphere and L stands for Left hemisphere.

3.4 Photoexcitation of Entorhino-Entorhinal Projection Neurons

3.4.1 Identifying Light-Responsive MEC Neurons

To identify medial entorhinal neurons in left hemisphere with direct projections to the contralateral right MEC neurons and vise versa, we used an optogenetic strategy where direct and indirect activation could be found based on response latencies. As mentioned before, neurons in both right and left MEC with projections terminating on the contralateral MEC neurons have been tagged by injection of AAV into the right MEC for the first group of rats (rat numbers; 18581 and 18916) as well as into the left MEC for the second group (rat numbers; 19081-19082 and 19083). Viral payload was successfully transported retrogradely to the superficial layers of MEC (Fig. 20, 21), which, in turn, presented optogenetic control (photoexcitation) on ChR2-expressing of contralateral MEC neurons. After identification of neurons recorded in MEC during the behavioral task, the same MEC neurons were stimulated by shinning ChR2-activating blue (473 nm) light. If functional contralateral MEC neurons showed light responses (i.e. action potential latency after laser stimulation), these cells for the first group could be either; i. those cells with direct projections to the right MEC region and are being activated directly as they express ChR2, whose gene was retrogradely transported from right MEC; ii. or those neurons that are being indirectly activated by ChR2-expressing left MEC neurons with excitatory synaptic connections to the cell of interest. However, these cells for second group with injection of vector into their left MEC could be either; i. those cells with direct projections to the left MEC region and are being activated directly as they express ChR2, whose gene was retrogradely transported from left MEC; ii. or those neurons that are being indirectly activated by ChR2-expressing right MEC neurons with excitatory synaptic connections to the cell of interest.

During the same surgical session, an assembly of tetrodes and a laser-coupled optical fiber were together implanted into the left and right MEC regions for the first and second group respectively.

The place of optical fiber was 500 µm above the tip of tetrode that enabled us to record neurons *in vivo* and delivering 473 nm blue light for ChR2 activation simultaneously. After behavioral task and functional identity of recorded neurons in MEC, the rat was put on a towel into a flower pot and, for light delivery purposes, an optical fiber connected to the head stage on animal's head. In the flower pot, a recording session together with laser stimulation followed for 2 min; laser stimulation was including 3.5 ms 473 nm light pulses with 1 Hz frequency. Note that, the power of light delivery at the tip of optical fiber measured at ~20 mW. The recorded cells in 10 min running session and cells found in 2 min laser stimulation session were considered as the same neurons if the position of isolated clusters in electrode-pair scatterplots as well as form of spike waveforms before and during the laser stimulation session seemed the same (Fig. 22).

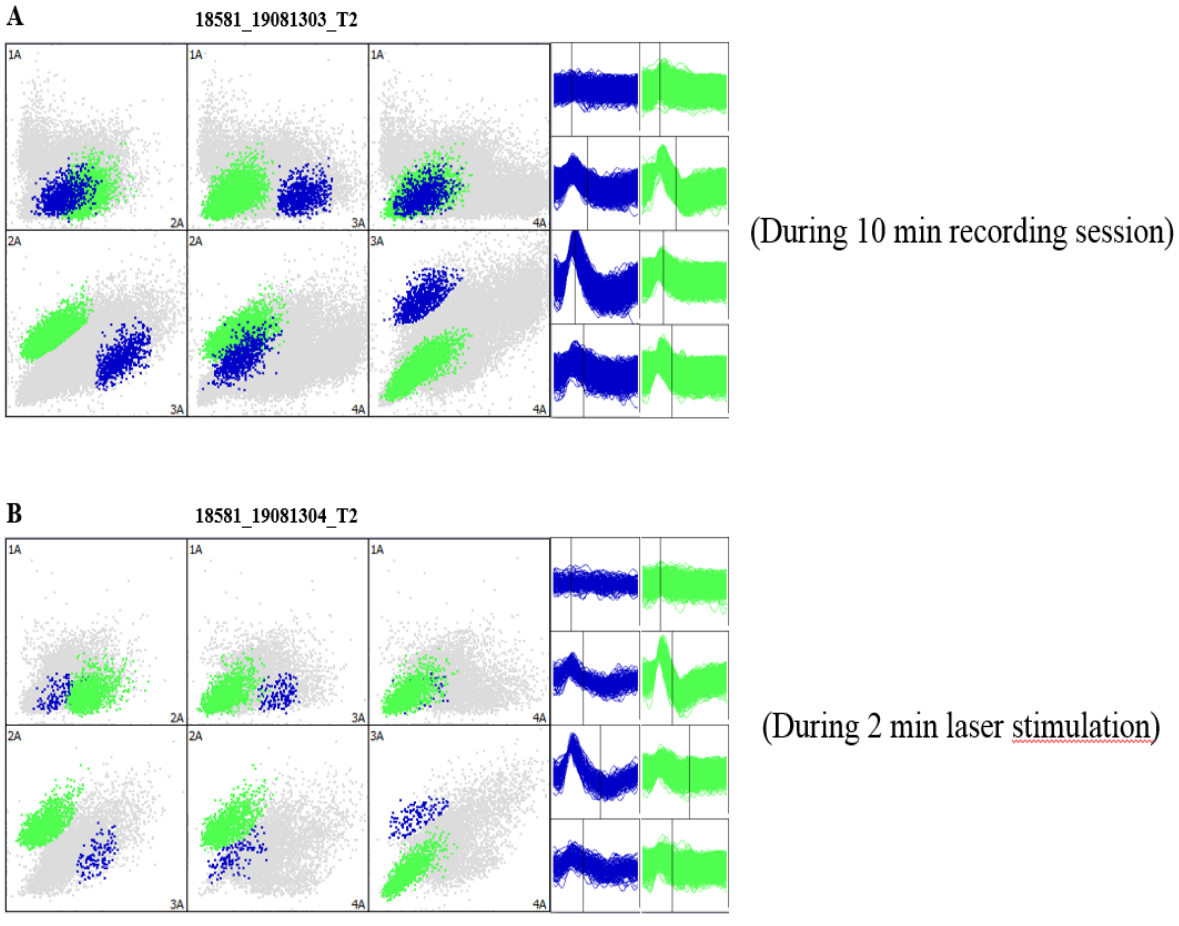

Fig. 22. Electrode-pair scatterplots representing the response of neurons recorded in left MEC to laser stimulation. Electrode-pair scatterplots of two neurons (represented by blue and green) before the laser stimulation (during 10 min recording session) **(A)** and during 2 min laser stimulation **(B).** Two cells in the left MEC of rat (number 18581) have been recorded while the rat was running in the square enclosure

for 10 min **(A),** whereas during 2 min laser stimulation rat was placed in a large flower pot. By comparing the position and waveform appearance of recorded neurons during 10 min running session **(A)** with cells recorded during laser stimulation **(B),** when no detectable changes could be observed from this comparison, then we assumed that cells before laser stimulation **(A)** and during laser stimulation **(B)** were the same cells . Then we were recording and stimulating the same cells by this simple comparison.

Moreover, to evaluate whether recorded neurons in MEC were responsive to 473 nm blue light during laser stimulation, two parameters were considered: number of evoked spikes and response latency in spike raster and spike histograms. Spike raster and the spike histogram both representing the distribution of action potentials of the neuron before and after laser stimulation (Fig 23). Note that spike raster and spike histograms presented in following figure, are representing the spike distribution (before and after stimulation) for unit 1 (blue cluster) detected by tetrode 2 of the same rat shown in (Fig. 23).

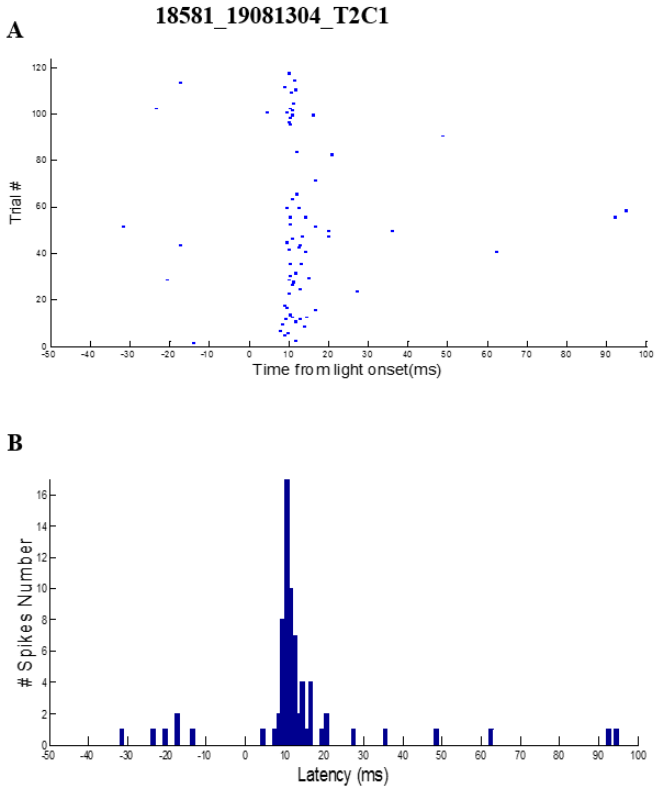

Fig. 23. Spike raster and spike histograms representing the response of the MEC recorded neuron in left MEC to laser stimulation. The spike raster (top) and the spike histogram (bottom) display the distribution of spike before and after 2 min laser stimulation. Each single dot in the spike raster **(A)** is a single spike recorded from the cluster in Fig. 22, A. The position of each action potential is represented by two parameters: the number of spikes when the action potential was recorded on *y* axis (each row represents

1 s stimulation period, adding up to ~120 trials for 2 min stimulation session of 1 Hz stimulation) and the [-50, 100] s time interval around the laser stimulation. Laser was on from 0 to 3.5 ms. If spikes are directly fired by light activation, they will probably have the same firing latency for every laser flash. This leads to a vertical line of dots (each dot representing a spike) after point 0 in the spike raster. In the spike histogram **(B),** the number of spikes is plotted by their firing latency around the laser stimulation moment. The response of the cell to the illuminated light is represented by the tallest columns in the histogram right after point 0 in *x* axis. By a short look at the spike raster and spike histogram, It can clearly be seen that the recorded cell has a fixed firing latency at around 10 ms.

Therefore, at this study, only those recorded cells with a clear dotted line in the spike raster (Fig. 23, A) and clear peaks in the spike histogram (Fig. 23, B) were considered as light-activated cells. After analysis of raster and spike histograms extracted by MATLAB program software, it was calculated that of 124 recorded cells in both left and right MEC of 5 rats, only 25 cells (~22%) were detected as responsive to the light activation. According to the aforementioned criteria for identification of the functional cell type of MEC neurons, 12 cells recognized as interneuron, 10 cells as unknown principal cells and 3 cells as grid cells.

Despite the low amount of light responsive cells detected in contralateral MEC, these results demonstrate that combined optogenetic-electrophysiological method can be applied for determining functional identity of entorhino-entorhinal projecting MEC cell.

3.4.2 Direct vs. Indirect Response of Cells to Light

Response latencies can be used to differentiate direct and indirect neuronal responses to the light. Those cells that stimulated directly by light should have minimal response latencies compared to indirectly activated cells. Those cells with an already expression ChR2 in their plasma membrane will quickly fire action potentials in response to light when their ChR2 channels get activated, whereas the synaptic activation by nearby light-responsive cells with synaptic connections to the cell of interest would lead to additional time for signal transduction. Light responsive cells with firing latencies at around ~10 ms were considered to be directly activated cells. However, those neurons with longer latencies were considered to be indirectly activated cells. These criteria for determining whether the recorded neuron is directly-light activated or indirectly-light activated, has been used in a recently published paper by *Zhang et al.(*40).

Then we looked into the response latencies which were acquired from grid cells, unknown principal cells and interneurons. In total, of 28 recorded unknown principal cells,10 cells showed responses to laser stimulation and of 16 recorded interneurons, 12 responsive cells and of 23 recorded grid cells, only 3 cells showed light responses. Principal cells including grid cells and unknown cells showed a minimal variation within the data acquired in their response latencies in different sessions or different animals. However, when looking at response latencies of light-responsive interneurons it is easily to see that the data spread is wider compared to that of light-responsive principal cells. There were no evidence of light responsiveness for other types of spatial cells in MEC at this study.

3.4.3 Light Activated Grid Cells

Of total 23 recorded grid cells in MEC, only 3 cells (~13%) found as responsive to laser stimulation. The grid pattern of firing with no preferred head direction properties was found in all three light responsive grid cells. However, as the Fig. 24 shows the responses (number of evoked spikes) of these grid cells are not strong.

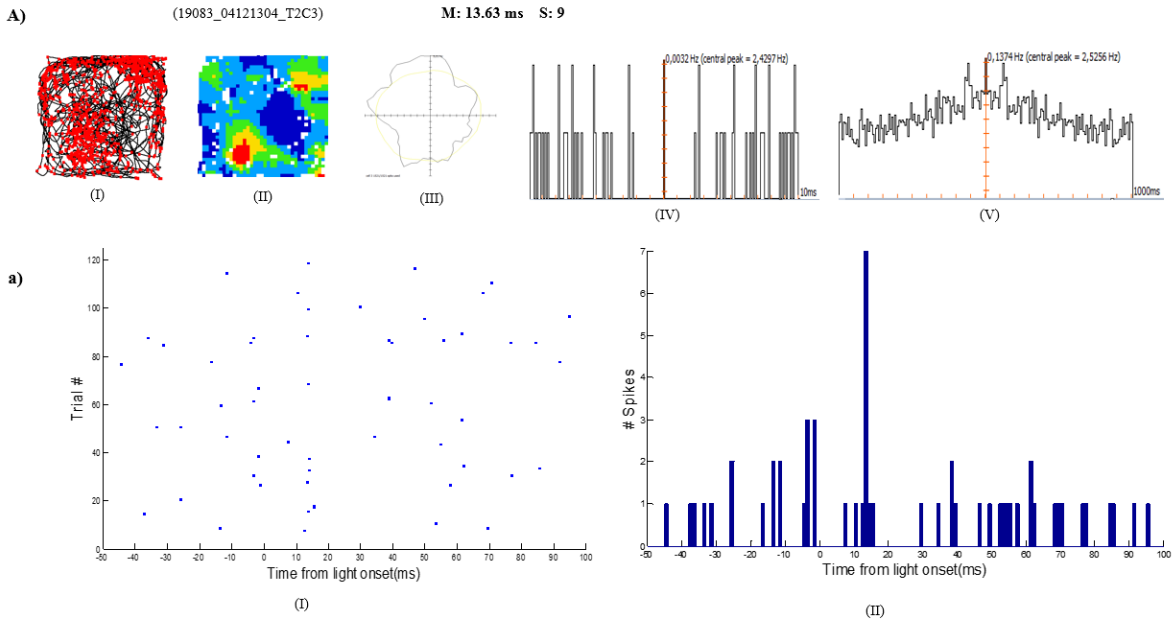

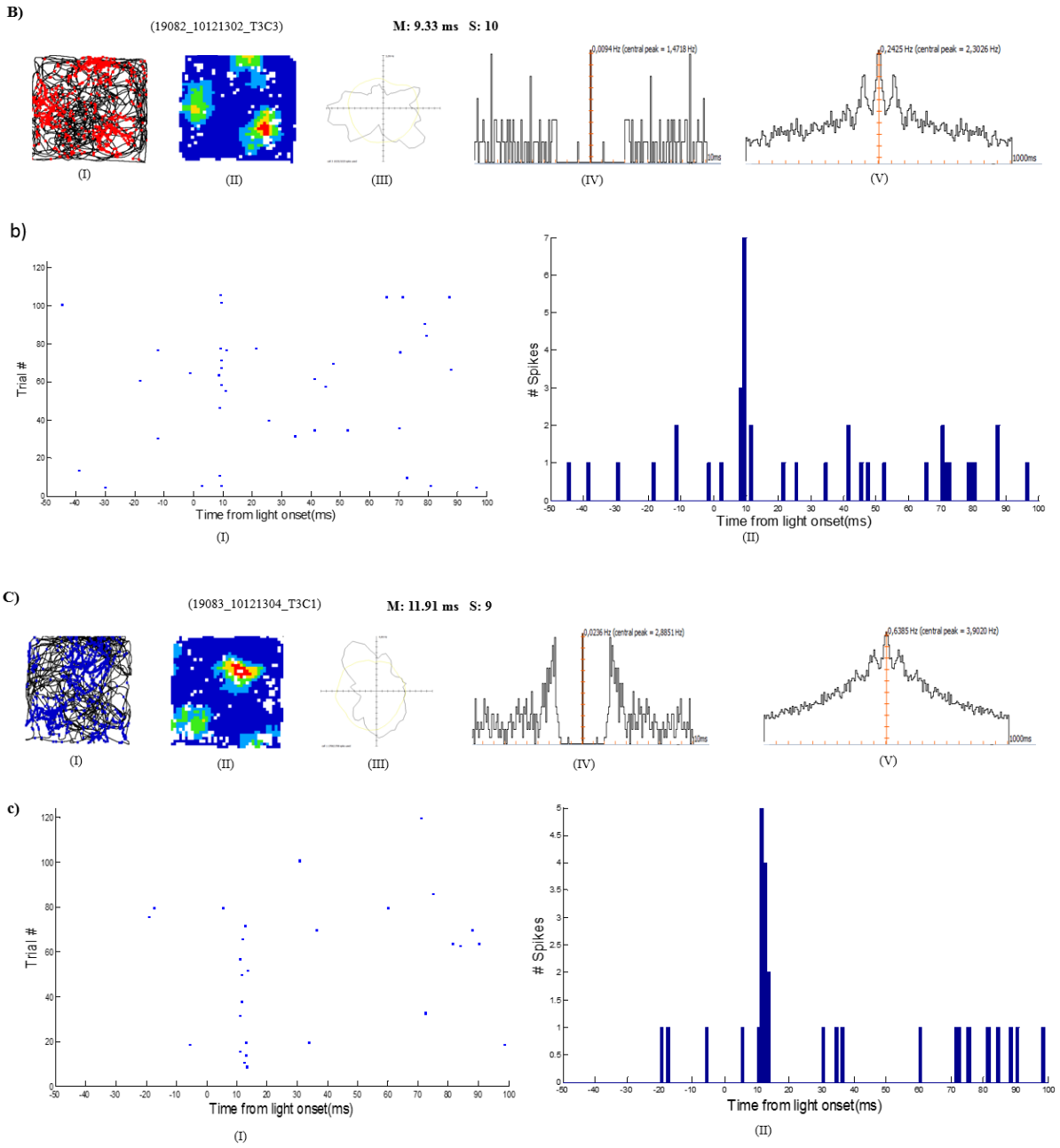

Fig. 24. Firing pattern of light responsive grid cells recorded in MEC. Three cells are represented in this figure by three letters **(A,B,C).** Note that ‘’**A and a’’** representing different data related to one cell and it is the same for B,b and C, c. **A, B** and **C,** from left to right: **(I),** spike locations (**A** and **B** in red and **C** in blue) superimposed on the trajectory of the animal (black lines) showing the locations of spikes as a triangular firing pattern of neural activity during 10 min recording period **(I).** Different colors (blue and red) here in spike locations map representing different cells recorded in neural clustering process by Tint program software. Color-coded rate maps **(II)** representing the triangular distribution of firing pattern with maximum rate of firing representing by red and absence of action potentials by dark blue color. Polar maps **(III)** showing firing rate as a function of rat’s head direction. As seen in polar plots of all three cells, there is no direction selectivity while navigation in enclosure resulting that these cells are not conjunctive cells. The next one, **(IV),** is -10/10 ms autocorrelogram confirming the isolation of extracellular neuronal spikes in all three cells (A,B,C) by the absence of firing activity over refractory time (the first 2 ms)**.**

However, a small correlation before 2ms to compare with other correlations in the -10/10 ms autocorrelograms for two last Cells (**B** and **C**) shows that a small amount of noise was isolated with these signals. The -1000/1000 ms autocorrelograms **(V)** show a small correlation with few distinct peaks. **a, b** and **c**, from left to right: spike raster **(I)** representing spike distribution before and after laser stimulation. Each blue dot shows a recorded spike from the cluster chosen. The x-axis shows the time from -50 to 100 milliseconds and y-axis is the trial number when each spike was recorded (ranging from 0 to 120 where each row represent 1 s stimulation period. 2 min stimulation session of 1Hz stimulation will give 120 trials).The next histogram **(II)** shows spike histogram where the number of spikes is plotted by their firing latency around the moment of stimulation (given at point 0 in the x-axis). The x-axis shows the time from light onset and ranges from – 50 to 100 milliseconds. The y-axis shows the number of spikes. At the front of session number presented on top of the data, ‘’**M’’** is the mean response time showing in x-axis of raster and spike histograms and ‘’**S’’** is the number of evoked spikes (y-axis).

3.4.4 Light Activated Unknown Principal Cells

10 light activated cells were classified as Unknown principal cells. They had neither no clear spatial characterization nor directional modulation (look at part I,II,III of each cell presented in Fig. 25) and the spike raster and spike histogram show clear peaks after point 0 (representing time of laser flash) (look at part VI,VII of each cell presented in Fig. 25). The peaks in both raster and spike histograms show a short latency of ~10 ms for 6 recorded responsive cells presented (from top to bottom) in Fig. 25, indicating direct activation of these cells in response to light (see mean responses ‘’M’’ at cells D,E,F,G,I,J Fig. 25). However, a slight longer latency of ~12 ms indicating indirect activation in several detected light responsive cells (see mean responses ‘’M’’ at cells A,B,C,H Fig. 25).

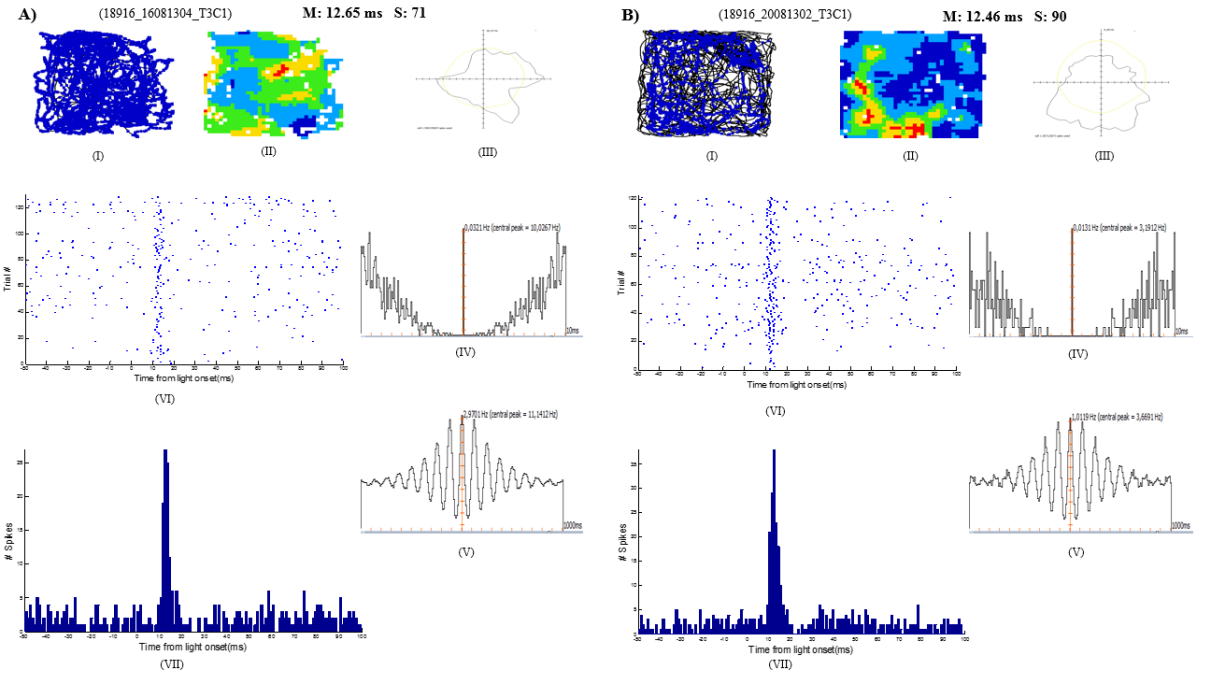
A)
(18916_16081304_T3C1)
M: 12.65 ms S: 71
(I)
(II)
(III)
(IV)
(V)
(VI)
(VII)
Trial #
Time from light onset(ms)
Spikes
B)
(18916_20081302_T3C1)
M: 12.46 ms S: 90
(I)
(II)
(III)
(IV)
(V)
(VI)
(VII)
Trial #
Time from light onset(ms)
Spikes

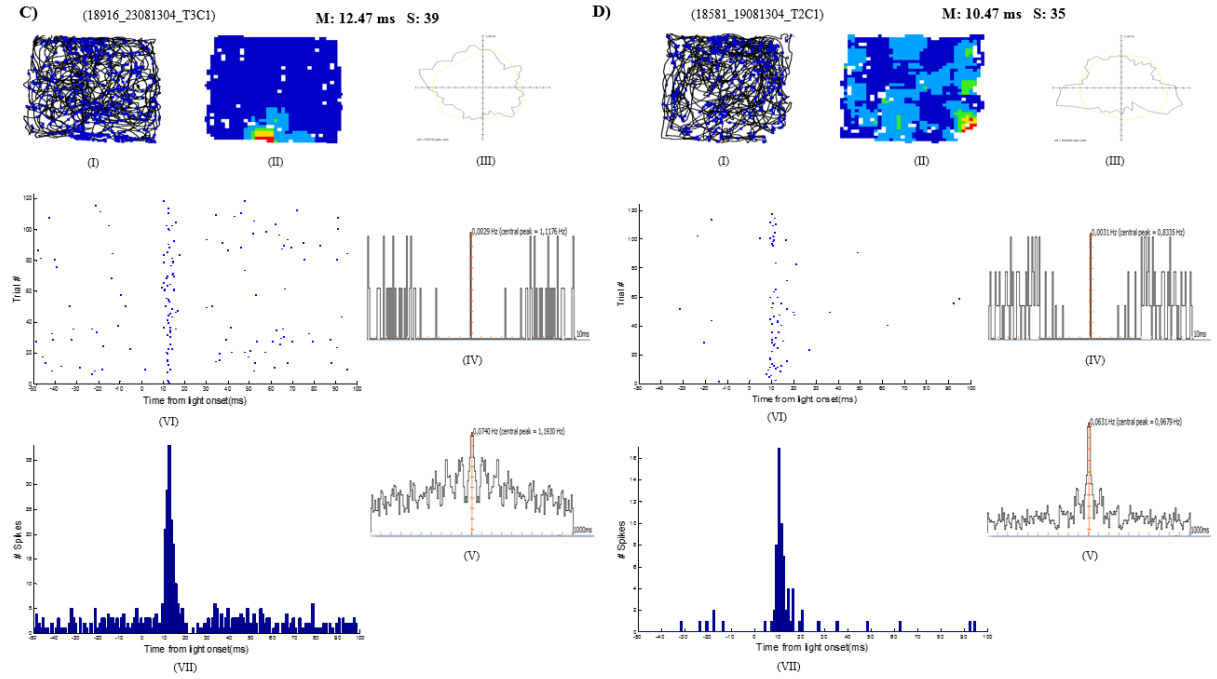
C)
(18916_23081304_T3C1)
M: 12.47 ms S: 39
(I)
(II)
(III)
(IV)
(V)
(VI)
(VII)
Trial #
Time from light onset(ms)
Spikes
D)
(18581_19081304_T2C1)
M: 10.47 ms S: 35
(I)
(II)
(III)
(IV)
(V)
(VI)
(VII)
Trial #
Time from light onset(ms)
Spikes

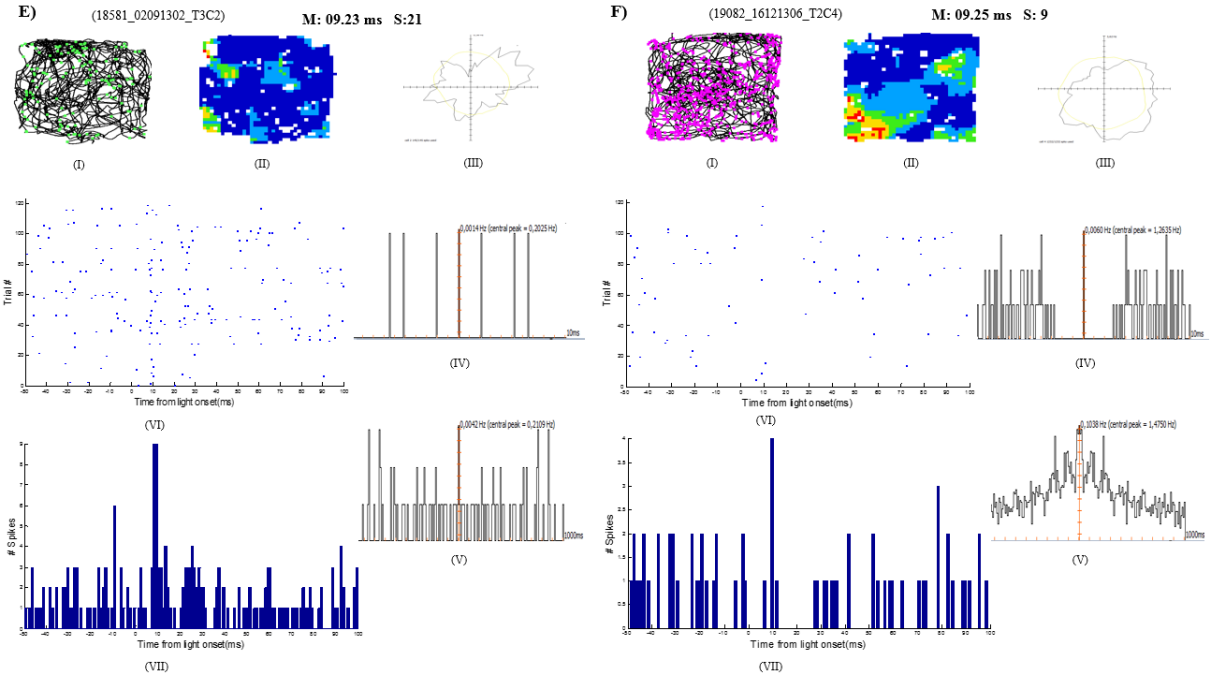
E)
(18581_02091302_T3C2)
M: 09.23 ms S:21
(I)
(II)
(III)
(IV)
(V)
(VI)
(VII)
Trial #
Spikes
Time from light onset(ms)
F)
(19082_16121306_T2C4)
M: 09.25 ms S: 9
(I)
(II)
(III)
(IV)
(V)
(VI)
(VII)
Trial #
Spikes
Time from light onset(ms)

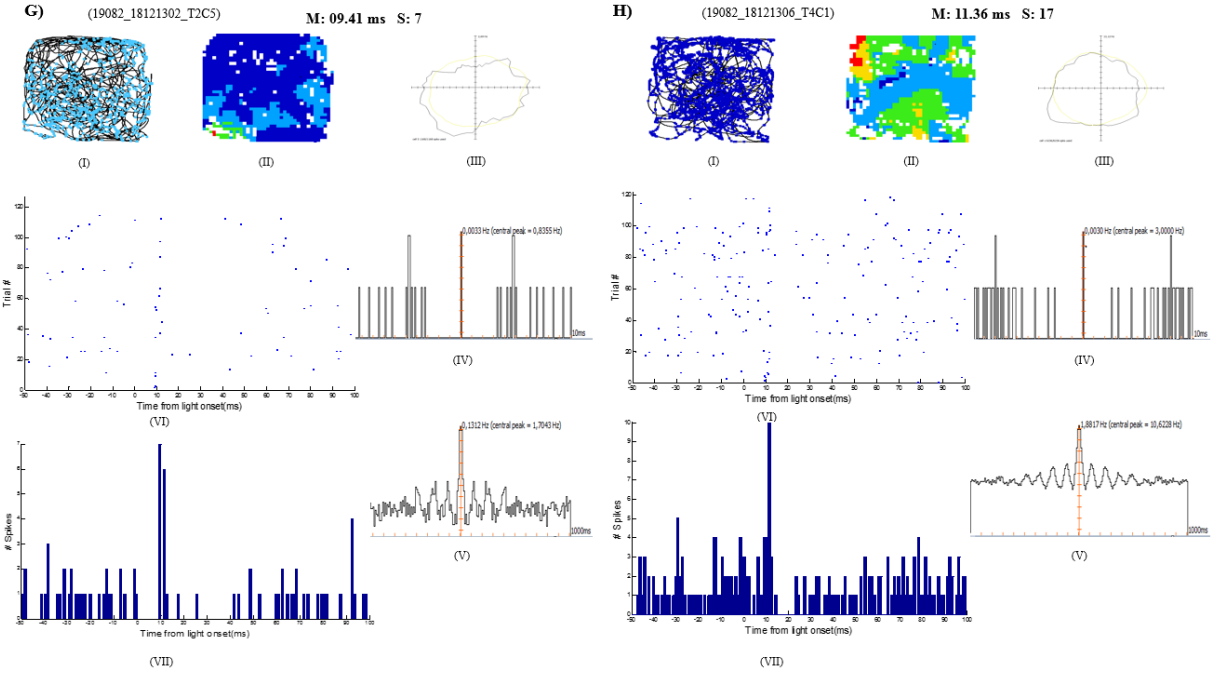
G)
(19082_18121302_T2C5)
M: 09.41 ms S: 7
(I)
(II)
(III)
(IV)
(V)
(VI)
(VII)
Trial #
Spikes
Time from light onset(ms)
H)
(19082_18121306_T4C1)
M: 11.36 ms S: 17
(I)
(II)
(III)
(IV)
(V)
(VI)
(VII)
Trial #
Spikes
Time from light onset(ms)

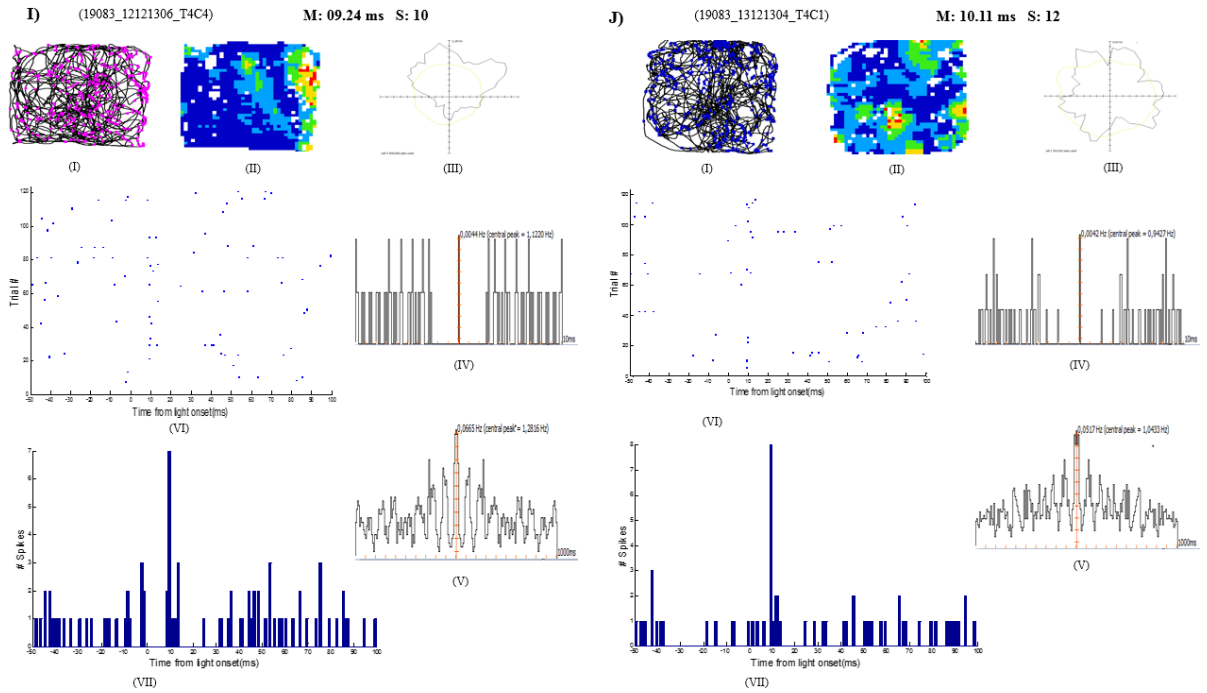

|**Fig. 25.** Firing pattern of light-responsive unknown principal cells recorded in MEC. Ten cells are represented in this figure. Each cell is represented by one letter (A-J) and different data collections are represented for each cell (I-VII). In each cell represented by one letter **(A-J)**: **(I),** spike locations (**E** in green and **F&I** in pink and **G** in light blue and the rest in blue) superimposed on the trajectory of the animal (black lines) showing the locations of spikes**.** Different colors (green, pink, light blue and blue) here in spike locations map, representing different cells recorded in neural clustering process by Tint program software. Color-coded rate maps **(II)** representing the distribution of firing pattern with maximum rate of firing representing by red and absence of action potentials by dark blue color. Polar maps **(III)** showing firing rate as a function of rat's head direction. As seen in polar plots of all cells, there is no direction selectivity while navigation in the enclosure. The next one, **(IV),** is -10/10 ms autocorrelogram confirming the isolation of extracellular neuronal spikes by the absence of spikes over the first 2 ms (refractory time)**.** However, in the first cell **(A),** a small firing activity of the cell before 2ms in the -10/10 ms autocorrelograms, shows that a small amount of noise was isolated with this signal. The -1000/1000 ms autocorrelograms **(V)** represents the pattern of rhythmicity over 1s. Spike raster **(VI)** representing spike distribution before and after laser stimulation. Each blue dot shows a recorded spike from the cluster chosen. The x-axis shows the time from -50 to 100 milliseconds and y-axis is the trial number when each spike was recorded (ranging from 0 to 120 where each row represent 1 s stimulation period. 2 min stimulation session of 1Hz stimulation will give 120 trials). The last histogram **(VII)** shows spike histogram where the number of spikes is plotted by their firing latency around the moment of stimulation (given at point 0 in the x-axis). The x-axis shows the time from light onset and ranges from – 50 to 100 milliseconds. The y-axis shows the number of spikes. At the front of session number presented on top of the data, ''**M''** is the mean response time showing in x-axis of raster and spike histograms and ''**S''** is the number of evoked spikes (y-axis).

3.4.5 Light Activated Interneurons

In total, Of 16 recorded interneurons, 12 cells (75%) were light-activated interneurons (Fig. 26). They had neither no clear spatial characterization nor directional modulation (look at part I,II,III of each cell presented in Fig. 26). In addition, these cells show a high firing rate and narrow waveforms. The spike raster and spike histogram show clear peaks after point 0 (representing time of laser flash) (look at part VI,VII of each cell presented in Fig. 26). 6 cells, by looking at peaks in these histograms, show a short latency of ~10 ms in response to laser stimulation (see mean responses ‘’M’’ at cells B,C,D,F,I,J Fig. 26), indicating direct activation and 6 cells show indirect activation by a slightly longer latency of ~12 m s . However, there are some cells showing multiple peaks responses (Fig. 26, cells; B,C,F,I,L). with a longer latency of ~25 ms (Fig. 26, I), ~30 ms (Fig. 26, B,C), and ~80 ms (Fig. 26, L) indicating indirect excitation with weaker synapses of the cells by synaptic connections with neighboring light activated cells.

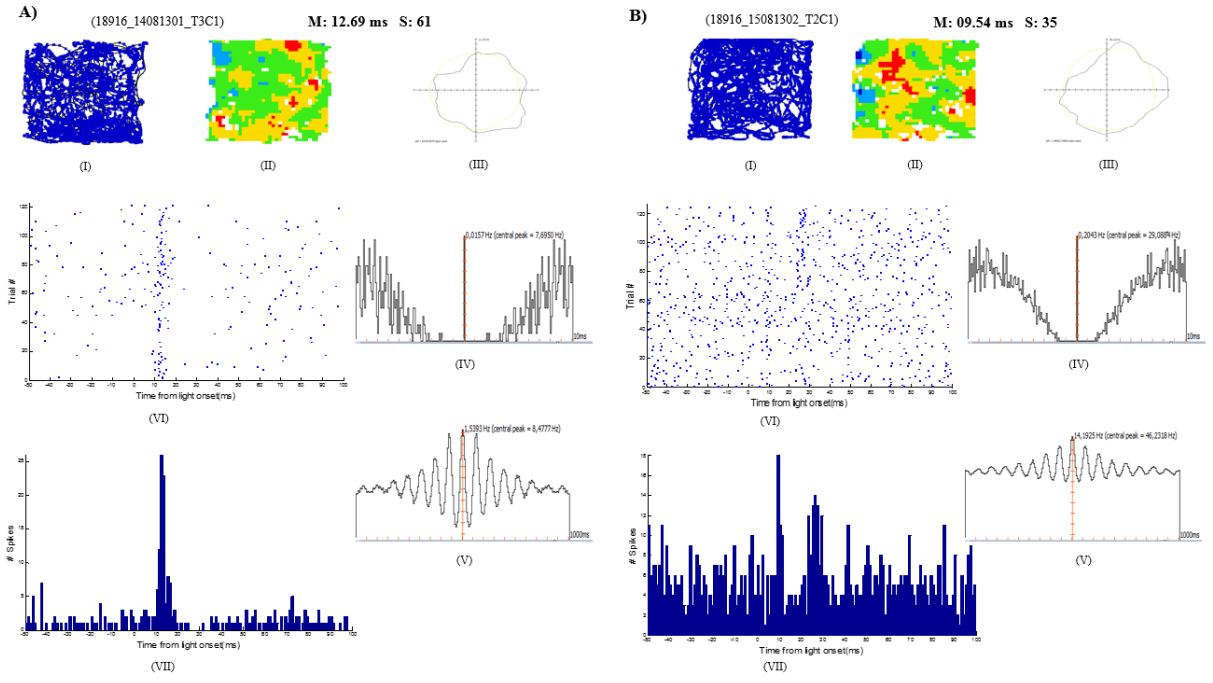

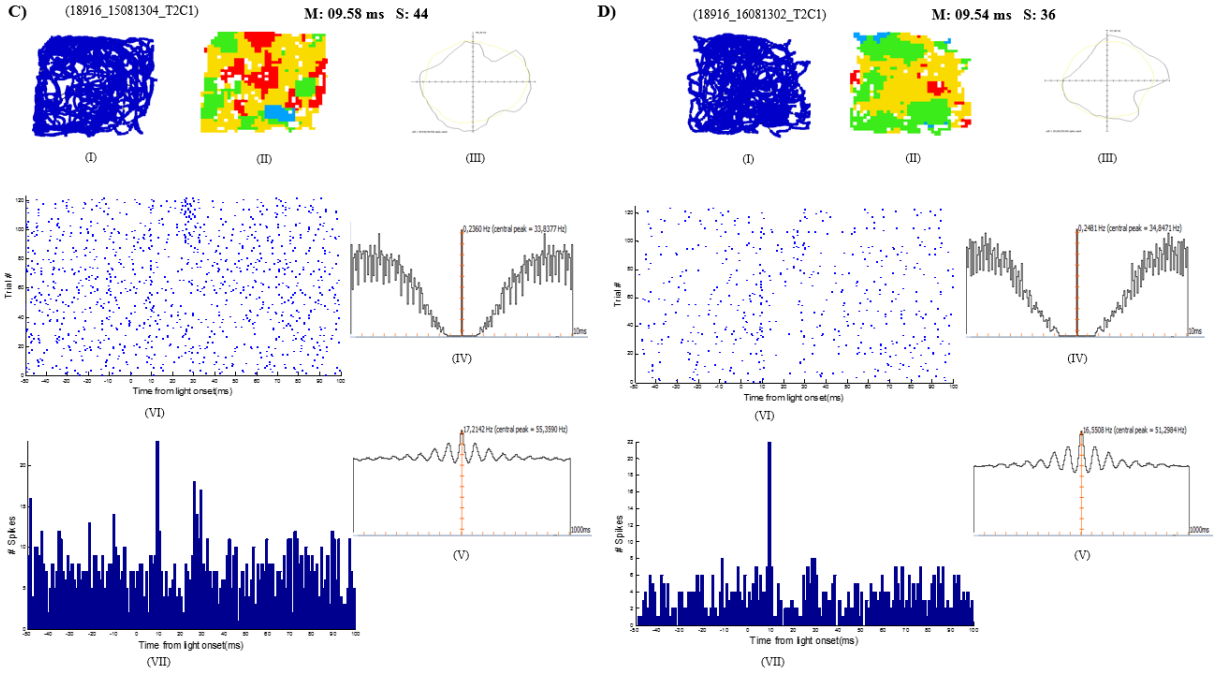
C)
(18916_15081304_T2C1)
M: 09.58 ms S: 44
(I)
(II)
(III)
(IV)
(V)
(VI)
(VII)
Trial #
Time from light onset(ms)
Spikes
D)
(18916_16081302_T2C1)
M: 09.54 ms S: 36
(I)
(II)
(III)
(IV)
(V)
(VI)
(VII)
Trial #
Time from light onset(ms)
Spikes

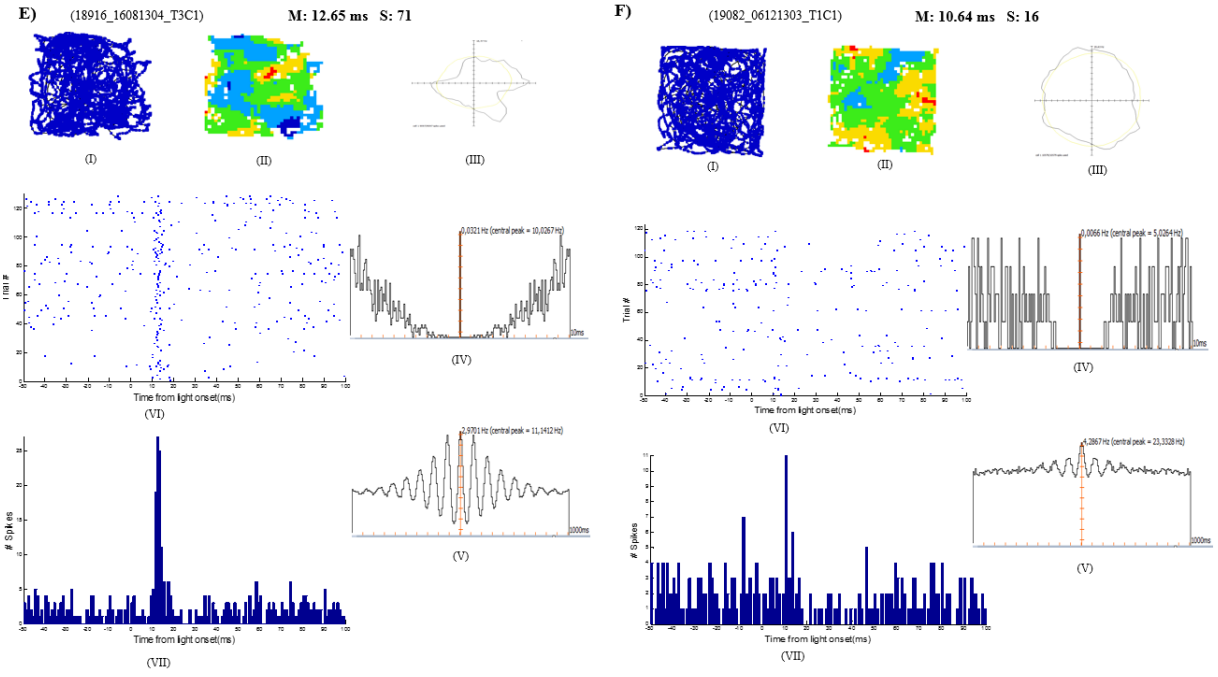
E)
(18916_16081304_T3C1)
M: 12.65 ms S: 71
(I)
(II)
(III)
(IV)
(V)
(VI)
(VII)
Trial #
Time from light onset(ms)
Spikes
F)
(19082_06121303_T1C1)
M: 10.64 ms S: 16
(I)
(II)
(III)
(IV)
(V)
(VI)
(VII)
Trial #
Time from light onset(ms)
Spikes

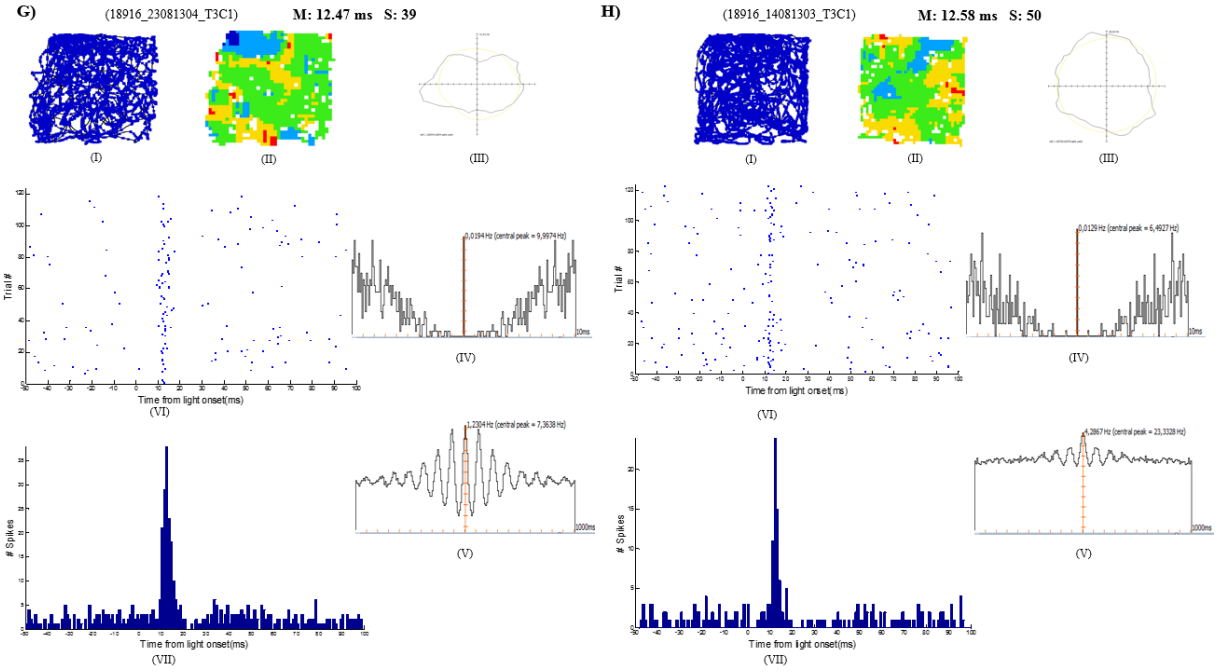
G)
(18916_23081304_T3C1)
M: 12.47 ms S: 39
(I)
(II)
(III)
(IV)
(V)
(VI)
(VII)
Trial #
Spikes
Time from light onset(ms)
H)
(18916_14081303_T3C1)
M: 12.58 ms S: 50

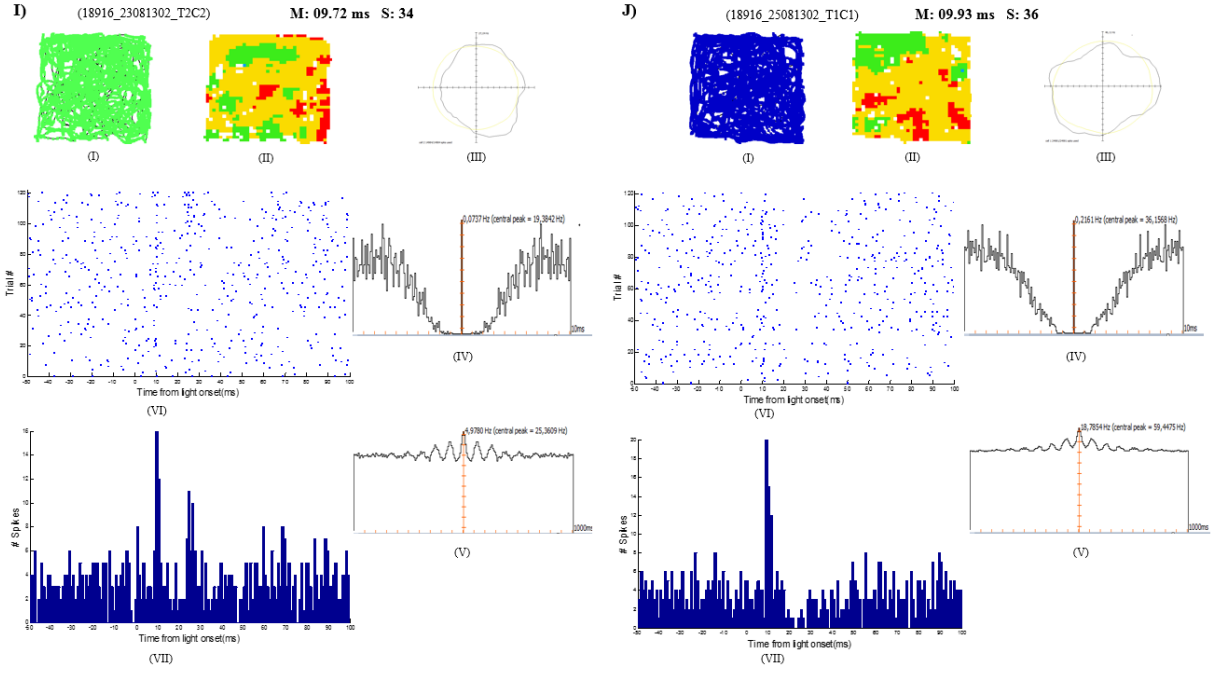
I)
(18916_23081302_T2C2)
M: 09.72 ms S: 34
(I)
(II)
(III)
(IV)
(V)
(VI)
(VII)
Trial #
Spikes
Time from light onset(ms)
J)
(18916_25081302_T1C1)
M: 09.93 ms S: 36

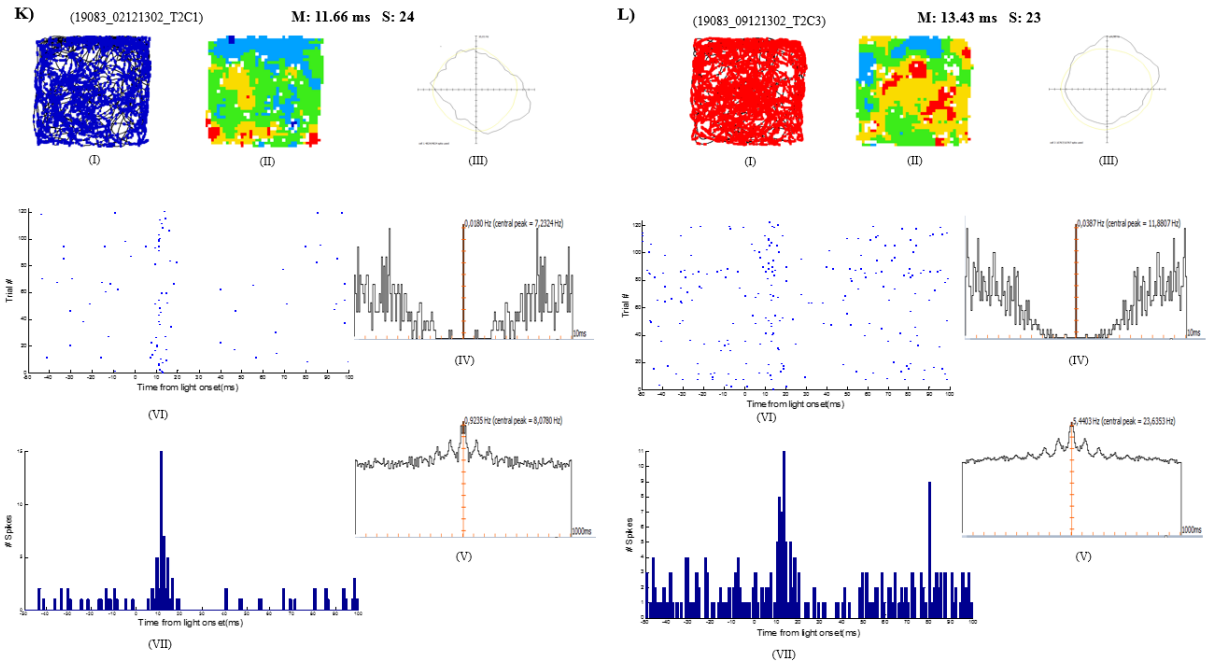

Fig. 26. Firing pattern of light-responsive interneurons recorded in MEC. Twelve cells are represented in this figure. Each cell is represented by one letter (A-L) and different data collections are represented for each cell (I-VII). In each cell represented by one letter **(A-L)**: **(I),** spike locations (**I** in green and **L** in red and the rest in blue) superimposed on the trajectory of the animal (black lines) showing the locations of spikes**.** Different colors (green, red, and blue) here in spike locations map, representing different cells recorded in neural clustering process by Tint program software. Color-coded rate maps **(II)** representing the distribution of firing pattern with maximum rate of firing representing by red and absence of action potentials by dark blue color. Polar maps **(III)** showing firing rate as a function of rat's head direction. As seen in polar plots of all cells, there is no direction selectivity while navigation in the enclosure. The next one, **(IV),** is -10/10 ms autocorrelogram confirming the isolation of extracellular neuronal spikes by the absence of spikes over the first 2 ms (refractory time)**.** However, in almost all presented cells, a small firing activity of the cell before 2ms can be seen shows that a small amount of noise was isolated with these signals. The -1000/1000 ms autocorrelograms **(V)** represents the pattern of theta rhythmicity over 1s. Spike raster **(VI)** representing spike distribution before and after laser stimulation. Each blue dot shows a recorded spike from the cluster chosen. The x-axis shows the time from -50 to 100 milliseconds and y-axis is the trial number when each spike was recorded (ranging from 0 to 120 where each row represent 1 s stimulation period. 2 min stimulation session of 1Hz stimulation will give 120 trials). The last histogram **(VII)** shows spike histogram where the number of spikes is plotted by their firing latency around the moment of stimulation (given at point 0 in the x-axis). The x-axis shows the time from light onset and ranges from – 50 to 100 milliseconds. The y-axis shows the number of spike. At the front of session number presented on top of the data, ''**M''** is the mean response time showing in x-axis of raster and spike histograms and ''**S''** is the number of evoked spikes (y-axis).

4. DISCUSSION

4.1 Aim of this research

Verga et al. showed that two distinct projections from different non-overlapping population of neurons located in the superficial layer II in MEC reaches neurons of hippocampus and extrahippocampally areas containing entorhinal cortex (110). This directed us to investigate further if the two cell populations contained different functional cell types. It has been demonstrated that the population of MEC neurons projecting to the hippocampus contain all MEC functional cell types, however the majority of these MEC-hippocampal projection cells types were grid cells (40). Hippocampal functions in connection with neural circuits in medial entorhinal cortex offer a good systems approach to understanding the basic functions of episodic memory formation. Then we draw our attention to the connections between both MEC hemispheres to investigate the connectivity of MEC-MEC neurons. In fact, by further analysis of the pattern of connectivity on entorhinal-entorhinal projections and identity of projection cells types, we could step up further steps to lighten up the way in which memory formation is done in navigational system and these data can be used for further research on this field. For this, we recorded neuronal activities in both left and right MEC by two different types of electrophysiological recording devices; i. microdrive device containing 4 tetrode bundles (Fig.7) and ii. versaderive device containing 8 tetrode bundles (Fig. 8) to see the differences in neuronal recording ability of these devices from superficial layers in MEC.

4.2 Optogenetics Technique Assessments

In order to identify controlaterally projecting MEC neurons, we used retrograde gene delivery strategy combined with optogenetics. By this approach, in addition to identification of various functional cell types of MEC, we could control their activities by light stimulations and, in turn, identifying their controlaterally target projections by retrograde viral transduction strategy. However, there is another approach by which the stimulation could have been carried out in MEC regions and recording at the same time from contralateral part. This strategy is called antidromic stimulation. However, this method has been less used as it would only allow us to get information about a small fraction of whole population of MEC neurons with projections to the contralateral MEC neurons. This is because of this fact that antidromic stimulations in a single location in the MEC would evoke action potentials in only those controlateral MEC axons that are in close

proximity of stimulating electrode. Since we need to study whole population of neurons in superficial layers of MEC, not only a small fraction of cells, then we chose optogenetic technique.

We used AAV2/1 viral vector to deliver optogenetic payload due to their excellent transduction efficiency. The reason to choose these viral vectors was due its low toxicity, high infectivity, long- term gene expression (*88*). We chose recombinant AAV2 serotype pseudotyped with AAV1 capsid proteins to produce AAV2/1. rAAV2/1 possess a high transgene transcription efficiency and, in turn, carried a plasmid that were coding ChR2-FLAG construct gene. As an optogenetic tool, we used ChR2 to detect infected neurons in the MEC, whereas FLAG was applied as a tag for immunohistology. Then during surgery, rAAV2/1, viral vector, was injected stereotactically into the left MEC for three rats with indicating numbers of 19081,19082 and 19083 (tetrodes implanted in right MEC). However, over the same period, rAAV2/1 was injected into the right MEC for two rats with indicating numbers of 18916 and 18581 and tetrodes were implanted to the left MEC for these two rats. For data recording, we applied microdrives for three rats with indication numbers of 18916-19081-19082 and Versadrive was used for two rats with indication numbers of 18581 and 19083. The number of cells detected in MEC of rats connected to versaderive was significantly larger than found MEC cells in rats recording by microdrives. As seen in Table 1, in MEC of rats with identity number of 18581 and 19083,in which, cells were recorded by versadrive system, 37 and 34 neurons was recorded respectively. However, this record was 20, 22 and 11 cells for rats 19082,19081 and 18916 respectively in which, MEC cells were recorded by microdrive system.

Behavioral data was collected while rats ran freely in 1 m^2 square box at the same time while recording neuronal spikes in the MEC. After experimental recordings were done (approximately 2 months), rats were transcardially perfused and their brains carefully extracted, sliced to sections and, in turn, brain sections stained with Nissl stain to track the trace of implanted tetrodes to see if the recording tetrodes are set truly in desired place that is superficial layers (II and III) of MEC. These Nissl-stained brain sections showed that the tetrodes were located in superficial layers of MEC (see Fig. 11). However, for rat number 18916 recording tetrodes seem to be initially sticked at superficial layers of MEC (Fig. 11 , Top to the right) and then we acquired less data (totally 11 cells) at this rat comparing with the other rats (Table. 1). ChR2-FLAG expression was observed around the injection sites (Fig. 20,21, left images) as well as the contralateral part of MEC (Fig. 20,21, right images).

4.3 Channelrhodopsin-2 Expression Assessment

By looking at immunohistochemical staining images (Fig. 20,21), we can easily see that ChR2-FLAG was expressed in superficial layers of contralateral MEC (mostly layer II and III). However, the following figure shows that ChR2 was not expressed in contralateral MEC in one rat with identification number of 19081 and as it was expected, no light responsive cells were detected around the implanted tetrodes in right MEC of this rat. Figure 27 shows a comparison in the level of ChR2 expression between this rat with indicating number 19081 and the other rat (rat number 18581). We can easily see that ChR2 was expressed undoubtedly in injection areas for both rats (shown in bright red, left images in Fig. 27). However, in contralateral MEC (right images in Fig. 27), there is no evidence of ChR2 expression for rat number 19081 (bottom image) while the expression of this channel in neurons of contralateral MEC of the rat 18581 is obvious and indicated by bright red (top image).

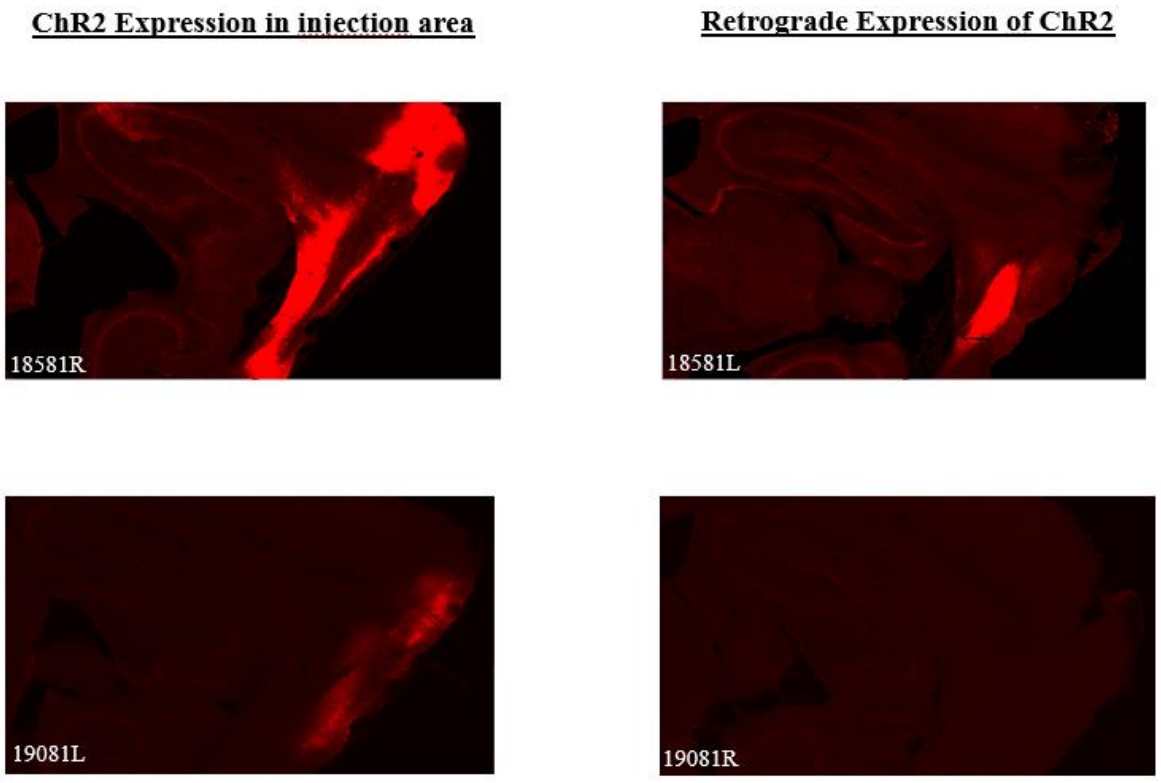

Fig. 27. Immunofluorescent images showing a comparison between ChR2-Flag expression level in injection area and contralateral MEC of two recorded cells in MEC of rats. The immunofluorescent images on the left side represent the expression level of ChR2 around

injection areas in MEC of two rats. While, the right images indicating the expression level of ChR2 in contralateral MEC. Areas containing ChR2 expression is indicated by bright red. Rats numbers are shown at the bottom of images where ‘’L’’ stands for left hemisphere and ‘’R’’ represents right hemisphere.

4.4 Identification and Classification of Recorded MEC Neurons

Please note that, the probability of correct identification and classification of functional cell types would be increased if we would apply the statistical analysis on recorded data. However, due to limited time, statistical analysis on the recorded data was not carried out and, instead, the MEC recorded cells were categorized by looking at the firing rate distributions maps, polar maps and spike location maps recorded over 10 min running session. To verify whether the recorded cell was light responsive or not, due to time limits, statistical analysis was not performed and, however, determined qualitatively by looking at spike raster and spike histograms that is leading to a decrease in certainty that these cells were light-responsive.

In total, 124 neurons were found in superficial layers II and III of both left and right MEC at this experiment. Based on the form of waveforms and the rate of firing activities in firing rate maps, 101 of total recorded neurons were categorized as putative principal cells and 23 cells as putative interneurons. According to specific criteria, Putative principal cells were further categorized into six categories: grid cells, head-direction cells, border cells, conjunctive grid x head direction cells, conjunctive border x head direction cells, unknown principal cells.

In total, Putative principal cells were sorted out by 25 grid cells, 16 head-direction cells, 9 border cells, 10 conjunctive grid x head direction cells, 7 conjunctive border x head direction cells and 34 unknown principal cells (see Table. 1).

To identify which cell types of the recorded MEC neuron population is connected to the contralateral part of MEC.

4.5 Identity of MEC Cells Projecting to Contralateral MEC by Laser Stimulations

To identify which recorded MEC neuron had projections terminating on contralateral MEC neurons, laser stimulations were carried out in the recording area of MEC. we applied laser stimulation in MEC with blue light of 473 nm with light pulses of approximately 20 mW light power at the fiber tips delivered at 1 Hz frequency for 2 min recording period. A recorded cell was counted as a light-responsive one if the number of spikes in spike raster and spike histogram of that cell reaches the level to form a clear dotted line and clear peaks respectively.

In total, 25 cells of all 124 recorded cells in MEC (~20%) showed responses in their spike raster and spike histograms and counted as light responsive cells. Of these photo-responsive cells, 3 cells were grid cells, 10 were unknown principal cells and 12 were interneurons. Some of these photo-responsive cells had weak responses in response to the light illumination with only few spikes in their spike raster and spike histograms (less than 10 spikes during 2 min laser stimulation). All three light-responsive grid cells (look at spike numbers indicated by ‘’S’’ at the top of each cell A, B and C in Fig. 24) as well as a number of unknown principal cells (F,G, I. Fig, 25) showed only few spikes in response to light illumination in their spike raster and spike histograms after laser stimulation. Three light-responsive grid cells; A, B and C shown in Fig. 24, displayed only 9, 10 and 9 spikes respectively. Furthermore, of 10 light responsive unknown principal cells, three cells; F, G and I had also weak responses of 9, 7 and 10 spikes in response to 2 min laser stimulation. Although, these cells sorted out as light-responsive cells set, these few responses (spikes) might be belong to other cells’ activities which manually isolated ,by mistake, in one cluster, as one cell in the same cluster during cluster-cutting in software TINT, Axona UK. This is further explained in the following figure, where a grid cell was supposed to possess few spikes (9 spikes) in response to the light illumination that these spikes might possibly be the property of the other cells activity adjacent to the grid cell that was clustered as one cell during cluster-cutting in analysis software (Tint, Axona). As shown in Fig. 28 A, amongst three isolated units (blue, green and red), the unit number 3, indicated by red cluster in the electrode-pair scatterplots, identified as grid cell, showed 9 spike at mean response time of 13.63 in response to the laser stimulation in their spike raster and spike histogram. However, due to weak responses (only 9 spikes), we carried out another test to see

the light responses activity of other cells adjacent to the identified grid cell (Blue, green and grey clusters adjacent to the grid cell that is indicated by red). As seen in Fig. 28, B, by selecting all activities around the grid cells (blue cluster in electrode-pair scatterplots adjacent to the grid cell), as one cluster, we found a huge mass of light response activities of 107 action potentials with mean response time of 10.59 in the spike raster and spike histogram. This suggests that these few spikes of grid cells in response to the light illumination might not certainly express that these cells are responsive to the light. The most responsess to the light illumination was found by grey dots, adjusent to the grid cell, in which indicating the signlas with no clear waveforms and isolated clusters. Then we called these unclear signals as noises.

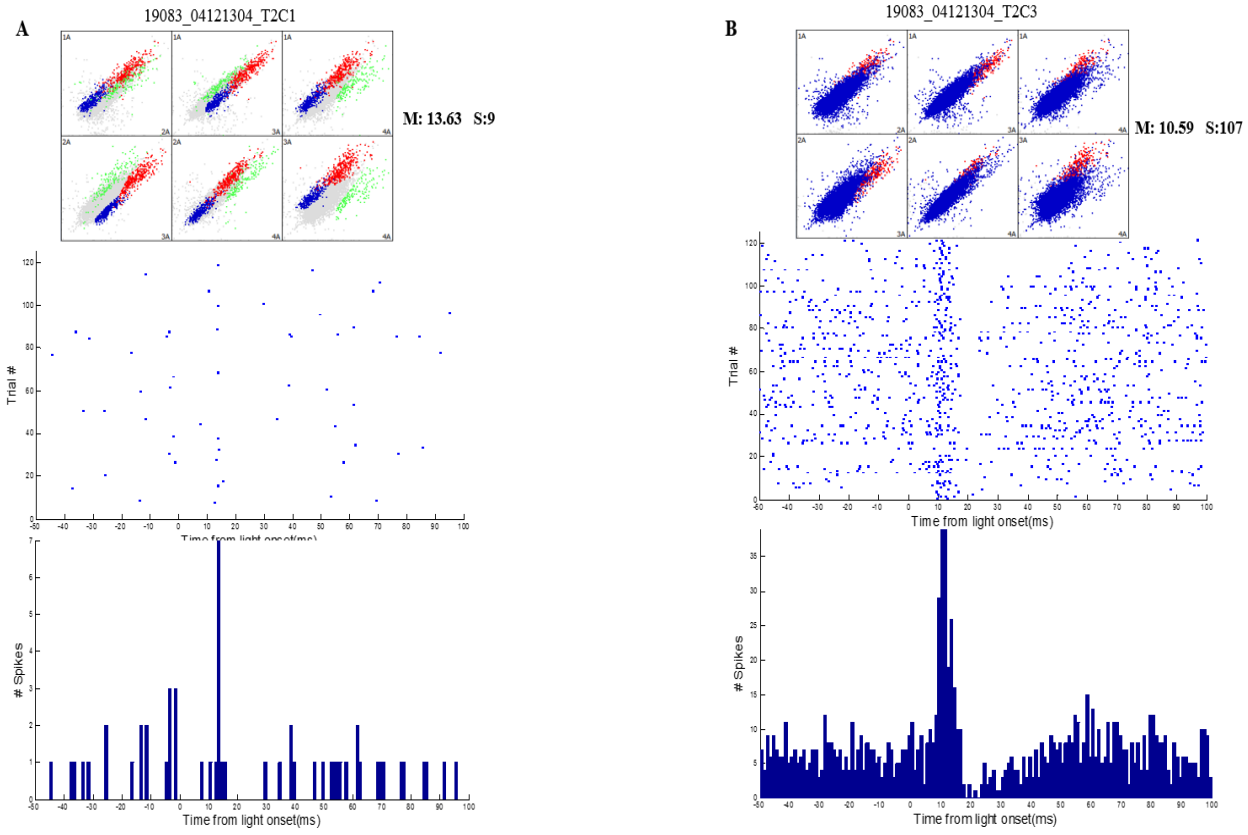

Fig. 28. A comparison between a grid cell activity and surrounding signals, Simultaneously, in response to the light illumination in MEC. (**A)** represents the response of grid cell to the light illumination. From top to bottom ; Electrode-pair scatterplots by 2 min recording of neuronal signals in MEC. Each individual grey dot in scatterplot is representative of one recorded spike plotted in accordance to its distance to 4 electrodes of the tetrode (1A–4A). Each box shows the recorded action potential by a single electrode. Three representative units (blue, green and red) shown in three distinct clusters identified manually by hand drawn polygons in which grid cell is the cell number 3 and indicated by red cluster. The spike raster (middle) and the spike histogram (bottom) display the distribution of spike before and after 2 min laser stimulation. Right to the scatterplots ‘’**M’’** is the mean response time showing in x-axis of raster and spike

histograms and ‘’**S’’** is the number of evoked spikes (y-axis). (**B)** representing the response of surrounding signals, adjacent to the grid cell, to the light illumination. From top to bottom ; the same electrode-pair scatterplots represented in (**A)**. Two representative units (blue, red) shown in two distinct clusters identified manually by hand drawn polygons in which surrounding signals around grid cell (red cluster) is indicated by blue cluster. The spike raster (middle) and the spike histogram (bottom) display the distribution of spike before and after 2 min laser stimulation. Right to the scatterplots ‘’**M’’** is themean response time showing in x-axis of raster and spike histograms and ‘’**S’’** is the number of evoked spikes (y-axis).

No light responses activities were detected for recorded spatial cells such as head direction cells, border cells and conjunctive grid x head-direction cells and conjunctive border x head-direction cells.

By looking at Nissl-stained sagittal brain section and then comparing it with immunofluorescent images, it can be seen if the final position of recording tetrodes, at their deepest locations, were located in the ChR2-FLAG-expressing MEC layers. Column A and C in the following figure shows the final position of recording tetrodes that is marked with yellow and white arrows in MEC of 5 studied rats (Fig. 29). Note that, both column A and C images are representing the same MEC hemisphere where the tetrodes were placed to record projections from contralateral MEC. As can be seen here, the recording tetrodes in the superficial layers of MEC (look at the white arrows in column C) were in adjacent with the ChR2-FLAG-expressing MEC areas (bright red) and not directly located in these areas, then decreasing the probability of detecting spatial cells responses to the light illumination. However, the recording tetrodes in rats with indicating numbers of 18916 and 19083 is slightly more in touch with chR2- expressed areas and then, of total 25 light activated cells, we found 12 and 6 light-responsive cells in MEC neurons of these two rats respectively. This is more evident in MEC of rat number 18581 where despite the strong retrograde expression of ChR2 in left MEC, only two light-responsive cells were detected and this is due to the distance between recording tetrodes (white arrows) and ChR2-expressed area (see column C rat number 18581). 5 light-responsive cells were recorded in MEC of rat number 19082 as well. Due to the absence of retrogradely gene expression of ChR2 in MEC of rat number 19081, then no light responses was discovered in this rat.

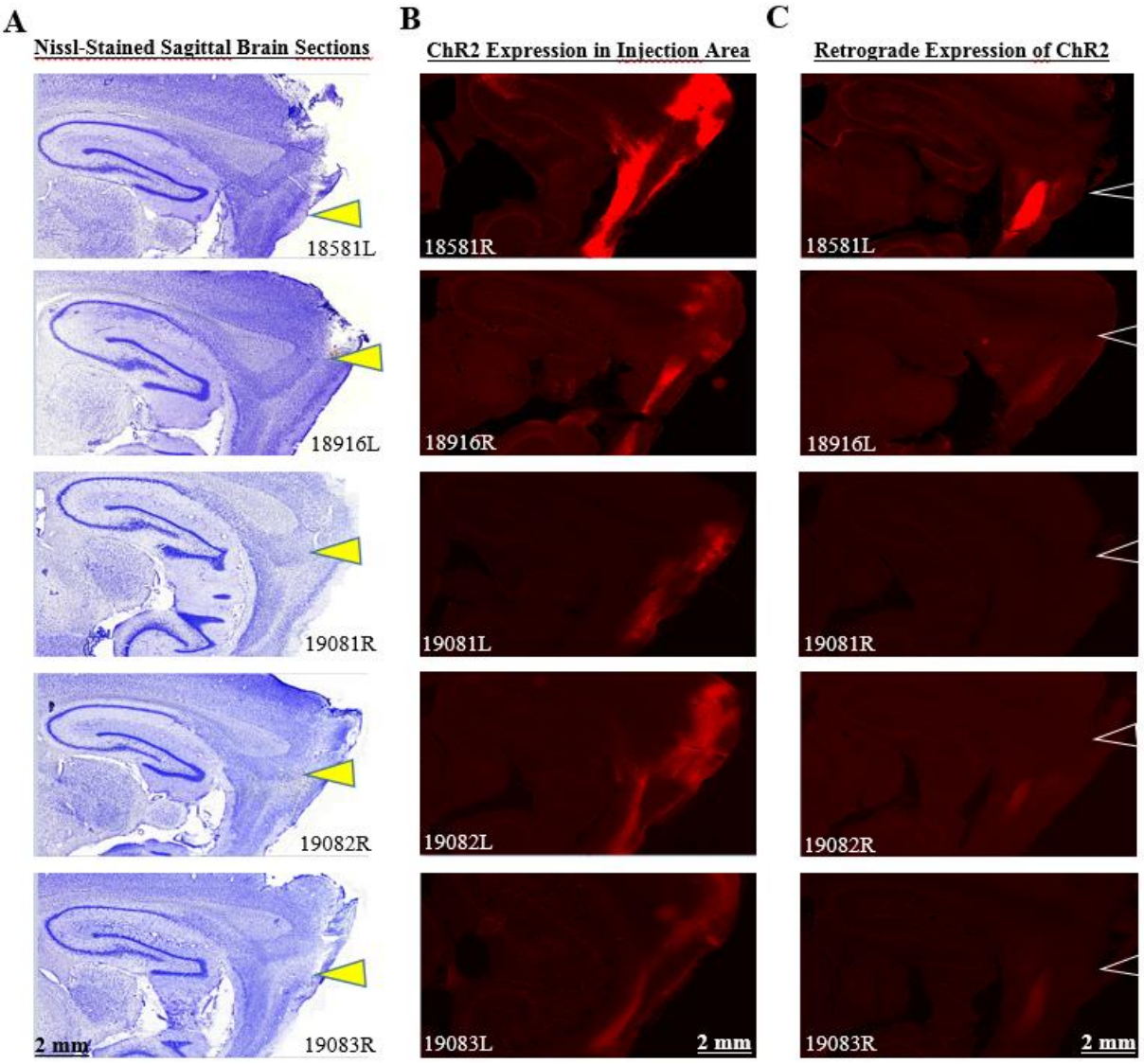

Fig. 29. A comparison between the final position of tetrodes and ChR2-FLAG expression areas in both left and right MEC of rats. Please note that, from top to bottom, for first two rats,18581 and 18916, the viral vectors were injected in the right MEC and recording area (the place where tetrodes were implanted) was in contralateral left MEC , whereas, injection area for the last three rats was the left MEC and tetrode were presented in contralateral right MEC. **(A)** Nissl stained sagittal brain sections representing the position of the tetrodes (deepest recording position is indicated by a yellow arrowhead). The number indicates the number of the rat, "R" stands for right brain hemisphere and ''L'' indicates the left brain hemisphere; 2 mm scale is shown on the bottom picture. **(B)** Immunofluorescent images of sagittal MEC sections showing ChR2-FLAG expressing around injection sites of MEC areas where expression of ChR2-FLAG is indicated by bright red fluorescence. **(C)** Immunofluorescent images of sagittal MEC sections showing the expression of ChR2-FLAG in contralateral MEC areas, correspond to the deepest recording position of tetrodes where that is indicated by the white arrowhead. Please note that tetrodes were located in the contralateral MEC areas where retrogradely expressing of ChR2-FLAG is been observed.

The function of opotogenetic control of neuronal signals is dependent on several criteria such as the absolute amount of light reaching in MEC neurons, the number of opsin molecules presented in the plasma membrane of the neuron and the light sensitivity of opsins (96). The control precision can also be influenced by the intrinsic membrane physiological properties of the recorded neuron and its surrounding neuronal signals which can not be controlled by experimenter. For instance, those recorded neurons in MEC that receive a massive inhibitory inputs from surrounding cells will be difficult to be activated by light illumination and neurons with electrically leaky plasma membrane will be hardly depolarized or hyperpolarized. The absolute amount of light reaching the recorded neuron in MEC depends upon the light power at the tip of light source (~20 mW at the tip of optical fiber) and the pattern of light propagation in MEC. The efficiency of optically controlling of neurons in MEC will not vary by location where neurons are at locations within the close proximity of the light source where light intensity is at the saturation level for opsin action. However, at locations further away from the light source (optic fiber tip), where light intensity falls below the saturation level, the efficiency of controlling MEC neurons will reduce with distance, and eventually at positions where light power falls below the threshold for opsin activation, light illumination will be unable to control neural activities. Moreover, the presence of electrodes and optical fibers in MEC also influences the pattern of light propagation (96).

These all abovementioned theories might be reasons leading to the absence of spikes recorded from these light-unresponsive MEC spatial cells in response to light illumination. While we found signals from three grid cells in response to the light illumination (Fig. 24), as explained above, these responses were not enough strong (less than 10 spikes over 2 min laser stimulation) to ensure us that these grid cells showed projections to the contralateral MEC. Indeed, these detected light-responsive spikes presented in grid cell signals might be of adjacent neuronal activities or unclear signals with no clear waveforms (named as noises) that was selected as one cluster as grid cell while cluster-cutting in analysis software Tint, Axona (please see Fig.28).

4.6 Analysis of Direct Vs. Indirect Photoexcitation

We speculated that minimal and stable response latencies, shown in spike raster and spike histograms, would suggest direct excitation, whereas longer and varied response latencies could be indicator of an indirect excitation as it requires synaptic transmission period. *Zhang et al*. in recently published paper defined neurons with short response latency of *~10* ms as directly-light-activated cells whereas those neurons with longer latency response of 11 ms or higher in their spike raster and spike histogram were considered as indirectly-light-activated cells (40). These criteria were used at this study to identify direct and indirect activation cells in response to the light illumination.

Table 2. Total number of Light-responsive neurons with direct and indirect activation detected in MEC of rats.

Light-responsive Cell Type	*Grid cells*	*Putative Unknown Principal Cell*	*Putative Interneuron*	*Total*
Number of Cells with Direct Excitation (Response latency of ~10 Ms)	1	6	6	13
Number of Cells with Indirect Excitation (Response latency of ≥11 Ms)	2	4	6	12
Total	3	10	12	25

Of total 25 recorded light-responsive cells in MEC, 13 cells (52%) showed a short response latency of *~10* ms and classified as direct-light-activated cells. Of these 13 direct-light-activated cells, 1 was grid cell, 6 were putative unknown principal cells and 6 were putative interneurons. Whereas, 12 cells (48%) showed a longer response latency of *11 ms* or higher and then considered as indirect-light-activated cells. Of these 12 indirect-light-activated cells, 2 were grid cells, 4 were

putative unknown principal cells and 6 were putative interneurons (See table. 2). Directly-light activated MEC neurons is due to expression of ChR2 in the cell membrane of cell by light illumination. All of these cells were recorded in either left MEC or right MEC whereas the virus carrying the ChR2 was injected in contralateral MEC. That is, if the virus was injected in left MEC, the neuron would be recorded in right MEC and vise versa. This suggests that the virus carrying ChR2 has travelled through the contralateral projection retrogradely from the left MEC to the right MEC and vise versa. Then, we can assume that all the directly-light activated cells recorded in MEC have projections to the contralateral MEC. Cells with longer latency response of *11 ms* are stimulated indirectly by the laser stimulation, meaning that, the recording tetrodes detect the spikes of the cell of interest which these spikes are as a result of synaptic connections with another cells activated by laser stimulation. That is, the illumination of light on ChR2-expressing neuron will lead to a depolarization of the cell leading to fire spikes and if this cell contains excitatory synapses with the cell of interest recorded in MEC, it would lead to a depolarization and then firing spikes in the cell of interest too.

Response latencies for interneurons were slightly longer and also possessed slightly higher variations to compare with putative principal cells. In addition to a longer response latency comparing with putative principal cells, interneurons, showed multiple peaks with different response latencies in their spike raster and spike histograms (see spike raster and spike histogram in interneurons indicating by B, C, F, I , L Fig. 26). These multiple peak latency cases are possibly including both direct and indirect excitations where the minimal response latency would correspond to a direct excitation and all the remaining peaks could be associated with indirect excitation arising through excitatory synapses with already-light-activated surrounding cells. The reason by which why these multiple peak latency responses were more observed in interneurons rather than principal cells could be due to a high number of synaptic connections between excitatory principal cells and inhibitory cells, which in our study these inhibitory cells probably resemble to interneuron category (*111*). In fact, 6 out of 13 (~46%) responsive principal cells showed response latencies higher than 11 ms, whereas for interneurons this number was 6 out of 12 (50%), which in turn, again supports the idea that indirect excitation was more often in light-responsive interneuron population.

In general, these findings suggest that both responsive cell type categories including principal cells and interneurons showed direct and indirect excitation, with almost equal number of 13 and 12 responsive cells respectively. This, in turn, lets us imply that both principal neurons (grid cells with low probability and unknown principal cells) and interneurons have projections terminating on contralateral MEC neurons.

Almost half of the responsive cells population was comprised of principal cells ,grid cells and unknown principal cells, (13 out of 25, 54%), and the other laser activated cells were interneurons (12 out of 25, 46%); note that the proportion of indirectly-light-activated cells in interneuron population is also larger than principal cells. A large portion of responsive principal cells were unknown principal cells (10 out of 13, ~77%), and grid cells (3 out of 13, 23%). However, interestingly, no responses was detected in head-direction cells, conjunctive grid x head-direction cells, conjunctive border x head-direction cells and borders cells.

However, it is far to understand the exact proportions of each functional cell type input projecting to the contralateral MEC and all the aforementioned numbers should be looked upon with caution. Indeed, the acquired quantities for different responsive cell types profoundly depend on several factors including; i. a sample size of recorded cells which plays a major role; for instance, it could be that with increased sample size the light responses in other spatial principal cells such as head-direction cells would be observed; ii. The differences in terminal distribution of projecting neurons could raise the probability of certain cell types being infected by virus more greatly due to this fact that their axons reach areas of virus injection, whereas some projections could be left out due to absence of virus in their terminal distribution in contralateral MEC; iii. Myelination could also be a noticeable factor as it was reported that myelination reduces the efficiency of retrograde AAV transduction (*112*); iv. delayed light propagation in brain tissue (*88*) could give rise to cases where MEC cells express ChR2 but because of overfilled light delivery in brain tissue or reaching light power being too low to activate ChR2, eventually those neurons would simply not be identified as light responsive cells. It is also of great significance to know that lowering down the tetrode in dorsal-ventral axis of superficial layers of MEC will record the neuronal signals of only a portion of cells presented there due to a high limitation in unit isolation range (*113*).

In brief, our study confirmed that unknown principal cells and interneurons, among various functional cell types presented in superficial layers II and III of MEC in rats' brain, showed a strong projection from left MEC to the contralateral right MEC and vise versa. Regardless of few spikes in response to light recorded from grid cells, as discussed earlier we could not support the idea that MEC grid cells projecting to the contralateral MEC and this is in contrast with MEC grid cells populations projecting to the hippocampus. In fact, to verify whether grid cells have contralateral projections to the MEC, broader population of neurons should be investigated. Although, other spatial cell types such as head-direction cells, border cells and conjunctive cells categories recorded in MEC showed no light responses at this study, these cells have been recently found to be responsive to light in another research and then could be counted as MEC cells projecting to the contralateral MEC (114). As illustrated, due to tetrode locations being far away from (rats number 18581 and 19082) or in adjacent with (rats numbers 18916 and 19083) ChR2-expressed in MEC areas studied at this research suggesting a less chance to recording signals from neurons containing expressed ChR2 (please see Fig.29). In addition to this, further issues leading to inability to record light-responses signals from these spatial cells have been discussed earlier. Then, further studies are needed to be carried out on MEC cells containing projections to the contralateral MEC to lighten up this pattern of activity between these two MEC hemispheres. This might further help to understanding a brighter mechanism by which Contralateral MEC neurons are involved in spatial memory formation and, furthermore, the role of these projections in spatial memory function need to be investigated.

5. CONCLUSION

Hippocampal functions in connection with neural circuits in medial entorhinal cortex offer a good systems approach to understanding the basic functions of episodic memory formation. Then we draw our attention to the connections between both MEC hemispheres to investigate the connectivity of MEC-MEC neurons.

By electrophysiological recordings *in vivo*, we found seven functional cell types presenting different spatial information within neuronal networks in medial entorhinal cortex including grid cells, head-direction cells, border cells, conjunctive grid x head-direction cells, conjunctive border x head-direction cells, unknown principal cells and interneurons. Retrograde gene delivery strategy enabled us to successfully tag neurons presented in superficial layers of MEC conveying information to the contralateral MEC. What's more, by combined optogenetics technique with electrophysiology recordings we could determined the identity of recorded MEC neuron that contained projections to the contralateral MEC. Our study showed that unknown principal cells and interneurons, among all functional cell types presented in superficial layers II and III of MEC, had a strong projection from left MEC to the contralateral right MEC and vise versa. Grid cells that are recently found to have a massive projections to the hippocampus, here in our study, only a small number, showed responses to light that might suggest the probability of their contralateral MEC connections. However, these responses were too much weak to convince us that these cells had projections to contralateral MEC. No more data were discovered to support projections of other detected spatial cell types to the contralateral MEC at this study. However, due to technical challenges fairly discussed, we could not get enough data to claim firmly on connection complexity of MEC-MEC neural circuits. Then, further studies are needed to lighten up this connection complexity between neurons of these two MEC hemispheres. This might further help to understanding a brighter mechanism by which Contralateral MEC neurons are involved in spatial memory formation. In the next stage, the role of these projections in spatial memory function need to be investigated too.

6. REFERENCES

1. B. L. McNamoserughton, F. P. Battaglia, O. Jensen, E. I. Moser, M.-B. Moser, Path integration and the neural basis of the 'cognitive map'. *Nat. Rev. Neurosci.* **7**, 663 (2006).
2. P. A. Naber, M. P. Witter, F. H. Lopes da Silva. Perirhinal cortex input to the hippocampus in the rat: evidence for parallel pathways, both direct and indirect. A combined physiological and anatomical study.European Journal of Neuroscience, **11**, 4119-4133 (1999).
3. J. O'Keefe, N. Burgess, Dual phase and rate coding in hippocampal place cells: Theoretical significance and relationship to entorhinal grid cells. *Hippocampus* **15**, 853 (2005).
4. D. C. Rowland, M.-B. Moser, From cortical modules to memories. Current Opinion in Neurobiology, **24**, 22-27(2014).
5. L. R. Howard, A. H. Javadi, Y. Yu, R. D. Mill, L. Staskute, H. J. Spiers. The Hippocampus and Entorhinal Cortex Encode the Path and Euclidean Distances to Goals during Navigation. Current Biology **24,** 1331-1340(2014).
6. B. L. McNaughton, F. P. Battaglia, O. Jensen, E. I. Moser, M.-B. Moser, Path integration and the neural basis of the 'cognitive map'. *Nat. Rev. Neurosci.* **7**, 663 (2006).
7. T. J. Wills, F. Cacucci. The development of the hippocampal neural representation of space. Current opinion in Neurobiology, **24**, 111-119(2014)
8. V. H. Brun et al., Place cells and place recognition maintained by direct entorhinal- hippocampal circuitry. *Science* **296**, 2243 (2002).
9. J. Taube, R. Muller, J. Ranck, Head-direction cells recorded from the postsubiculum in freely moving rats. I. Description and quantitative analysis. *The Journal of Neuroscience* **10**, 420 (1990).
10. T. Hafting, M. Fyhn, S. Molden, M.-B. Moser, E. I. Moser, Microstructure of a spatial map in the entorhinal cortex. Nature 436, 801 (2005).
11. H. Stensola *et al.*, The entorhinal grid map is discretized. *Nature* **492**, 72 (2012).
12. J, Kealy, S. Commins, The rat perirhinal cortex: A review of anatomy, physiology, plasticity, and function. progress in Neurobiology **93**, 552 (2011).
13. N. M. van Strien, N. L. M. Cappaert, M. P. Witter, The anatomy of memory: an interactive overview of the parahippocampal-hippocampal network. *Nat. Rev. Neurosci.* **10**, 272 (2009).
14. C. B. Canto, F. G. Wouterlood, M. P. Witter, What Does the Anatomical Organization of the Entorhinal Cortex Tell Us? Neural Plasticity 2008, Article ID 381243 (2008).
15. B. Tahvildari, A. Alonso, Morphological and electrophysiological properties of lateral entorhinal cortex layers II and III principal neurons. The Journal of Comparative Neurology. **491**, 123-140, (2005).

16. G. P. Gutierrez-Figueroa, C. Dalmaz, I. Izquierdo. Effects of entorhinal cortex lesions on memory in different tasks. Brazilian Journal of Medical and Biological Research, **30**, 769(1997).
17. T. V. Groen, I. Kadish, J. M. Wyss, Species differences in the projections from the entorhinal cortex to the hippocampus. Brain Reasearch bulletin, **57**, 553 (2002).
18. E. A. Tolner, F. Kloosterman, E. A. van Vliet, M. P. Witter. F H. Silva, J. A. Gorter, Presubiculum stimulation in vivo evokes distinct oscillations in superficial and deep entorhinal cortex layers in chronic epileptic rats. J. Neurosci. **25**, 8755 (2005).
19. B. F. Jones, M. P. Witter, Cingulate cortex projections to the parahippocampal region and hippocampal formation in the rat. Hippocampus **17**, 957 (2007).
20. M. T. Shipley. Presubiculum afferents to the entorhinal area and the papez circuit. Brain Research, **67**, 162 (1974).
21. M. P. Witter, D. Amaral, in Hippocampal Formation. The Rat Nervous System. G. Paxinos. Amsterdam, 635-704 (2004).
22. B. Poucet, C. Thinus-Blanc, R. U. Muller, Place cells in the ventral hippocampus of rats. **16**, 2045-8 (1994).
23. M.-B. Moser, D. C. Rowland, E. I. Moser, Places Cells, Grid Cells, and Memory. Cold Spring Harbor Perspectives in Biology, 1, 1 (2015).
24. D. Derdikman, E. I. Moser, A manifold of spatial maps in the brain. Trends in CognitiveSciences **14**, 561 (2010)
25. R. U Muller, J. L Kubie, E. M. Bostock, J. S. Taube, G. J. Quirk, in Spatial firing correlates of neurons in the hippocampal formation of freely moving rats. (Oxford University Press, 296–333 (1991).
26. G. J. Quirk, et al., The firing of hippocampal place cells in the dark depends on the rats recent experience. J. Neurosci. **10**, 2008 (1990).
27. M.-B. Moser, Y. Roudi, M. P. Witter, C. Kentros, T. Bonhoeffer, M.-B. Moser. Grid Cells and cortical representation. Nature Reviews, **15**, 466 (2014).
28. T. Solstad, E. I. Moser, G. T. Einevoll, From grid cells to place cells: A mathematical model.*Hippocampus* **16**, 1026 (2006).
29. V. H. Brun et al., Impaired Spatial Representation in CA1 after Lesion of Direct Input from Entorhinal Cortex. Neuron **57**, 290 (2008).
30. T. Solstad, C. N. Boccara, E. Kropff, M.-B. Moser, E. I. Moser, Representation of GeometricBorders in the Entorhinal Cortex. Science **322**, 1865 (2008).
31. T. L. Bjerknes, E. I. Moser, M.-B. Moser, Representation of geometric borders in the developing rat. Neuron **82**, 71-78(2014).
32. J. R. Whitlock, R. J. Sutherland, M. P. Witter, M.-B. Moser, E. I. Moser, Navigating from hippocampus to parietal cortex. Pnas **105** , 14755 (2008).
33. K.Jeffery, Spatial Mapping: graded precision of entorhinal head direction cells. Current biology **24**, 3 (2013).

34. H. M. Tan, J. P. Bassett, F. Cacucci, T. J. Wills, The development of the head direction system before eye opening in the rat. Current Biology **25**, 479(2015).
35. F. Sargolini et al., Conjunctive representation of position, direction, and velocity in entorhinal cortex. Science 312, 758 (2006).
36. T. Sasaki, S. Leutgeb, J. K. Leutgeb, Spatial and memory circuits in the medial entorhinal cortex. Current Opinion in Neurobiology **32**, 16(2015).
37. T. Hafting, M. Fyhn, S. Molden, M.-B. Moser, E. I. Moser, Microstructure of a spatial map in the entorhinal cortex. *Nature* **436**, 801 (2005).
38. J. O'Keefe, L. Nadel, in The hippocampus as a cognitive map. (Clarendon Press, Oxford,1978).
39. C. Köler, Intrinsic connections of the retrohippocampal region in the rat brain III. The medial entorhinal area. J. Comp. Neurol. 271, 208 (1988).
40. A. S. Etienne, R. Maurer, V. Seguniot, Path integration in mammals and its interaction with visual landmarks. The Journal of Experimental Biology **199**, 201(1996).
41. M. L. Mittelstaedt, H. Mittelstaedt, Homing by path integration in a mammal. Naturwissenschaften 67, 566 (1980).
42. J. O'Keefe, J. Dostrovsky, The hippocampus as a spatial map. Preliminary evidence from unit activity in the freely-moving rat. *Brain Res.* **34**, 171 (1971).
43. R. Muller, J. Kubie, The effects of changes in the environment on the spatial firing of hippocampal complex-spike cells. The Journal of Neuroscience 7, 1951 (1987).
44. E. I. Moser, M.-B. Moser, A metric for space. Hippocampus 18, 1142 (2008).
45. A. S. Etienne, K. J. Jeffery, Path integration in mammals. Hippocampus 14, 180 (2004).
46. T. Hafting, M. Fyhn, T. Bonnevie, M.-B. Moser, E. I. Moser, Hippocampus-independent phase precession in entorhinal grid cells. Nature 453, 1248 (2008).
47. A. M. Turing. The chemical basis of morphogenesis. Phil. Trans. R. Soc. B **237,** 37-72(1953).
48. E. I. Moser, M.-B. Moser, Y. Roudi, Network mechanism of grid cells. Phil. Tran. R. Soc. B **369**,(2015).
49. E. I. Moser, E. Kropff, M. -B. Moser, Place Cells, grid Cells and the brain's spatial representation system. Annu. Rev. Neurosci. **31**,61-89 (2008).
50. L. M. Giocomo, M. –B. Moser, E. I. Moser, Computational models of grid cells. *Neuron* **71**, 589 (2011).
51. N. Burgess, C. barry, J. Okeefe. An oscillatory interference model of grid cell firing. Hippocampus **17**, 801-812 (2007).
52. A. C. Welday, I. G. Shlifer, M. L Bloom, K. Zhang, H. T. Blair, Cosine directional tuning of theta cell burst frequencies: evidence for spatial coding by oscillatory interference. J. Neurosci. **31**, 16157-16176 (2011).
53. M.M. Yartsev, M.P. Witter, N. Ulanovsky, Grid cells without theta oscillations in entorhinal cortex of bats. Nature **479**, 103-107 (2011).

54. Y. Burak, I. R. Fiete, Accurate path integration in continous attractor network models of grid cells. PLos Compt. Biol. **5**. (2009).
55. M.C. Fuhs, D. S. Touretzky, A spin glass model of path integration in rat medial entorhinal cortex. J. Neurosci. **26**, 4266-4276 (2006).
56. B. L. McNaughton, F. P. Battaglia, O. Jensen, E. I. Moser, M.-B. Moser, Path integration and the neural basis of the 'cognitive map'. *Nat. Rev. Neurosci.* **7**, 663 (2006).
57. O. Yizhar, E. Fenno, Thomas J. Davidson, M. Mogri, K. Deisseroth, Optogenetics in neural systems. Neuron 71, 9 (2011).
58. Q. Chen, Z. Zeng, Z. Hu, Optogenetics in neuroscience: what we gain from studies in mammals, Neurosci Bull **28**, 423 (2012).
59. R. T. LaLumiere, A new technique for controlling the brain: optogenetics and its potential for use in research and the clinic, Brain Stimulation **4**, 4-6(2011).
60. O. P. Ernst, D. T. Lodowski, M. Elstner, P. Hegemann, L. S. Brown, H. Kandori. Microbial and animal rhodopsin: structure, functions, and Molecular mechanisms. American chemical society, **114**, 126-163 (2014).
61. L. Fenno, O. Yizhar, K. Deisseroth, The development and application of optogenetics. *Annu. Rev. Neurosci.* **34**, 389 (2011).
62. O. Yizhar, L. Fenno, F. Zhang, P. Hegemann, K. Diesseroth, Microbial opsins: a family of single- component tools for optical control of neural activity. Cold Spring Harbor Protocols 3, 273 (2011).
63. O. Beja, E. N. Spudich, J. L. Spudich, M. Leclerc, E. F. DeLong, Proteorhodopsin photography in the ocean. Nature **411**,786-789 (2001).
64. G. Varo, L. S. Brown, M. Lakatos, J. K. Launi, Characterization of the photochemical reaction cycle of proteorhodopsin. Biophys. J. **84**, 1202-1207 (2003).
65. A. Matsuno-Yagi, Y. Mulohata , Tow possible roles of bacteriorhodopsin; a comparative study of strains of halobacterium halobium differing in pigmentation. Biochem. Biophys. Re. Commun.**78**,237-243 (1977).
66. J. Klare, I. Chizhov, M. Engelhard, in Bioenergetics, G. Schäfer, H. Penefsky, Eds. (Springer Berlin / Heidelberg), **45**, 73-122 (2008).
67. V. A. Lorez-Fonfria, J. Heberle, Channelrhodopsin unchained: Structure and mechanism of a light-gated cation channel. Biochimica et Biophysica Acta 1837 626-642 (2014).
68. G. Nagel, D. Ollig, M. Fuhrmann, S. Kateriya, A. Musti, E. Bamberg, P. Hegemann, channelrhodopsin-1: a light-gated proton channel in green algae . Science **296**, 2395-2398 (2002).
69. G. Negal, T. Szells, W. Huhn, S. Kateriya,N. Adeishvili, P. Berthold, D. Ollig, P. Hegemann, E. Bamberg, Channelrhodopsin-2, a directly light –gated cation-selective membrane channel, proc. Nati. Sci. U. S. A. **100**, 13940-13945 (2003).

70. T. P. Sakmar, Structure of rhodopsin and the superfamily of sevenhelical receptors: the same and not the same. Curr. Opin. Cell Biol. **14**, 189 (2002).
71. F. Zhang *et al.*, The microbial opsin family of optogenetic tools. *Cell* **147**, 1446 (2011).
72. A, Berndt, O. Yizhar, LA. Gunaydin, P. Hegemann, K. Deisseroth, Bi-stable neural state switches. Nat. Neurosci. **12**, 229–34 (2009).
73. ES. Boyden, F. Zhang, E. Bamberg, G. Nagel, K. Deisseroth, Millisecond-timescale, genetically targeted optical control of neural activity. Nat. Neurosci. **8**, 1263–68 (2005).
74. LA. Gunaydin, O. , Yizhar, A. Berndt, VS. Sohal, K. Deisseroth, P. Hegemann, Ultrafast optogenetic control. Nat. Neurosci. 13, 387–92 (2010).
75. J. A. Cardin, M. Carlen, K. Meletis, U. Knoblich, F. Zhang, et al.Targeted optogenetic stimulation and ´ recording of neurons in vivo using cell-type-specific expression of channelrhodopsin-2. Nat. Protoc. 5, 247– 54 (2010).
76. S. J. Cruikshank, H. Urabe, A.V. Nurmikko, B. W. Connors, Pathway-specific feedforward circuits between thalamus and neocortex revealed by selective optical stimulation of axons. Neuron **65**,230–45 (2010).
77. L. Petreanu, T. Mao, S. M. Sternson, K. Svoboda, The subcellular organization of neocortical excitatory connections. Nature **457**,1142–45 (2009).
78. M.S. Grubb, J. Burrone, Channelrhodopsin-2 localised to the axon initial segment. PloS One **5**, e13761 (2010).
79. H. Wang, Y. Sugiyama, T. Hikima, E. Sugano, H. Tomita, et al. Molecular determinants differentiating photocurrent properties of two channelrhodopsins from chlamydomonas. J. Biol. Chem. **284**, 5685–96 (2009).
80. N. Grossman, V. Poher, M. S. Grubb, G.T. Kennedy, K. Nikolic, et al. Multi-site optical excitation using ChR2 and micro-LED array. J. Neural Eng. **7**, 16004 (2010).
81. A.R. Adamantidis, F. Zhang, A.M. Aravanis, K. Deisseroth, L. de Lecea, Neural substrates of awakening probed with optogenetic control of hypocretin neurons. Nature **450**, 420–24 (2007).
82. A.M. Aravanis, L.P. Wang, F. Zhang, L.A. Meltzer, M.Z. Mogri, et al. An optical neural interface: in vivo control of rodent motor cortex with integrated fiberoptic and optogenetic technology. J. Neural Eng. **4,** S143–56 (2007).
83. F. Zhang, V. Gradinaru, A.R. Adamantidis, R. Durand, R.D. Arian, et al. Optogenetic interrogation of neural circuits: technology for probing mammalian brain structures. Nat. Protoc. **5,** 439–56 (2010).
84. J. Wang, D.A. Borton, J. Zhang, R.D. Burwell, A.V. Nurmikko, A neurophotonic device for stimulation and recording of neural microcircuits. Conf. Proc. IEEE Eng. Med. Biol. Soc. **1**, 2935–38 (2010).
85. R. Y. Pan, X. Xiao, S. L, Chen, H. J. Wang, et al. Disease- inducible transgene expression from a recombinant adeno associated virus vector in a rat modelds. J Viral, 73,3410-7 (1999).

86. Y. Mei, F. Zhang, Molecular tools and approaches for optogenetics. Biol. Psychiatry 71, 1033 (2012).
87. M. Rein, J. Deussing, The optogenetic (r)evolution. Molecular Genetics and Genomics 287, 95 (2012).
88. O. Yizhar, Lief E. Fenno, Thomas J. Davidson, M. Mogri, K. Deisseroth, Optogenetics in neural systems. Neuron 71, 9 (2011).
89. J. Dai, A. B. M. Rabie, The use of recombinant adeno-associated virus for skeletal gene therapy. Orthod craniofacial Res 10, 1- 14 (2007).
90. J. E. Rabinowitz, F. Rolling, C. Li, H. Conrath, W. Xiao, X. Xiao, *et al*. Cross-packaging of a single adeno-associated virus (AAV) type 2 vector genome into multiple AAV serotypes enables transduction with broad specificity. *J Virol*. **76**, 791–801 (2002).
91. G. Gao, M. R. Alvira, S. Somanathan, Y. Lu, L. H. Vandenberghe, J. J. Rux *et al.* Adeno-associated viruses undergo substantial evolution in primates during natural infections. Proc Natl Acad Sci U. S. A. **100**, 6081–6 (2003).
92. D. Grimm, M.A. Kay, J. A. Kleinschmidt, Helper virus-free, optically controllable, and two-plasmid-based production of adeno-associated virus vectors of serotypes 1 to 6. Mol Ther **7**,839–50 (2003).
93. D. Grimm, M. A. Kay, From virus evolution to vector revolution: use of naturally occurring serotypes of adeno-associated virus (AAV) as novel vectors for human gene therapy. Curr Gene Ther. **3**, 281–304 (2003).
94. C. Burger et al. Recombinant AAV viral vectors pseudotyped with viral capsids from serotypes 1, 2, and 5 display differential efficiency and cell tropism after delivery to different regions of the central nervous system. Mol Ther 10, 302 (2004).
95. Y. Mey, F. Zhang, Molecular tools and approaches for optogenetics, Biol Psychiatry, **71**, 1033-1038 (2012).
96. X. Han, In vivo application of optogenetics for neural circuit analysis.pubs.acs.org, chemneuro, Neurosci. **3**, 577-584 (2012).
97. T. T. Jonathan, F. Guoping, Development of transgenic animals for optogenetic manipulation of mammalian nervous system function: progress and prospects for behavioral neuroscience. Behave Brain Res, 15, 3-18 (2013).
98. B. R. Arenkiel, P. Joao, I. g. Davison, C. Feliciano, K. Deisseroth, G. J. Augustine, G. Feng, In vivo light induced activation of neural circuitry in transgenic mice expressing channelrhodopsin-2.Neuron, 54, 205-218 (2007).
99. V.S. Sohal, F. Zhang, O. Yizhar, K. Deisseroth Parvalbumin neurons and gamma rhythms enhance cortical circuit performance Nature, **459**, pp. 698–702 (2009),
100. H.C. Tsai, F. Zhang, A. Adamantidis, G. D. Stuber, A. Bonci, L. de Lecea, K. Deisseroth Phasic firing in dopaminergic neurons is sufficient for behavioral conditioning Science, **324**, pp. 1080–1084 (2009),

101. J. K. Chapin, Using multi-neuron population recordings for neural prosthetics. Nature Neuroscience, **7**, no 5 (2004).
102. E. H. Chang, S. A. Frattini, S. R. Robbiati, P. T. Huerta, Construction of Microdrive arrays for chronic neural recordings in awake behaving mice. Journal of Visualized Experiments.**77**, 1-8, (2013).
103. C. M. Gray, P. E. Maldonado., et al. Tetrodes markedly improve the reliability and yield of multiple single-unit isolation from multi-unit recordings in cat striate cortex. J. Neurosci. Methods. **63,** 43-54 (1995).'
104. VersaDrive 8 Optical construction Manual: 8 tetrode versaDrive (2012). www.Neuralynx.com.
105. Y. Jeantet, Y. H. Cho, Design of a twin tetrode Microdrive and headstage for hippocampal single unit recordings in beahaving mice, Journal of Neuroscience Method, **129,** 129-134 (2003).
106. E. Tran, Electrophysiological characterization of spatial memory cells in the anterior thalamic nuclei, bachelors thesis presented to Trinity collage Dublin, university of Texas at Austin, Page 12 (2012).
107. L. Santos, L. Opris, J. Fuqua, R. Hampson, S. Deadwyler, A novel tetrode Microdrive for simultaneous multi-neuron recording from different regions of primate brain. J. Neurosci Methods. **205,** 368-374, (2012).
108. J. D. Kralik, D. F. Dimitrove, D. J. Krupa, D. B. Katz, D. Cohen, M. A. L. Nicoletis. Techniques for long term multisite neuronal ensemble recordings in behaving animals. Methods, **25,** 121-150, (2001).
109. L. M. Frank, E. N. Brown, M. A. Wilson, A comparison of the firing properties of putative excitatory and inhibitory neurons from CA1 and the entorhinal cortex. *J.Neurophysiol.* **86**,2029 (2001).
110. C. Varga, S. Y. Lee, I. Soltesz, Target-selective GABAergic control of entorhinal cortex output. *Nat. Neurosci.* **13**, 822 (2010).
111. J. J. Couey *et al.*, Recurrent inhibitory circuitry as a mechanism for grid formation. *Nat. Neurosci.* **16**, 318 (2013).
112. E. R. Hollis *et al.*, Transient demyelination increases the efficiency of retrograde AAV transduction. *Mol Ther* **18**, 1496 (2010).
113. G. Buzsaki, Large-scale recording of neuronal ensembles. *Nat. Neurosci.* **7**, 446 (2004).
114. R. S. Wågan, Functional dissection of local medial entorhinal cortex subcircuits, master thesis , Norwegian University of Science and Technology, Faculty of Medicine. (2013).